Dissertation

submitted to the
Combined Faculties for the Natural Sciences and for Mathematics
of the Ruperto-Carola University of Heidelberg, Germany
for the degree of
Doctor of Natural Sciences

presented by

Diplom-Physiker:	Jan Unkelbach
born in:	Darmstadt, Germany

Oral examination: February, 15th 2006

Inclusion of organ motion in IMRT optimization using probabilistic treatment planning

Referees: Prof. Dr. Uwe Oelfke
Prof. Dr. Josef Bille

Zusammenfassung

Berücksichtigung von Organbewegungen in der IMRT Optimierung durch probabilistische Bestrahlungsplanung

Die vorliegende Arbeit beschreibt ein Verfahren zur Berücksichtigung von Organbewegungen in der Bestrahlungsplanung für die fraktionierte intensitätsmodulierte Strahlentherapie (IMRT). Organbewegungen werden durch ein mathematisches Modell beschrieben welches die Grundlage der Bestrahlungsplan-Optimierung darstellt. Das Modell enthält Zufallsvariablen um die stochastische Natur von Organbewegungen zu beschreiben. Die vorausgesagte Dosisverteilung im Patienten muss daher ebenfalls als Zufallsvariable aufgefasst werden und wird durch einen Erwartungswert der Dosis und dessen Varianz charakterisiert. Zur Optimierung des Bestrahlungsplans unter Berücksichtigung des Bewegungsmodells wird der Erwartungswert einer quadratischen Kostenfunktion minimiert, der sich als Summe der Dosisvarianz und der quadratischen Differenz von Solldosis und Erwartungswert der Dosis darstellen lässt. Die daraus resultierenden Bestrahlungspläne haben die Eigenschaft, dass Bereiche in denen Tumorgewebe nur relativ selten lokalisiert ist mit einer geringeren Dosis bestrahlt werden. Dies wird ausgeglichen durch eine Dosisüberhöhung in benachbarten Bereichen, so dass sich durch den Einfluss der Bewegung im Verlauf der gesamten Therapie eine näherungsweise homogene Gesamtdosisverteilung im Tumor ergibt. Das Verfahren erlaubt eine potentiell bessere Schonung von angrenzenden gesunden Geweben im Vergleich zur Sicherheitsrand-Methode.

Abstract

Inclusion of organ motion in IMRT optimization using probabilistic treatment planning

The presented thesis describes an off-line approach to incorporate organ motion into the treatment plan optimization for fractionated intensity modulated radiotherapy (IMRT). Organ movement is described in terms of a mathematical model that represents the basis of the treatment plan optimization process. The motion model contains random variables in order to describe the stochastic nature of organ movements. As a consequence, the predicted dose distribution in the patient must be considered as a random variable as well. It is characterized by the expectation value and the variance of the dose. For treatment plan optimization incorporating the motion model, the expectation value of a quadratic cost function is minimized, which can be expressed as the sum of the variance of the dose and the quadratic difference of expected and prescribed dose. The resulting treatment plans show a reduction of the dose in regions where tumor tissue is only rarely present. This is compensated for by delivering a higher dose to neighboring regions that are mostly occupied by tumor tissue. Due to organ movement during the course of treatment, a widely homogeneous cumulative dose distribution is delivered to the tumor. This method, compared to the standard safety margin approach, potentially allows for a better sparing of healthy tissues from dose burden.

Acknowledgments

I would like to thank my supervisor Prof. Uwe Oelfke for providing me the opportunity to work on this subject. I always enjoyed working with him and his group. I appreciate his friendly personality, which is one of the reasons for the pleasant atmosphere in his group.

I am grateful to all colleagues in the department who made my stay at the DKFZ a very enjoyable period of my life, both at work and at various social events. In particular, I would like to thank Simeon Nill and Jan Wilkens for their exceptional helpfulness and their valuable support in countless situations.

I would like to thank Prof. Wolfgang Schlegel for his support and for providing a productive and friendly work environment in his department. I also thank Prof. Josef Bille as the second referee of this thesis. I am grateful to Annette Seeber for her careful proof reading and to Daniel Maleike for his work as a diploma student.

Preface

This PhD thesis was carried out at the German Cancer Research Center (DKFZ) between November 2002 and December 2005. The thesis describes an approach to incorporate organ movements that occur during the course of fractionated radiotherapy into the optimization of a treatment plan for intensity modulated radiotherapy. This approach is referred to as probabilistic treatment planning.

The manuscript does not contain a general introduction to radiotherapy and assumes the reader to be familiar with the concept of intensity modulated radiation therapy (IMRT). A brief introduction to different methods to deal with organ motion in radiotherapy is provided in order to integrate this work into the field of Adaptive Radiotherapy (section 1.1).

Parts of this work have already been published as a series of three peer-reviewed papers. Chapter 2 is mainly covered by the papers [1] and [2], and section 3.2 is widely covered by the paper [3]. Parts of the work were also presented at five international conferences [4, 5, 6, 7, 8]. For the contribution at the ICCR Congress 2004 in South Korea [5], a young investigator's prize was awarded. Under the supervision of the author and Prof. Uwe Oelfke, one diploma thesis was prepared which is closely related to Chapter 3 of this work [9].

Contents

Dependencies of the Contents

The table lists all sections which should be read before working over a certain section. For example, understanding section 2.4 requires that the reader is familiar with parts of the content of section 2.2, whereas section 1.3 is not absolutely necessary.

		1				2							3						4					5				6	
		1	2	3	4	1	2	3	4	5	6	7	1	2	3	4	5	6	1	2	3	4	5	1	2	3	4	1	2
1	1	-																											
	2		-																										
	3		x	-																									
	4		x		-																								
2	1		x			-																							
	2						-																						
	3		x		x		x	-																					
	4		x		x		x	x	-																				
	5		x		x	x	x	x	x	-																			
	6		x		x	x	x	x	x	x	-																		
	7		x		x	x	x	x		x		-																	
3	1		x		x								-																
	2		x		x								x	-															
	3		x		x	x							x	x	-														
	4		x		x	x							x	x	x	-													
	5		x		x	x							x	x	x		-												
	6		x		x	x							x	x	x	x	x	-											
4	1																		-										
	2																		x	-									
	3																		x	x	-								
	4																		x	x	x	-							
	5		x		x														x	x	x	x	-						
5	1																		x	x	x	x		-					
	2		x		x								x	x					x	x	x	x		x	-				
	3		x		x								x	x					x	x	x	x	x	x	x	-			
	4		x		x								x	x					x	x	x	x	x	x	x	x	-		
6	1		x		x																							-	
	2		x		x				x																				-

Chapter 1

Introduction

In external beam radiotherapy to treat cancer, a tumor inside the patient body is irradiated from multiple directions. For most clinical treatments, high energy X-ray radiation is applied to irradiate the tumor. The radiation causes DNA damage in the cell nuclei, leading to the death of tumor cells and patient cure in the ideal situation. In order to achieve local tumor control with a high probability, a tumor type dependent therapeutic dose has to be applied to the tumor. In many situations the tumor is located close to so-called organs at risk (OAR) which are sensitive to radiation and limit the escalation of the dose. The objective in radiotherapy treatment planning is to deliver a prescribed dose to the tumor while minimizing the dose burden of adjacent healthy tissues. Nowadays, intensity modulated radiation therapy (IMRT) is considered the most advanced technique to achieve this goal. However, the precision of IMRT is to some extent compromised by organ motion. For example, the prostate may move due to changes in the filling of the rectum or a lung tumor may move due to the expansion of the lung during respiration. During treatment, the tumor may not be in the same position as in the pre-treatment CT image (computed tomography image), which is usually the basis for treatment planning. Therefore, different strategies to deal with organ movements in radiotherapy have been developed. This thesis focuses on a particular approach which we refer to as *probabilistic treatment plan optimization*.

1.1 Organ motion in radiotherapy

1.1.1 Classification of organ movements

Organ movements in radiotherapy can be classified with respect to different criteria. Usually, a distinction is made between *inter-fraction* and *intra-fraction* motion. Intra-fraction motion refers to organ movements that occur during the irradiation in a single fraction of the treatment. The standard example for intra-fraction motion are lung tumors or liver tumors that move due to respiration. Inter-fraction motion refers to the idealized case that the anatomy of the patient is stationary during one fraction but changes between fractions.

A standard example for inter-fraction motion is the prostate which changes its position due to variations in rectum and bladder filling.
For inter-fraction motion, one further distinguishes between random errors and systematic errors. A random error is a random displacement of the tumor from its mean position which is different in different fractions. A systematic error is a shift of the actual mean position of the tumor from its estimated mean position for treatment planning. This shift impacts all fractions in the same way and is therefore referred to as a systematic error.

1.1.2 Dealing with organ motion

The standard method to deal with organ motion in radiotherapy is the safety margin approach. The volume that should be irradiated with the prescribed tumor dose is referred to as the *clinical target volume* (CTV) and is contoured on the planning CT scan of the patient. To account for organ motion using the safety margin approach, the CTV is expanded to form a *planning target volume* (PTV) which is irradiated with the prescribed dose. The size of the CTV-to-PTV margin is chosen in such a way that the PTV is expected to cover the moving tumor at almost all times during treatment. Among others van Herk *et al* [10] quantified the required margin as a function of the magnitude of random errors and systematic errors. Roughly spoken, the safety margin approach ensures that the prescribed dose is delivered to the moving tumor by irradiating the entire area where the tumor may be with the prescribed dose. Obviously, this method leads to an increased dose burden of the healthy tissues adjacent to the tumor.

In recent years, *image-guided radiation therapy* (IGRT) or *adaptive radiation therapy* (ART) have evolved into a central issue in radiotherapy research. Traditionally, radiotherapy treatment planning is based on a single CT scan which is aquired prior to treatment. Nowadays, imaging modalities located within the treatment room allow for several CT scans of a patient prior to each fraction [11, 12, 13]. In addition, 4D CT imaging was developed to account for respiratory motion during image acquisition. As a result, a series of CT images (in the order of 10 images) is obtained to represent the patient's geometry in different phases of the breathing cycle. Repeated imaging of the patient provides the basis for an improved way of dealing with organ motion in radiotherapy.

Regarding strategies to deal with organ motion in adaptive radiotherapy, one distinguishes *online* and *offline* approaches. The aim of online correction methods is to directly react to geometric changes of the patient anatomy and adapt treatment plan parameters accordingly. An example would be that a CT scan of the patient performed directly before a treatment fraction can show a displacement of the patient's bony anatomy relative to the planning situation. The information is subsequently used to correct for the misalignment by shifting the treatment couch accordingly. In contrast, offline strategies incorporate aggregated information about the patient's organ mobility into the treatment plan optimization. An example would be that during the first week of a fractionated treatment, a CT scan of the patient is performed each day. After the first week, a new treatment plan

is created that incorporates the information of all images acquired so far. Yan *et al* [14] suggested to define a PTV based on the hull of the individual CTVs contoured in each CT image. In this approach, the multiple CT images are used to reduce the volume of the PTV by reducing the systematic error.

In the context of respiratory motion, tumor movements occur within seconds and the amplitude of motion can be considerably large. Especially tumors in the caudal region of the lung are reported to move up to 2 cm, primarily in cranial-caudal direction [15]. The average breathing period is typically in the order of 3 to 4 seconds. A bunch of approaches to deal with respiratory motion are proposed in the literature. One of the most promising approaches is referred to as *gating*. The idea of gating is as follows: the treatment beam is switched on only when the patient is in a certain phase of the breathing cycle and is blocked for the rest of the time. Usually, the exhale position is chosen as the so-called *gating window* where the beam is on. In most cases, an external signal is used to determine the breathing phase as a function of time. For example, the position of a marker on the skin of a patient's belly is tracked using infrared-cameras. It is then assumed that the internal position of the tumor correlates with the external signal. The ultimate online correction method for respiratory motion is referred to as *tracking*. The aim is to adapt the treatment machine parameters in real time to the tumor motion, i.e. to track the moving tumor with the radiation beam in real time. This approach is technically the most demanding approach and has only been investigated theoretically or applied to phantoms. A clinical implementation is not feasible so far. In addition, some other methods have been suggested, e.g. *active breathing control* (ABC) [16] or the *deep inspiration breath hold technique* [17]. A problem that is common to most correction methods is the variability of the breathing pattern. Patients usually do not breath regularly. The trajectory of the tumor is not reproduced in subsequent breathing cycles. For an overview of clinical studies on organ motion and its management see e.g. the review article by Langen *et al* [18].

In this thesis, an offline strategy to account for organ motion during treatment planning is investigated. The method can be applied to both interfractional and respiratory motion and can deal with both random and systematic errors. We call this approach *probabilistic treatment planning* but no general naming convention has been established yet. Another term associated with this approach is *4D optimization*. The motivation and the underlying idea of the concept is introduced in section 1.2.

1.2 Philosophy of probabilistic treatment planning

In this section, the general idea of probabilistic treatment planning is introduced and several aspects are discussed that motivate the development of a new optimization concept of IMRT in the presence of organ motion.
Roughly spoken, the idea of the safety margin approach is to deliver the prescribed tumor dose to the entire area where the tumor may be located during treatment. This implies

that the treatment planner primarily looks at the dose that is delivered to a certain point in space independent of the tissue that is located at that point. Due to organ motion, different volume elements of tissue can be located at a certain point in space. As a consequence, the dose that is actually delivered to a certain volume element of tissue is not investigated. However, this is the dose distribution which is of interest first of all. It is one idea of probabilistic treatment planning to optimize the dose distribution in a coordinate system that is attached to the moving and deforming tissue instead of optimizing the dose distribution in a coordinate system that is fixed in space.
Interfractional motion is essentially a random process. Assuming that the rectum and bladder filling of a patient with prostate carcinoma at the time of treatment is random, the prostate is at a random position in each fraction. As a consequence, the dose delivered to a volume element of tissue is a stochastic property. It can not be predicted with absolute certainty. It is one aspect of probabilistic treatment planning that one has to deal with the dose uncertainties and the fact that the dose that will finally be delivered can not be predicted precisely. It has to be assessed by appropriate surrogates. This aspect motivates the terminology *probabilistic* treatment planning. In principle, this applies also to conventional treatment planning using the safety margin approach but the issue is usually not addressed.
The safety margin approach leads to a significant dose burden of the healthy tissue because even regions, where tumor tissue is located only rarely, are irradiated with the prescribed tumor dose. It was suggested that a better sparing of the healthy tissue can be achieved by delivering less dose to those regions. In order to ensure that each part of the tumor receives its prescribed dose, this has to be compensated for by delivering higher doses to regions where tumor tissue is located most of the time. In other words, the dose distribution that would be delivered to a stationary geometry is inhomogeneous. However, the inhomogeneities are shaped in such a way that initial dose inhomogeneities are leveled out during the course of treatment due to organ motion and a widely homogeneous cumulative dose distribution is delivered to the moving tumor. Section 1.3 provides a mathematical motivation for this point of view.

How can probabilistic treatment planning be implemented practically? Generally, knowledge about organ motion can be obtained from two sources: first, from clinical studies on organ motion with a larger number of patients involved and second, from patient specific imaging. Traditionally, treatment planning is based on a single CT scan of a patient and organ motion is incorporated into the treatment planning process by the safety margin concept. Since only a single CT scan is performed, no patient specific knowledge on his organ mobility is available and the quantification of the required safety margin is purely based on population based studies. Nowadays, imaging modalities within the treatment room allow for several CT scans of a patient prior or during the course of fractionated treatment. These multiple CT scans provide individualized knowledge on organ mobility for the specific patient. For respiratory motion 4D CT images provide patient specific information on organ motion. For probabilistic treatment planning, the available information is used to derive a mathematical model that describes the organ movements of

the patient. Practically, the model of organ motion represents a probability distribution, which describes the probability that the patient's anatomy is in a certain geometric state. The probability distribution of patient geometries is the basis for the optimization of the treatment plan, i.e. the probability distribution is incorporated into the formulation of the optimization problem for IMRT planning. Section 1.4 introduces the general framework for the formulation of the optimization problem, which will become explicit in chapters 2 to 5. The idea of optimizing a treatment plan based on a probability distribution has been described before [19, 20, 21, 22, 23]. This thesis significantly extends the work published previously by assessing the uncertainties and risks of a treatment in the presence of organ motion. The probability distribution of patient geometries has to be estimated from a small number of images. In addition it is only sparsely sampled since the patient is irradiated in a finite number of fractions, typically about 30. Dealing with the resulting uncertainty of the delivered dose in the context of IMRT optimization has not been subject to detailed investigation before.

1.3 A mathematical paradigm

This section provides a mathematical motivation for probabilistic treatment planning. For idealized assumptions, we demonstrate that a better sparing of healthy tissue can be achieved compared to the safety margin approach without compromising the dose to the tumor. Let us consider a static coordinate system in space and a grid of volume elements (voxels) in that coordinate system. A tumor moves within that static coordinate system as a rigid object according to the three translational degrees of freedom. The tumor is as well divided into a grid of volume elements of the same resolution. We assume that the tumor can move in discrete steps of one voxel. Let D_j^{stat} denote the dose delivered to the voxel j in the static coordinate system. For now, it is assumed that the dose distribution D_j^{stat} can be realized by some external irradiation fields. We assume that D_j^{stat} remains unaffected by the tumor motion. Let D_i denote the dose that is delivered to the moving voxel i in the tumor. The relation between the dose distributions in both voxel grids is determined by

$$D_i = \sum_j P_{ij} D_j^{stat} \tag{1.1}$$

where P_{ij} is the relative frequency of finding the moving tumor voxel i at the static voxel j during the course of fractionated treatment. Assuming that there are n moving tumor voxels and m static voxels, equation 1.1 can be rewritten as a matrix equation

$$\boldsymbol{D} = \boldsymbol{P}\boldsymbol{D}^{stat} \tag{1.2}$$

where $\boldsymbol{D} \in \mathbb{R}^n$ and $\boldsymbol{D}^{stat} \in \mathbb{R}^m$ are vectors and $\boldsymbol{P}$ is a $n \times m$-matrix. Given a static dose distribution $\boldsymbol{D}^{stat}$ and the frequency matrix $\boldsymbol{P}$, the dose distribution in the tumor $\boldsymbol{D}$ can easily be calculated.

In the context of probabilistic treatment planning, the inverse problem of equation 1.2 is of prior interest. The question is: given a desired dose distribution $\boldsymbol{D}$ in the tumor and the frequency matrix $\boldsymbol{P}$, how does $\boldsymbol{D}^{stat}$ have to look like? Since the tumor is moving, $m > n$ holds. Consequently, $\boldsymbol{P}$ is not a diagonal matrix and therefore not invertible. The mapping $\boldsymbol{P}$ is not injective, i.e. generally there are multiple vectors $\boldsymbol{D}^{stat}$ that generate the same vector $\boldsymbol{D}$. This is not a problem but exactly the desired feature for probabilistic treatment planning. Roughly spoken, there are different static dose fields that deliver the prescribed dose to the tumor and the treatment planner can choose one of them according to a second criterion. E.g. he may choose the one that is most appropriate in terms of sparing the adjacent healthy tissue.

Let us make this point more explicit: Let $\boldsymbol{D}$ be the prescribed dose distribution in the moving tissue. All static dose fields $\boldsymbol{D}^{stat}$ that generate $\boldsymbol{D}$ form the solution set of the linear set of equations defined in (1.2). In order to characterize the solution set of (1.2) we assume that the rank of the matrix $\boldsymbol{P}$ is equal to n, i.e. all rows of the matrix are linearly independent. The solution set of (1.2) is an affine subspace of $\mathbb{R}^m$ denoted as

$$S(\boldsymbol{P}, \boldsymbol{D}) = \boldsymbol{D}_0^{stat} + K(\boldsymbol{P}) \tag{1.3}$$

where $\boldsymbol{D}_0^{stat}$ is an arbitrary solution of (1.2) and $K(\boldsymbol{P})$ is the kernel of the mapping $\boldsymbol{P}$, i.e. the set of all $\boldsymbol{D}^{stat}$ that satisfy

$$\boldsymbol{P}\boldsymbol{D}^{stat} = 0 \tag{1.4}$$

Let us assume that we want to deliver a homogeneous dose to the tumor, i.e. $D_i = 1$ $(i = 1, \cdots, n)$. Then we know one explicit solution of (1.2), namely $D_{0j}^{stat} = 1$ $(j = 1, \cdots, m)$. This corresponds to the safety margin solution which delivers the prescribed tumor dose to all static voxels where a moving tumor voxel may be located. Mathematically, this solution holds due to the normalization condition $\sum_{j=1}^{m} P_{ij} = 1$ $(i = 1, \cdots, n)$ which has to be satisfied by each row of the matrix $\boldsymbol{P}$. Assuming that $\text{rank}(\boldsymbol{P}) = n$, the dimension of the kernel is $\dim(K(\boldsymbol{P})) = m - n$. Hence, the kernel $K(\boldsymbol{P})$ is a $(m-n)$-dimensional subspace of $\mathbb{R}^m$ that can be represented by a set of $m-n$ linearly independent basis vectors $\boldsymbol{B}_k$. Every solution of (1.2) can then be written in the form

$$\boldsymbol{D}^{stat} = \boldsymbol{D}_0^{stat} + \sum_{k=1}^{m-n} \lambda_k \boldsymbol{B}_k \tag{1.5}$$

The basis vectors $\boldsymbol{B}_k$ correspond to inhomogeneous modes that modulate the homogeneous safety margin solution while preserving the dose distribution $D_i = 1$ everywhere in the tumor.

Figure 1.1 illustrates the mathematical formalism above. We consider a two-dimensional voxel grid and a quadratic tumor consisting of 25 voxels. The tumor may be in 5 different positions: a central position and 4 additional positions in which the tumor is shifted by one voxel towards the 4 directions up, right, down and left. The frequency of being there

shall be equal for all 5 positions. The red lines in figure 1.1 mark the tumor in its central position and the blue line marks the set of all static voxels. Figure 1.1a shows the safety margin solution where the prescribed dose is delivered to each static voxel. Figure 1.1b shows an example for an inhomogeneous mode $\boldsymbol{B}_k$. Figure 1.1c shows an inhomogeneous solution that preserves the homogeneous dose distribution in the moving tumor. It results from the safety margin solution plus 0.1 times the mode in figure 1.1b.

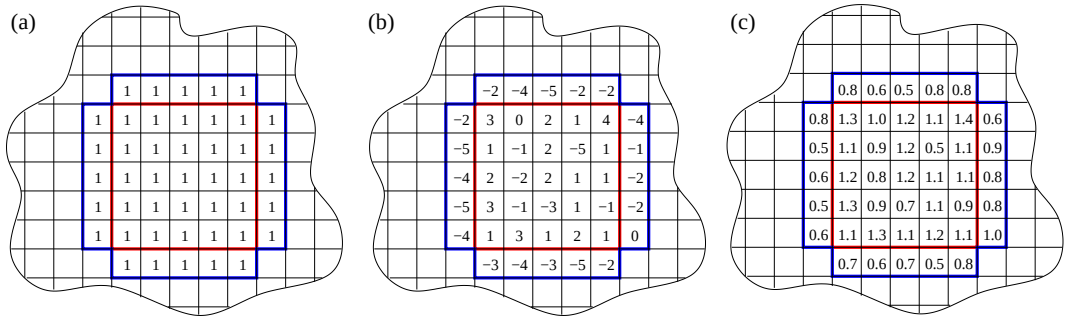

Figure 1.1: Illustration of the mathematical formalism in section 1.3 (a) safety margin solution (b) example for an inhomogeneous mode $\boldsymbol{B}_k$ (c) inhomogeneous solution that preserves the homogeneous dose distribution in the moving tumor

We have a look at the integral dose $\sum_{j=1}^{m} D_j^{stat}$. For the safety margin solution the integral dose is obviously 45.0. For the inhomogeneous solution in figure 1.1c, the integral dose is 40.8. Since the tumor receives its prescribed dose in both cases, the sparing of healthy tissue must have improved for the inhomogeneous solution. By delivering less dose to static voxels where only rarely a tumor voxel is located, the sparing of healthy tissue is improved. The dose coverage of the tumor is achieved by delivering higher doses to other static voxels where mostly or always a tumor voxel is located.

From a practical point of view, it is not realistic to apply the above concept to a clinical IMRT treatment planning scenario. The static dose distribution cannot be chosen arbitrarily but it has to be realized by external beams. Therefore, it is more practical to directly optimize the dose distribution in the moving tissue as a function of the intensity map of the external beams. This will be done throughout this thesis.

On a conceptual level, figure 1.1 also illustrates the intrinsic problems of the approach. In order to be sure that the prescribed dose is delivered to each tumor voxel, the displacement frequencies P_{ij} must be known in the case of an inhomogeneous static dose field. Realistically, this is not the case. In a first attampt, P_{ij} could be interpreted as a probability of finding the tumor voxel i at the static voxel j. In this case, D_i would correspond to the expectation value of the dose in voxel i. However, the expectation value would usually not be realized. The relative frequency of finding the tumor voxel i at the static voxel j would converge to P_{ij} only in the limit of an infinite number of fractions. For a realistic number

of fractions the frequency would differ from the probability. Hence, even if the probabilities P_{ij} were known, one would have to take into account that they are not realized during the actual treatment. The safety margin solution is more robust in terms of tumor coverage. For the safety margin solution, it is garantied that the prescribed dose is delivered to each tumor voxel independent of the values for P_{ij} (as long as the set of m static voxels covers the tumor at all times). Parts of this thesis are related to the question of how to make the trade-off between the two contradictory objectives: first, delivering a prescribed dose to a moving tumor, and second, optimizing the sparing of adjacent healthy tissue.

1.4 A probabilistic optimization postulate

First, let us consider IMRT optimization in general without considering organ motion. Inverse IMRT treatment planning is usually formulated as an optimization problem. The intensity profiles of the radiation beams are determined so that the resulting dose distribution becomes optimal in the sense that it corresponds to the minimum of an objective function. In the widely used beamlet-based IMRT optimization (also referred to as fluence map optimization), each beam is devided into a grid of beamlets (also referred to as bixels). It is the aim of the beamlet based optimization to determine the fluence values Φ_j of all beamlets j so that the dose distribution in the patient becomes optimal. Due to the linear relation between fluence and dose, the dose D_i in voxel i in the patient can be written as

$$D_i = \sum_j d_{ij}\Phi_j \tag{1.6}$$

where d_{ij} is the dose contribution of beamlet j to voxel i for unit fluence. The objective function E is usually formulated as a function of the dose distribution in the first place and can then be rewritten as a function of the beamlet intensities Φ using equation 1.6. The aim of IMRT optimization is to find the optimal set of fluence values $\boldsymbol{\Phi}^{opt}$ that minimizes the objective function $E(\boldsymbol{D}(\boldsymbol{\Phi}))$. The optimization problem is thus: determine

$$\boldsymbol{\Phi}^{opt} = \operatorname{argmin}\left(E(\boldsymbol{D}(\boldsymbol{\Phi}))\right) \tag{1.7}$$

subject to a set of constraints. One constraint that usually applies is $\Phi_j \geq 0$, saying that only positive intensities make sense physically. There may be additional constraints depending on the formulation of the optimization problem.

Let us now make the transition to probabilistic treatment planning and the incorporation of organ movements into the optimization. This section is very general and different aspects will become explicit in later chapters. At the time of treatment planning, it is unknown how the patient will move during the course of treatment. Only estimates about the shape and magnitude of the motion can be made. Therefore, the dose distribution in the patient becomes a stochastic property in the presence of organ movements. The dose delivered to the patient depends on a set of random variables $\boldsymbol{G}$ that characterize the geometric states

of the patient during treatment. We assume that a probability distribution $P(\boldsymbol{G})$ exists that describes the probability of finding the patient in the geometric state characterized by the vector $\boldsymbol{G}$. This distribution has to be derived from clinical studies on organ motion, measurements for the individual patient to be treated and heuristic assumptions. Due to the stochastic properties of organ motion, the delivered dose distribution $\boldsymbol{D}(\boldsymbol{\Phi}, \boldsymbol{G})$ and the objective function value $E(\boldsymbol{D}(\boldsymbol{\Phi}, \boldsymbol{G}))$ become random variables as well. Generally, there are multiple options to formulate the optimization problem in the presence of motion. This work follows one particular approach. We postulate, that the treatment of most patients will be good if we optimize the expectation value of the objective function. We thus suggest to solve the optimization problem

$$\boldsymbol{\Phi}^{opt} = \operatorname{argmin} \left(\langle E(\boldsymbol{D}(\boldsymbol{\Phi}, \boldsymbol{G})) \rangle \right) \tag{1.8}$$

where

$$\langle E(\boldsymbol{D}(\boldsymbol{\Phi}, \boldsymbol{G})) \rangle = \int E(\boldsymbol{D}(\boldsymbol{\Phi}, \boldsymbol{G})) P(\boldsymbol{G}) d\boldsymbol{G} \tag{1.9}$$

Generally, the objective function is a weighted sum of objectives for the different tissues and organs in the patient. A widely used objective function for the tumor is the quadratic objective function. If D^{pres} is the dose prescribed to the tumor, the quadratic objective function reads

$$E(\boldsymbol{D}) = \sum_i (D_i - D^{pres})^2 \tag{1.10}$$

where the sum runs over all voxels in the tumor. In the case of organ motion, the expectation value of the objective is

$$\begin{aligned} \langle E(\boldsymbol{D}) \rangle &= \int \sum_i (D_i(\boldsymbol{G}) - D^{pres})^2 \, P(\boldsymbol{G}) d\boldsymbol{G} \\ &= \sum_i \left[\int (D_i(\boldsymbol{G}) - D^{pres})^2 \, P(\boldsymbol{G}) d\boldsymbol{G} \right] \qquad (1.11) \\ &= \sum_i \left[(\langle D_i \rangle - D^{pres})^2 + \int (D_i(\boldsymbol{G}) - \langle D_i \rangle)^2 \, P(\boldsymbol{G}) d\boldsymbol{G} \right] \qquad (1.12) \end{aligned}$$

where

$$\langle D_i \rangle = \int D_i(\boldsymbol{G}) P(\boldsymbol{G}) d\boldsymbol{G} \tag{1.13}$$

is the expectation value of the dose in voxel i. Equation 1.11 shows that the expectation value of the quadratic objective function can be evaluated by considering every voxel seperately although the movement of neighboring voxels is obviously highly correlated. This simplifies the evaluation of the objective function compared to a more general case. If, for example, a non-linear equivalent uniform dose (EUD) function is used, all voxels in the tumor would be coupled. Equation 1.12 allows for an interpretation of the expectation value of the quadratic objective function, which turns out to be the sum of the variance of the dose and the quadratic difference of expected and prescribed dose. In order to deliver

approximately the prescribed dose to the tumor, the expectation value of the dose has to be close to the prescribed dose. And in addition, the variance of the dose has to be small so that the expectation value is approximately realized in most cases. This work deals with the evaluation of the quadratic objective function. For different types of movements, motion models are evaluated in order to derive explicit expressions for the set of random variables $\boldsymbol{G}$ and its respective probability distribution $P(\boldsymbol{G})$ that describe the motion-induced geometric changes of the patient. Chapters 2 and 3 deal with inter-fractional motion and chapters 4 and 5 deal with respiratory motion.

Chapter 2

Probabilistic treatment plan optimization for interfractional motion

This chapter deals with the application of probabilistic treatment plan optimization in the presence of interfractional motion. We develop the mathematical model of organ motion, formulate the optimization problem for inverse IMRT treatment planning and derive the mathematical formalism to evaluate the objective function. The method is then applied to a patient model of idealized geometry in order to analyze the generic features of the approach. An application to clinical data of a prostate patient is provided in chapter 3.

The assumptions which build the basis for this chapter have been described in section 1.2: It is assumed that multiple CT scans of a patient exist. In addition, population based knowledge from clinical studies on organ motion may exist. Based on that data, a model that describes the interfractional motion is derived, which is the basis of a probabilistic treatment planning approach. This will be done in section 2.1. It is assumed that the interfractional displacements of the tumor can be described by a Gaussian distribution. The concept of Bayesian inference is applied to derive probability distributions for the parameters mean and width of the Gaussian motion model. The method allows for a unified description of random and systematic errors. In section 2.2 a patient model of idealized geometry is introduced which originates from rotation therapy. An idealized geometry is considered where the movement is restricted to rigid translations. In this case, one CT scan corresponds to one measurement of the tumor position. Section 2.3 defines the optimization problem according to the general postulate introduced in section 1.4. The expectation value of a quadratic objective function which is customized to the geometry under consideration is optimized. Sections 2.4, 2.5 and 2.6 demonstrate the results of probabilistic optimization for the idealized patient. The generic features of the approach are analyzed.

Naturally, a number of assumptions and approximations have to be made in order to formulate a mathematical model of the real world. In this case, we assume that the

patient changes his geometry between fractions, i.e. we focus on the idealized case of pure inter-fraction organ motion and neglect intra-fraction motion. The positions of the patient in different fractions are assumed to be uncorrelated, i.e. the geometry of the latest fraction does not have an impact on the geometry in the next fraction. Furthermore, the motion model that describes the interfractional changes is assumed to be time-invariant, i.e the same motion model holds for the whole course of fractionated treatment. This means we do not consider time trends during treatment, e.g. weight loss or radiation effects on the tumor and healthy tissues.

2.1 The motion model

2.1.1 Preliminaries

We consider interfractional rigid motion of the patient. We assume that the translations of the patient in different spatial dimensions are statistically independent. To simplify the notation, this section is formulated for the one-dimensional case, but the generalization to two or three spatial dimensions is straightforward.
The patient is not always located in the same position but can be located in different positions from day to day. We assume that M CT scans of a patient exist and that these images can be used to determine the positions $\{\Delta p_\mu\}_1^M$ that describe the M positions of the tumor relative to a fixed reference point. The set of M positions $\{\Delta p_\mu\}_1^M$ is referred to as the measured data.
We now assume that the data can be modelled by a deterministic law plus noise. In this case we just assume that the measured positions scatter randomly around an average position Δs, i.e. we assume the following parameterized model of the data:

$$\Delta p_\mu = \Delta s + \delta_\mu \tag{2.1}$$

where δ represents a random number, i.e. the noise. We further assume Gaussian noise, i.e. the probability distribution for δ is given by

$$P(\delta) = \frac{1}{\sqrt{2\pi}\sigma} \exp\left(-\frac{\delta^2}{2\sigma^2}\right) \tag{2.2}$$

The data model is parameterized by the parameters Δs and σ, where the parameter of the noise model σ describes the magnitude of the random motion. From the equations 2.1 and 2.2 we find that the probability to measure a position Δg of the volume element given both model parameters Δs and σ is determined by

$$P(\Delta g|\Delta s, \sigma) = \frac{1}{\sqrt{2\pi}\sigma} \exp\left(-\frac{(\Delta g - \Delta s)^2}{2\sigma^2}\right) \tag{2.3}$$

2.1.2 Maximum likelihood estimate of the most probable data model

We are interested in calculating the expectation value of the dose. In a first approach, this can be done by determination of the most likely model of the data, i.e. we determine the parameters $(\Delta s^\star, \sigma^\star)$ which describe the measured data the best. A well known method to do this is to maximize the data likelihood [24]. The likelihood is defined as the probability to obtain the data set $\{\Delta p_\mu\}_1^M$ given the model parameterized by $(\Delta s, \sigma)$:

$$P(\{\Delta p_\mu\}|\Delta s, \sigma) = \prod_{\mu=1}^{M} \frac{1}{\sqrt{2\pi}\sigma} \exp\left(-\frac{(\Delta p_\mu - \Delta s)^2}{2\sigma^2}\right) \tag{2.4}$$

Maximizing the likelihood is equivalent to minimizing the negative of the logarithm of the likelihood, i.e. in order to determine the optimal (or most probable) data model $(\Delta s^\star, \sigma^\star)$ we have to solve the optimization problem

$$\begin{aligned} L &= -\ln\left[\prod_{\mu=1}^{M} \frac{1}{\sqrt{2\pi}\sigma} \exp\left(-\frac{(\Delta p_\mu - \Delta s)^2}{2\sigma^2}\right)\right] \\ &= M \ln\left(\sqrt{2\pi}\sigma\right) + \sum_{\mu=1}^{M} \frac{(\Delta p_\mu - \Delta s)^2}{2\sigma^2} \qquad \rightarrow \min \end{aligned} \tag{2.5}$$

Solving

$$\frac{\partial L}{\partial \Delta s} \stackrel{!}{=} 0 \qquad and \qquad \frac{\partial L}{\partial \sigma} \stackrel{!}{=} 0 \tag{2.6}$$

yields the intuitive result

$$\Delta s^\star = \frac{1}{M} \sum_{\mu=1}^{M} \Delta p_\mu \tag{2.7}$$

$$\sigma^\star = \sqrt{\frac{1}{M} \sum_{\mu=1}^{M} (\Delta p_\mu - \frac{1}{M} \sum_{\eta=1}^{M} \Delta p_\eta)^2} \tag{2.8}$$

The optimal model $(\Delta s^\star, \sigma^\star)$ can now be used to predict the possible locations Δg of the volume element: $\Delta g = \Delta s^\star + \delta$ where the probability for obtaining a position Δg given the optimal model is given by

$$P(\Delta g|\Delta s^\star, \sigma^\star) = \frac{1}{\sqrt{2\pi}\sigma^\star} \exp\left(-\frac{(\Delta g - \Delta s^\star)^2}{2\sigma^{\star 2}}\right) \tag{2.9}$$

The expectation value of the dose per fraction at a given point in the moving tumor can be calculated according to

$$\langle D \rangle = \int D(\Delta g) P(\Delta g|\Delta s^\star, \sigma^\star) d\Delta g \tag{2.10}$$

$D(\Delta g)$ is the dose delivered to the point in the tumor in a single fraction given a displacement Δg of this tumor point. Using equation 2.10 corresponds to the widely used convolution method to calculate the expectation value of the dose. However, equation 2.10 considers only the most likely model of the data to predict the dose. This is a reasonable approximation if the probability distribution $P(\Delta s, \sigma|\{\Delta p_\mu\})$, that describes the probability of a model $(\Delta s, \sigma)$ given the data, is sharply peaked around the optimal model. This would be true if the number of measured positions M was large. However, the number of CT scans of a patient will typically be small. Apart from the potentially unreliable estimate of the expectation value of the dose there is another weakness of this approach. When considering the optimal model alone, all information about the expected variance of the dose due to an imperfect knowledge of the parameters Δs and σ is lost. One can only calculate the variance of the dose that arises from the sparse sampling of the probability distribution 2.9 due to a finite number of fractions. This will be discussed extensively in the result sections 2.4, 2.5 and 2.6.
The maximum likelihood approach is a very general and widely used method for model parameter estimation. However, the maximum likelihood method does not always yield an unbiased estimate of the model parameters [24]. For the problem considered, this applies to the estimate of the optimal distribution width $\sigma^\star$. Equation 2.8 underestimates the distribution width since it does not account for the shift between the estimated mean position and the real mean position. For the current problem, the model parameters are rather simple since they just represent the first and second power moment of the distribution of displacements. In this case the method of moments yields

$$\sigma^\dagger = \sqrt{\frac{1}{M-1}\sum_{\mu=1}^{M}(\Delta p_\mu - \frac{1}{M}\sum_{\eta=1}^{M}\Delta p_\eta)^2} \tag{2.11}$$

as an estimate of the distribution width which is proven to be unbiased. $\sigma^\dagger$ is also referred to as the empirical standard deviation. From equations 2.8 and 2.11 we obtain $\sigma^\dagger = \sqrt{\frac{M}{M-1}}\sigma^\star$.

2.1.3 The concept of Bayesian inference

We will now extend the dose calculation method from the previous section 2.1.2. This will be done by applying the concept of Bayesian inference [25]. The basic idea is as follows: Not only the most probable model of the data shall be used to calculate the dose but all models $(\Delta s, \sigma)$ weighted with their respective probabilities. This will further enable us to calculate the uncertainty of the expected dose, often characterized by its variance. In other words, we are now interested in the probability distribution $P(\Delta g|\{\Delta p_\mu\})$ that describes the probability of a position Δg given the data $\{\Delta p_\mu\}_1^M$. $P(\Delta g|\{\Delta p_\mu\})$ is given by

$$P(\Delta g|\{\Delta p_\mu\}) = \int\int P(\Delta g|\Delta s, \sigma)P(\Delta s, \sigma|\{\Delta p_\mu\})d\Delta s d\sigma \tag{2.12}$$

To evaluate equation 2.12 one has to calculate the *posterior probability* $P(\Delta s, \sigma|\{\Delta p_\mu\})$, that describes the probability for a model $(\Delta s, \sigma)$ given the data $\{\Delta p_\mu\}_1^M$. This is done by using the Bayes theorem:

$$P(\Delta s, \sigma|\{\Delta p_\mu\}) = \frac{P(\{\Delta p_\mu\}|\Delta s, \sigma)P(\Delta s, \sigma)}{P(\{\Delta p_\mu\})} \tag{2.13}$$

The term $P(\{\Delta p_\mu\})$ is referred to as *Evidence* and can be considered as a normalization factor since it is independent of Δs and σ. The term $P(\Delta s, \sigma)$ is called *Prior* and describes the probability of a model $(\Delta s, \sigma)$ without knowing the data. The Prior therefore represents previous knowlegde about the model parameters which can for example be obtained from a clinical study involving a population of patients.

No previous knowledge:

We first consider the case that no previous knowledge exists, i.e. $P(\Delta s, \sigma)$ is constant. The posterior probability $P(\Delta s, \sigma|\{\Delta p_\mu\})$ is therefore determined by the data likelihood alone:

$$P(\Delta s, \sigma|\{\Delta p_\mu\}) \propto \frac{1}{\left(\sqrt{2\pi}\sigma\right)^M} \exp\left(-\frac{\sum_{\mu=1}^M (\Delta p_\mu - \Delta s)^2}{2\sigma^2}\right) \tag{2.14}$$

This can be rearranged to give

$$\begin{aligned} P(\Delta s, \sigma|\{\Delta p_\mu\}) \propto \quad & \frac{1}{\left(\sqrt{2\pi}\sigma\right)^M} \exp\left(-\frac{(\Delta s - \frac{1}{M}\sum_{\mu=1}^M \Delta p_\mu)^2}{2\frac{\sigma^2}{M}}\right) \\ & \times \exp\left(-\frac{\frac{1}{M}\sum_{\mu=1}^M (\Delta p_\mu - \frac{1}{M}\sum_{\eta=1}^M \Delta p_\eta)^2}{2\frac{\sigma^2}{M}}\right) \end{aligned} \tag{2.15}$$

The posterior probability can be written in the form

$$P(\Delta s, \sigma|\{\Delta p_\mu\}) = P(\Delta s|\sigma, \{\Delta p_\mu\})P(\sigma|\{\Delta p_\mu\}) \tag{2.16}$$

where equation 2.15 gives us the probability distributions

$$P(\Delta s|\sigma, \{\Delta p_\mu\}) = \frac{1}{\sqrt{2\pi\frac{\sigma^2}{M}}} \exp\left(-\frac{(\Delta s - \frac{1}{M}\sum_{\mu=1}^M \Delta p_\mu)^2}{2\frac{\sigma^2}{M}}\right) \tag{2.17}$$

$$P(\sigma|\{\Delta p_\mu\}) \propto \frac{1}{\left(\sqrt{2\pi}\sigma\right)^{M-1}} \exp\left(-\frac{\frac{1}{M}\sum_{\mu=1}^M (\Delta p_\mu - \frac{1}{M}\sum_{\eta=1}^M \Delta p_\eta)^2}{2\frac{\sigma^2}{M}}\right) \tag{2.18}$$

We introduce the parameter

$$\sigma_{data} = \sqrt{\frac{1}{M}\sum_{\mu=1}^M (\Delta p_\mu - \frac{1}{M}\sum_{\eta=1}^M \Delta p_\eta)^2} \tag{2.19}$$

that describes the distribution width that was estimated from the measured data. The probability distribution for Δs for a given value of σ is a Gaussian distribution of width $\sigma/\sqrt{M}$ centered at the average position $\frac{1}{M}\sum_{\mu=1}^{M}\Delta p_\mu$ that is obtained from the measured data. The probability distribution for σ is displayed in figure 2.1a for different values of M, the number of measurements. For large M the distribution is sharply peaked at σ_{data}, the value of σ that corresponds to the optimal model. For smaller M the distribution is broader and especially allows for much larger values of σ. Δs and its associated probability distribution describe systematic errors, i.e. a shift between the "true" mean position of the patient and the estimated mean position based on a finite number of measurements. A wrong estimate of the mean position influences all fractions in the same way and is therefore called a systematic error. The probability distribution $P(\sigma|\{\Delta p_\mu\})$ describes an uncertain knowledge of the magnitude of motion.

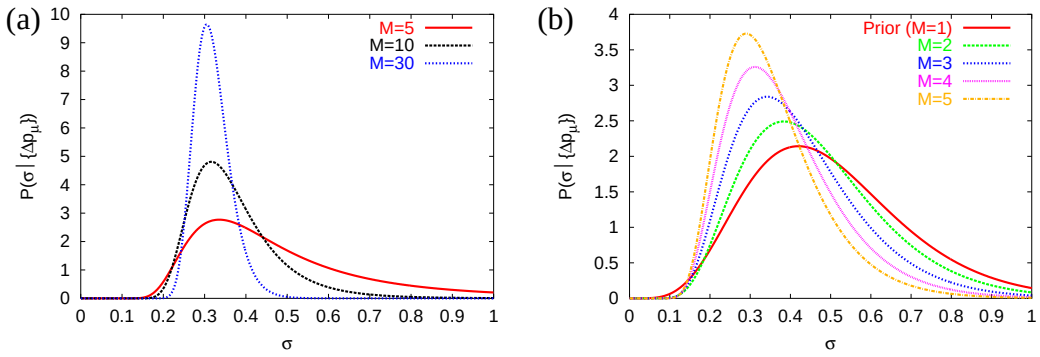

Figure 2.1: (a) Posterior probability distribution for σ without prior knowledge according to equation 2.18 for different values of M and $\sigma_{data} = 0.3$. (b) Posterior probability distribution for σ with a gamma prior according to equation 2.22 for different values of M and the parameters $\sigma_{data} = 0.2$, $\sigma_{pop} = 0.5$ and $\sigma_{var} = 0.2$. The solid line shows the prior.

Use of Priors:

The Bayes theorem also provides a method to incorporate knowledge about a population of patients into the calculation of the posterior probability $P(\Delta s, \sigma|\{\Delta p_\mu\})$ when patient specific data is sparse. In particular, this affects the parameter σ. We assume that no previous knowledge on Δs exists but focus on the prior probability $P(\sigma)$. By analyzing the organ movements for a very large number of patients one could in principle determine the entire distribution $P(\sigma)$ empirically (see e.g. [18] for a review of existing studies). We will assume that each patient is characterized by his individual value of σ and that within the population of patients the values of σ scatter around a mean value σ_{pop} with a width σ_{var}. For the prior distribution we adopt the gamma prior [26] that is often used when the range of a parameter is bounded on one side like the positive distribution width σ in this

case:

$$P(\sigma) = \begin{cases} \frac{\lambda^\alpha}{\Gamma(\alpha)} \sigma^{(\alpha-1)} \exp(-\lambda\sigma) & (\sigma > 0) \\ 0 & otherwise \end{cases} \tag{2.20}$$

where Γ is the Gamma function and $\alpha, \lambda > 0$ are parameters of the distribution. Both parameters are relatively simple functions of the expectation value σ_{pop} and the standard deviation σ_{var} of the distribution $P(\sigma)$:

$$\alpha = \frac{\sigma_{pop}^2}{\sigma_{var}^2} \qquad \lambda = \frac{\sigma_{pop}}{\sigma_{var}^2} \tag{2.21}$$

The posterior probability is then given by

$$P(\sigma|\{\Delta p_\mu\}) \propto \frac{\sigma^{(\alpha-1)}}{\left(\sqrt{2\pi}\sigma\right)^{M-1}} \exp(-\lambda\sigma) \exp\left(-\frac{\sigma_{data}^2}{2\frac{\sigma^2}{M}}\right) \tag{2.22}$$

Figure 2.1b shows the posterior probability $P(\sigma|\{\Delta p_\mu\})$ for different values of M and the parameters $\sigma_{data} = 0.2$, $\sigma_{pop} = 0.5$ and $\sigma_{var} = 0.2$. This corresponds to the situation that the patient specific measurements give rise to a value of σ that is small compared to the average patient. The method interpolates automatically between the patient specific data and the population based knowledge. When only a single measurement exists ($M = 1$), $P(\sigma|\{\Delta p_\mu\})$ is given by the prior $P(\sigma)$ alone. This corresponds to the situation where only a single planning CT is performed which is common practice today. In this case all information on potential organ movements is taken from population based knowledge. When little data is available (M small) the maximum of $P(\sigma|\{\Delta p_\mu\})$ is located between σ_{data} and σ_{pop}. When the amount of data increases (M large) the influence of the prior is reduced and the posterior probability distribution is determined by the data alone.

The expectation value of the dose per fraction is now calculated according to

$$\langle D \rangle = \int D(\Delta g) P(\Delta g|\{\Delta p_\mu\}) d\Delta g \tag{2.23}$$

where $P(\Delta g|\{\Delta p_\mu\})$ is given by equation 2.12 with the probability distributions given in equations 2.17, 2.18, 2.22 and 2.3. By substitution we get

$$\begin{aligned} \langle D \rangle \;=\; & \int\int\int D(\Delta g) P(\Delta g|\Delta s, \sigma) \\ & \times P(\Delta s|\sigma, \{\Delta p_\mu\}) P(\sigma|\{\Delta p_\mu\})\, d\Delta g\, d\Delta s\, d\sigma \end{aligned} \tag{2.24}$$

The more important change however is that one can now estimate the variance of the dose due to the model parameter uncertainty. This will be discussed in detail in sections 2.5 and 2.6

2.2 An idealized geometry

To gain some basic understanding of inverse planning based on probability distributions of patient geometries, we consider a model of idealized geometry that originates from rotation therapy with high energy photons. We consider the planar irradiation of a circularly shaped CTV of radius R_T with a rotating gantry. The CTV is surrounded by a healthy tissue of radius R (see Fig. 2.2).

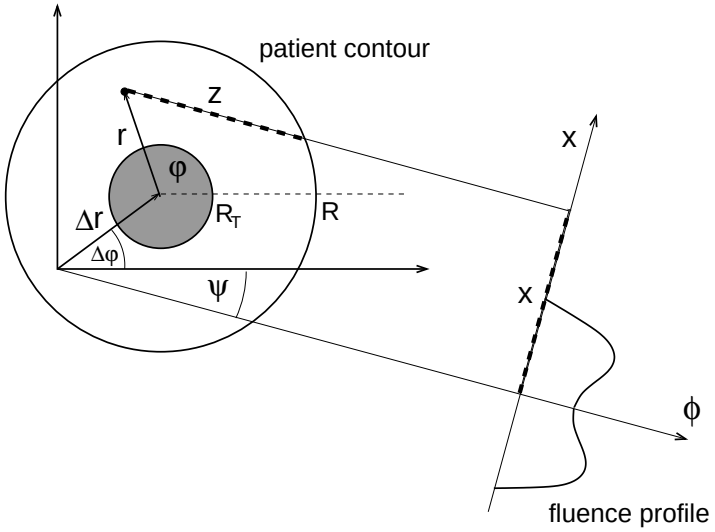

Figure 2.2: Geometry of the model

Organ movements are simulated by rigid translations of the entire body for simplicity. This allows us to track each point of the body during movement and to calculate the cumulative dose in each point. The geometry of the patient can then be parameterized by a single vector $\Delta\boldsymbol{r} = (\Delta r, \Delta\varphi)$ denoting the position of the center of mass. In the following text, vectors in two spacial dimensions are denoted by bold characters and scalars by italic characters. The interfractional displacements $(\Delta r, \Delta\varphi)$ of the patient are described by the motion model derived in section 2.1. To retain the rotational symmetry of the system we assume that the displacements in both spatial directions are uncorrelated and that the probability distribution for the displacements is of equal width in both directions. This means, the parameter σ of the Gaussian motion model is not a vector.

For the dose calculation we adopt the BRL approximation (Brahme, Roos, Lax) of the photon beam [27], i.e. the beam is assumed to be parallel, lateral scattering of the photons is neglected, and the photon fluence in the medium is assumed to attenuate exponentially according to $exp(-\mu z)$ with increasing depth z and constant attenuation coefficient μ. To calculate the dose at point $\boldsymbol{r} = (r, \varphi)$ for a given displacement $(\Delta r, \Delta\varphi)$ the following

equation applies:

$$D\left(r,\varphi|\Delta r\Delta\varphi\right)=\frac{1}{2\pi}\int_0^{2\pi}\Phi\left(x\right)\exp\left(-\mu z\right)d\psi \tag{2.25}$$

where x and z are given by

$$x\left(r,\varphi,\Delta r,\Delta\varphi,\psi\right)=r\sin\left(\varphi-\psi\right)+\Delta r\sin\left(\Delta\varphi-\psi\right) \tag{2.26}$$

$$z\left(r,\varphi,\psi\right)=\sqrt{R^2-r^2\sin^2\left(\varphi-\psi\right)}-r\cos\left(\varphi-\psi\right) \tag{2.27}$$

as illustrated in figure 2.2. The gantry angle is denoted by ψ and $\Phi(x)$ is the fluence profile. Due to the rotational symmetry of the system we restrict ourselves to fluence profiles which are symmetric ($\Phi(x)=\Phi(-x)$) and are independent of the gantry angle ψ. For the objective functions used later in this thesis it can be shown that the global minimum corresponds to a state of ψ-independent fluence profiles. This simplification is thus valid for our purpose. For the results presented in this chapter we adopt the following set of dimensionless parameters if not stated differently: $\mu=0.1$, $R_T=1$, $R=3$.

2.2.1 The static solution of the inverse problem

For the static situation without motion, i.e. $\Delta r\equiv 0$, the inverse problem of radiotherapy treatment planning can be solved analytically [27, 28]. We prescribe a constant dose $D_{pres}\equiv 1$ ($r<R_T$) to the CTV whereas the dose to the surrounding normal tissue is unspecified. The solution for the fluence profile is then given by

$$\Phi\left(x\right)=\begin{cases}\cos\left(\mu x\right)\exp\left(\mu\sqrt{R^2-x^2}\right) & \left(|x|<R_T\right)\\ 0 & otherwise\end{cases} \tag{2.28}$$

The analytical fluence profile and the corresponding dose distribution are shown in figure 2.3.

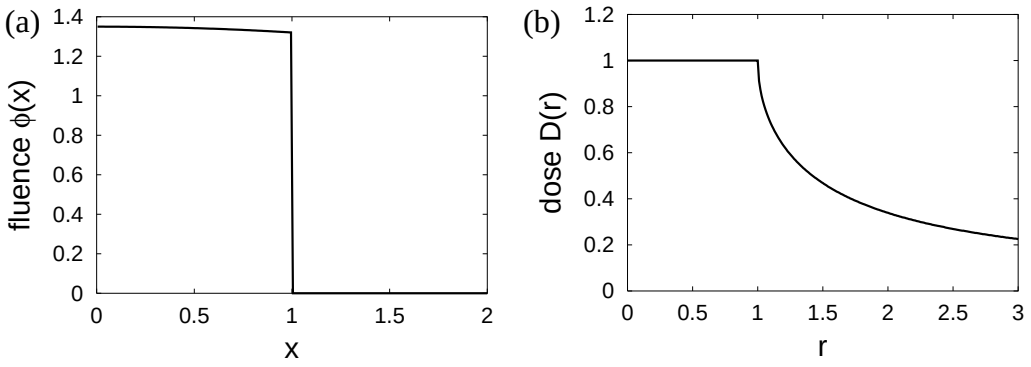

Figure 2.3: (a) Static fluence profile according to equation 2.28, (b) corresponding dose distribution

2.3 The optimization problem

The standard quadratic objective function for a static geometry in the inverse planning process can be written in the form

$$E_{stat} = \int_0^R \alpha\left(r\right)\left[D\left(r\right) - D_{pres}\left(r\right)\right]^2 r dr \tag{2.29}$$

for a dose distribution of rotational symmetry. The factor r is due to the integration with respect to the radial coordinate r in polar coordinates. α and D_{pres} are a penalty factor and a prescribed dose, respectively. For the results presented in this thesis we chose the standard parameter values

$$\alpha\left(r\right) = \begin{cases} 1 & (r < R_T) \\ 0.001 & (r > R_T) \end{cases} \tag{2.30}$$

$$D_{pres}\left(r\right) = \begin{cases} 1 & (r < R_T) \\ 0 & (r > R_T) \end{cases} \tag{2.31}$$

Calculating the fluence profile that minimizes 2.29 gives a close approximation of the analytical solution 2.28.

For probabilistic treatment planning we consider the cumulative dose distribution delivered to the patient in N fractions:

$$D_c(\boldsymbol{r}) = \sum_{\mu=1}^{N} D(\boldsymbol{r}|\Delta\boldsymbol{g}_\mu) \tag{2.32}$$

where $D(\boldsymbol{r}|\Delta\boldsymbol{g}_\mu)$ is the dose delivered to point $\boldsymbol{r}$ given a displacement $\Delta\boldsymbol{g}_\mu$. For a static geometry, the cumulative dose distribution is just a multiple of the dose per fraction. Therefore, objective function 2.29 would be identical when formulated in terms of the cumulative dose. For probabilistic treatment plan optimization we optimize the expectation value of 2.29 for the cumulative dose, which is the sum of the variance of the cumulative dose and the quadratic difference of expected and prescribed dose:

$$E = \int_0^R \alpha(r)\left[\left[\langle D_c\rangle\left(r\right) - N D_{pres}(r)\right]^2 + \left[\left\langle D_c^2\right\rangle\left(r\right) - \langle D_c\rangle^2\left(r\right)\right]\right] r dr \tag{2.33}$$

The following sections will evaluate objective function 2.33 using the motion model derived in section 2.1. Section 2.6 considers the most general case where all parameters $\Delta\boldsymbol{g}$, $\Delta\boldsymbol{s}$ and σ are random variables. Section 2.4 starts with a simplified version which only considers random errors.

2.4 Probabilistic treatment planning incorporating random errors

This section considers a simplified version of the motion model derived in section 2.1. The distribution width σ and the mean position $\Delta\boldsymbol{s}$ of the patient are assumed to be known exactly. This means, we only deal with random errors and neglect systematic errors and uncertainties in the knowledge of the magnitude of motion. In this case the calculation of the expectation values $\langle D_c \rangle$ and $\langle D_c^2 \rangle$ is given by

$$\langle D_c \rangle = N\langle D \rangle \tag{2.34}$$

$$\langle D_c^2 \rangle = N\langle D^2 \rangle + N(N-1)\langle D \rangle^2 \tag{2.35}$$

$$\langle D \rangle = \int D(\boldsymbol{r}|\Delta\boldsymbol{g}) P(\Delta\boldsymbol{g}|\Delta\boldsymbol{s},\sigma) d\Delta\boldsymbol{g} \tag{2.36}$$

$$\langle D^2 \rangle = \int D^2(\boldsymbol{r}|\Delta\boldsymbol{g}) P(\Delta\boldsymbol{g}|\Delta\boldsymbol{s},\sigma) d\Delta\boldsymbol{g} \tag{2.37}$$

with the probability distribution

$$P(\Delta\boldsymbol{g}|\Delta\boldsymbol{s},\sigma) = \frac{1}{2\pi\sigma^2} \exp\left(-\frac{(\Delta\boldsymbol{g}-\Delta\boldsymbol{s})^2}{2\sigma^2}\right) \tag{2.38}$$

A derivation of the expectation values in 2.36 and 2.37 can be found in appendix A.1. For the mean position, one would usually choose $\Delta\boldsymbol{s} = \Delta\boldsymbol{s}^\star$. Without loss of generality we assume $\Delta\boldsymbol{s}^\star = 0$, i.e. we place the isocenter at the mean position of the patient. For the distribution width one could also choose the optimal model value $\sigma = \sigma^\star$. In general, especially when population based knowledge exists, one could derive the value of σ from the distribution $P(\sigma|\{\Delta\boldsymbol{p}_\mu\})$ in equation 2.22. One could for example choose the expectation value of σ, i.e. $\sigma = \int P(\sigma'|\{\Delta\boldsymbol{p}_\mu\}) d\sigma'$. Here, we choose $\sigma = 0.2$.

Using equation 2.34 to 2.37 the objective function 2.33 can be rewritten as

$$E = \int_0^R \alpha(r) \left[\left[\langle D \rangle (r) - D_{pres}(r)\right]^2 + \frac{1}{N} \left[\left\langle D^2 \right\rangle (r) - \langle D \rangle^2 (r) \right] \right] r dr \tag{2.39}$$

Both terms, $\langle D \rangle$ and $\langle D^2 \rangle$ can be expressed as a function of the fluence and the optimization can be performed using a standard gradient method (see appendix A.2). Equation 2.39 shows explicitly that the objective function depends on the number of fractions N. Therefore, we obtain different optimal fluence profiles $\Phi(x)$ for different numbers of fractions.

Figure 2.4a shows the optimal fluence profiles for 1, 10 and 30 fractions. The optimization for $N = 1$ reproduces a safety margin like solution. The profile is essentially flat within the tumor and the irradiated region is expanded towards the healthy tissue to account for the

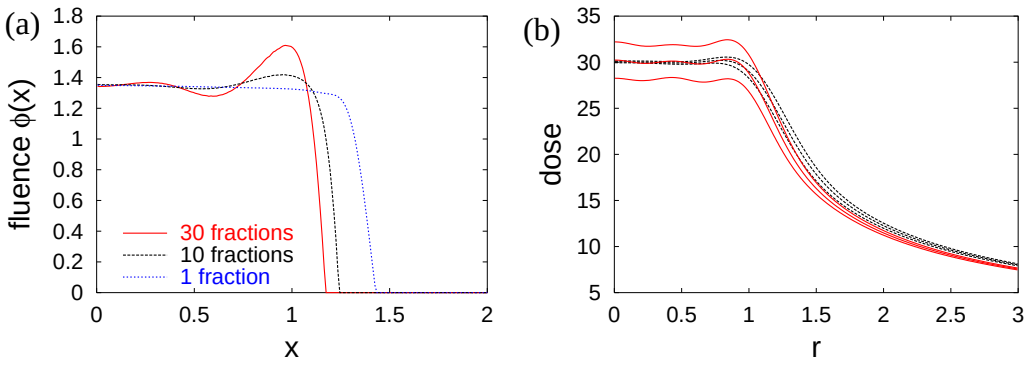

Figure 2.4: (a) fluence profiles that minimize objective function 2.39 for different numbers of fractions, (b) expectation value of the dose and its standard deviation for 30 fractions: for the fluence profile that minimizes 2.39 for $N \to \infty$ (black solid line) and $N = 30$ (red dashed line). The three lines show the expectation value $N\langle D\rangle$ and the expectation value plus and minus one standard deviation $\sqrt{N(\langle D^2\rangle - \langle D\rangle^2)}$, respectively.

positioning uncertainty of the tumor. The optimization automatically chooses an appropriate size of the margin based on the probability distribution of the displacements. For $N = 30$ the optimal fluence profile shows a moderate peak near the edge of the tumor. Initial dose inhomogeneities within the tumor resulting from this peak are likely to be leveled out during later fractions when the patient is in different positions. Points near the edge of the tumor may move out of the high dose region in some fractions. This is compensated for by delivering higher doses than the prescribed dose in other fractions. The peak in the fluence profile allows for a reduction of the irradiated area compared to the solution for $N = 1$. For $N = 1$ the fluence profile is smooth since initial dose inhomogeneities could never be compensated for by later fractions. For $N = 10$ an intermediate result is obtained which shows a slight peak near the edge of the tumor but less pronounced than for $N = 30$. Figure 2.5 shows the expectation value of the dose and the corresponding variance as a function of the radial coordinate r for the fluence profiles in figure 2.4a. The expectation values indicate a better sparing of the healthy tissue when the fluence profile is optimized for a larger number of fractions. The variance in 2.5b is normalized to 30 fractions, i.e. the different values $N = 1$, $N = 10$ and $N = 30$ were used in the optimization but for recalculating the variance after the optimization, 30 fractions are assumed for all profiles to allow for a meaningful comparison. The peak in the fluence profile for $N = 30$ leads to a larger variance at the edge of the tumor compared to the safety margin like solution for $N = 1$. The largest dose uncertainties arise in the adjacent healthy tissue since the largest dose gradients are located in this region.

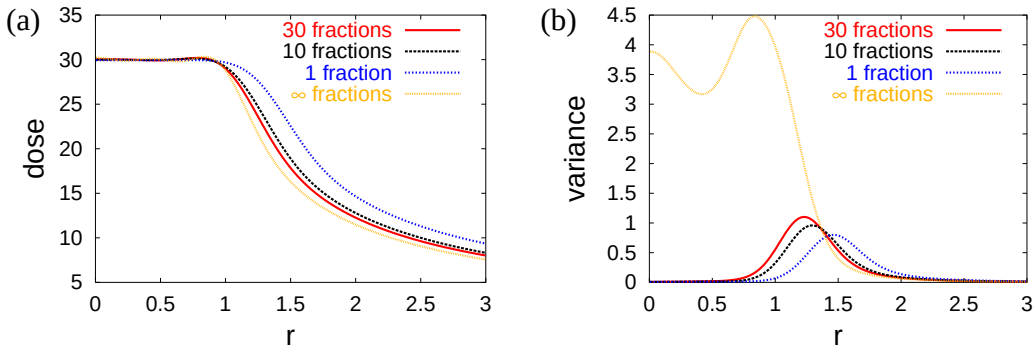

Figure 2.5: (a) expectation values of the dose distribution for the fluence profiles in figure 2.4a and 2.6a (b) corresponding variance distributions, normalized to 30 fractions

2.4.1 Optimization of the expectation value

In the limit $N \to \infty$ the variance term in equation 2.39 vanishes. If an infinite number of fractions was delivered, the expectation value of the dose would be realized. In this case, the objective function is easier to evaluate since only the expectation value of the dose has to be considered. We investigate the question whether the limit $N \to \infty$ provides a useful approximation for inverse treatment planning. Mathematically, this corresponds to approximating the expectation value of the objective function by the objective function evaluated at the expectation value of the random variable, i.e. $\langle E(D) \rangle \approx E(\langle D \rangle)$.

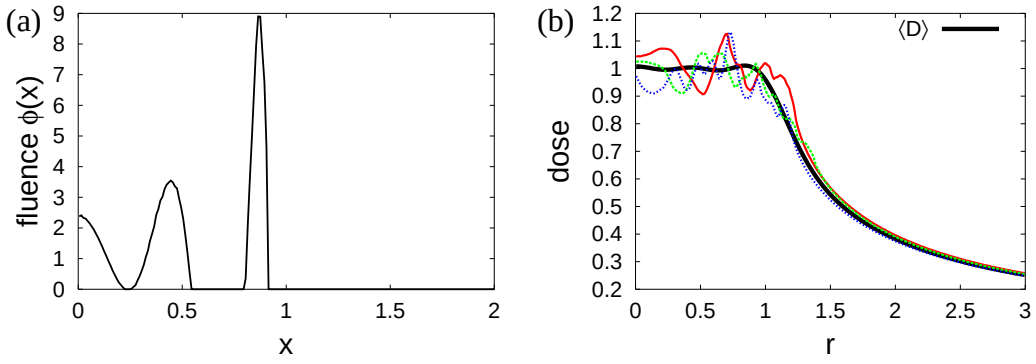

Figure 2.6: (a) fluence profile that minimizes objective function 2.39 for $N \to \infty$, (b) corresponding expectation value of the dose per fraction (thick solid line) and three examples for realistic dose distributions for $N = 30$ fractions (colored dashed lines)

The result for the respective optimal fluence profile is depicted in figure 2.6a. Figure 2.6b shows the corresponding expectation value of the dose distribution (solid line). The fluence profile is characterized by a sharp peak near the edge of the tumor that allows for an optimal sparing of the healthy tissue. However this optimize expectation value

would only be achieved for an infinite number of treated fractions. In this case, initial dose inhomogeneities that result from the sharp peaks in the fluence profile would be smoothed out by later fractions. For a realistic number of 30 fractions this process can only partly occur. Figure 2.6b shows three cumulative dose distributions as a function of the radial coordinate r for $\varphi = 0$ and $N = 30$ randomly chosen treatment positions from the distribution 2.38. This plot clearly demonstrates that patients do not benefit from the optimized expectation value. For the fluence profile optimized for $N = 30$, the profile is also peaked near the edge of the tumor but the peak is less pronounced. The complete objective function including the variance term allows for the correct compromise between an acceptable expectation value of the dose and a small value for its corresponding variance which can be seen from 2.4b. Compared to the optimization for $N = 30$, optimizing 2.39 in the limit $N \to \infty$ yields a slightly steeper dose gradient in the expectation value of the dose at the edge of the tumor (figure 2.5a). This indicates a potentially better sparing of the healthy tissue. For the individual patient this is, however, not beneficial since the expectation value is not realized for a realistic number of fractions as indicated by the large standard deviation. Also figure 2.5b shows the dramatically increased variance that results from neglecting the variance term during the optimization. The standard deviation is in the order of 7% of the prescribed dose for points within the tumor.

2.5 Incorporating systematic errors into the optimization

In this section we still consider the distribution width σ of the motion model as a fixed parameter, but we allow for uncertainties in the estimated mean position $\Delta\boldsymbol{s}$ of the patient, i.e. we account for systematic errors. In this case, the expectation values $\langle D_c \rangle$ and $\langle D_c^2 \rangle$ are given by (appendix A.1)

$$\langle D_c \rangle = N \langle D \rangle \tag{2.40}$$

$$\langle D_c^2 \rangle = N(N-1) \langle DD \rangle + N \left\langle D^2 \right\rangle \tag{2.41}$$

$$\langle D \rangle = \int\int D(\boldsymbol{r}|\Delta\boldsymbol{g}) P(\Delta\boldsymbol{g}|\Delta\boldsymbol{s},\sigma) P(\Delta\boldsymbol{s}|\sigma,\{\Delta\boldsymbol{p}_\mu\})\, d\Delta\boldsymbol{g}\, d\Delta\boldsymbol{s} \tag{2.42}$$

$$\langle D^2 \rangle = \int\int D^2(\boldsymbol{r}|\Delta\boldsymbol{g}) P(\Delta\boldsymbol{g}|\Delta\boldsymbol{s},\sigma) P(\Delta\boldsymbol{s}|\sigma,\{\Delta\boldsymbol{p}_\mu\})\, d\Delta\boldsymbol{g}\, d\Delta\boldsymbol{s} \tag{2.43}$$

$$\langle DD \rangle = \int\int\int D(\boldsymbol{r}|\Delta\boldsymbol{g}_\mu) D(\boldsymbol{r}|\Delta\boldsymbol{g}_\eta) P(\Delta\boldsymbol{g}_\mu|\Delta\boldsymbol{s},\sigma) P(\Delta\boldsymbol{g}_\eta|\Delta\boldsymbol{s},\sigma) \times P(\Delta\boldsymbol{s}|\sigma,\{\Delta\boldsymbol{p}_\mu\})\, d\Delta\boldsymbol{g}_\mu\, d\Delta\boldsymbol{g}_\eta\, d\Delta\boldsymbol{s} \tag{2.44}$$

with the probability distributions

$$P(\Delta \boldsymbol{g}|\Delta \boldsymbol{s},\sigma) = \frac{1}{2\pi\sigma^2}\exp\left(-\frac{(\Delta \boldsymbol{g}-\Delta \boldsymbol{s})^2}{2\sigma^2}\right) \tag{2.45}$$

$$P(\Delta \boldsymbol{s}|\sigma,\{\Delta p_\mu\}) = \frac{1}{2\pi\frac{\sigma^2}{M}}\exp\left(-\frac{(\Delta \boldsymbol{s}-\frac{1}{M}\sum_{\mu=1}^{M}\Delta \boldsymbol{p}_\mu)^2}{2\frac{\sigma^2}{M}}\right) \tag{2.46}$$

Objective function 2.33 can be rearranged to give

$$\begin{aligned} E &= \int_0^R \alpha(r)\left[\langle D\rangle(r)-D_{pres}(r)\right]^2 r dr \\ &\quad + \int_0^R \alpha(r)\left[\frac{N-1}{N}\langle DD\rangle(r)+\frac{1}{N}\left\langle D^2\right\rangle(r)-\langle D\rangle^2(r)\right] r dr \end{aligned} \tag{2.47}$$

Concerning the expectation value of the dose, there is no real discrimination between random error and systematic error. The expectation value would be identical for a pure random error with a distribution width $(1+\frac{1}{M})\sigma$. In other words, two averaging processes are mixed up: first, the averaging over the random displacements during the course of treatment for a single patient. And second, the averaging over the systematic displacements for a population of patients. The distinction between random errors and systematic errors in the optimization is warranted by the variance term and becomes manifest in the expectation value $\langle DD\rangle$. The systematic error in equation 2.44 leads to a coupling of the displacement $\Delta \boldsymbol{g}_\mu$ in fraction μ and the displacement $\Delta \boldsymbol{g}_\eta$ in another fraction η. The total probability for obtaining the displacements $\Delta \boldsymbol{g}_\mu$ and $\Delta \boldsymbol{g}_\eta$ given by $P(\Delta \boldsymbol{g}_\mu,\Delta \boldsymbol{g}_\eta|\sigma\{\Delta \boldsymbol{p}_\mu\}) = \int P(\Delta \boldsymbol{g}_\mu|\Delta \boldsymbol{s},\sigma)P(\Delta \boldsymbol{g}_\eta|\Delta \boldsymbol{s},\sigma)P(\Delta \boldsymbol{s}|\sigma,\{\Delta \boldsymbol{p}_\mu\})d\Delta \boldsymbol{s}$ does not factorize.

For the simulation in this section we again assume $\frac{1}{M}\sum_{\mu=1}^{M}\Delta \boldsymbol{p}_\mu = 0$, i.e the isocenter is placed at the estimated mean position of the patient. For the distribution width we choose $\sigma = 0.2$ and we assume $N = 30$ fractions. Figure 2.7a depicts the optimal fluence profiles for different values of M, the number of position measurements. M essentially determines the width of the Gaussian probability distribution for the systematic error (equation 2.46). For $M \to \infty$, the systematic error is eliminated and the simplified case discussed in section 2.4 is obtained. For $M = 1$, which corresponds to common practice today, the distribution width of the systematic error is as large as for the random error, i.e. σ. As expected the fluence profile is expanded while the systematic error increases. All profiles are characterized by a peak at the edge of the tumor which arises due to the random error that is the same for all profiles. Figure 2.8 shows the corresponding expectation values of the dose and the variances. The expectation values in figure 2.8a show that the sparing of healthy tissue is significantly improved when the systematic error is reduced ($M > 1$). In case of a large systematic error ($M = 1$) the high dose region is significantly expanded. Figure 2.8a shows also that five measurements of the patient position ($M = 5$) already provide a strong improvement compared to $M = 1$, whereas a further increase of the number of measurements yields only minor benefits. The variance in figure 2.8b shows that the optimization

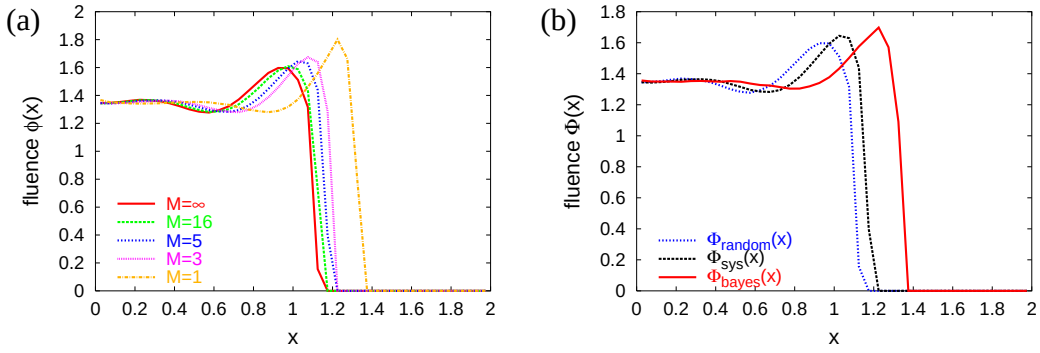

Figure 2.7: (a) fluence profiles that minimize objective function 2.47 for different numbers of position measurements M prior to treatment and $N = 30$ fractions (b) fluence profiles that minimize objective function 2.33 for three different methods to evaluate the expectation values $\langle D_c \rangle$ and $\langle D_c^2 \rangle$ according to sections 2.4, 2.5 and 2.6 for $N = 30$, $M = 5$ and $\sigma_{data} = 0.2$

makes the uncertainty small within the tumor. The large variance in the healthy tissue adjacent to the tumor is due to the steep dose gradients which arise in the transition region.

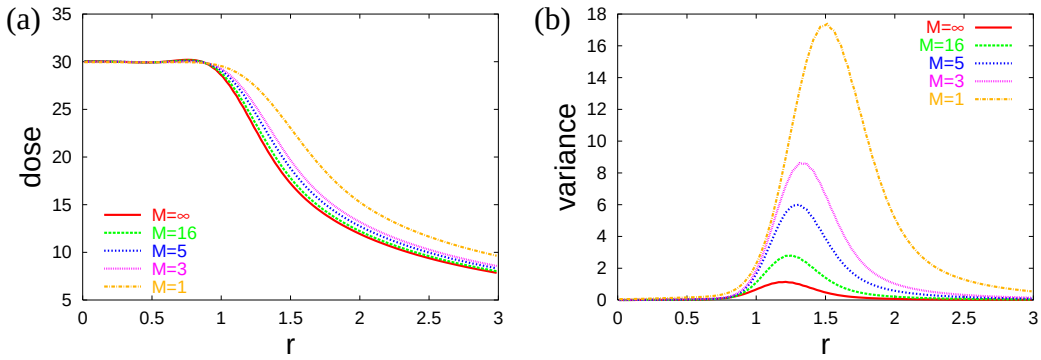

Figure 2.8: (a) expectation values of the dose $\langle D_c \rangle$ for the fluence profiles in 2.7a (b) corresponding variances $\langle D_c^2 \rangle - \langle D_c \rangle^2$

It should be noted that the expectation value of the dose is not a good surrogate for the dose distribution delivered to the patient. It includes the averaging over the systematic error which only occurs among a population of patients but not for the individual patient. The expectation value has to be interpreted pointwise. For every point $\boldsymbol{r}$, the expectation value provides the best estimate for the dose delivered to that point. The variance provides the uncertainty of that prediction. If the variance is small, the delivered dose will be close to the expectation value. However, the spatial distribution of expectation values as depicted

in figure 2.8 can never be realized at each point simultaneously. Realistically, the delivered dose distribution will not be radially symmetric.

2.6 Accounting for an uncertain magnitude of motion

In this section we allow for uncertainties in all model parameters, i.e. a random displacement $\Delta\boldsymbol{g}$ in every fraction, a systematic displacement $\Delta\boldsymbol{s}$ and an uncertainty in the distribution width σ. In this case, the expectation values $\langle D_c\rangle$ and $\langle D_c^2\rangle$ are given by

$$\langle D_c\rangle = N\langle D\rangle \tag{2.48}$$

$$\langle D_c^2\rangle = N(N-1)\langle DD\rangle + N\left\langle D^2\right\rangle \tag{2.49}$$

$$\begin{aligned}\langle D\rangle = \int\int\int & D(\boldsymbol{r}|\Delta\boldsymbol{g})P(\Delta\boldsymbol{g}|\Delta\boldsymbol{s},\sigma) \\ & \times P(\Delta\boldsymbol{s}|\sigma,\{\Delta\boldsymbol{p}_\mu\})P(\sigma|\{\Delta\boldsymbol{p}_\mu\})\,d\Delta\boldsymbol{g}\,d\Delta\boldsymbol{s}\,d\sigma\end{aligned} \tag{2.50}$$

$$\begin{aligned}\langle D^2\rangle = \int\int\int & D^2(\boldsymbol{r}|\Delta\boldsymbol{g})P(\Delta\boldsymbol{g}|\Delta\boldsymbol{s},\sigma) \\ & \times P(\Delta\boldsymbol{s}|\sigma,\{\Delta\boldsymbol{p}_\mu\})P(\sigma|\{\Delta\boldsymbol{p}_\mu\})\,d\Delta\boldsymbol{g}\,d\Delta\boldsymbol{s}\,d\sigma\end{aligned} \tag{2.51}$$

$$\begin{aligned}\langle DD\rangle = \int\int\int\int & D(\boldsymbol{r}|\Delta\boldsymbol{g}_\mu)D(\boldsymbol{r}|\Delta\boldsymbol{g}_\eta)P(\Delta\boldsymbol{g}_\mu|\Delta\boldsymbol{s},\sigma)P(\Delta\boldsymbol{g}_\eta|\Delta\boldsymbol{s},\sigma) \\ & \times P(\Delta\boldsymbol{s}|\sigma,\{\Delta\boldsymbol{p}_\mu\})P(\sigma|\{\Delta\boldsymbol{p}_\mu\})\,d\Delta\boldsymbol{g}_\mu\,d\Delta\boldsymbol{g}_\eta\,d\Delta\boldsymbol{s}\,d\sigma\end{aligned} \tag{2.52}$$

with the probability distributions

$$P(\Delta\boldsymbol{g}|\Delta\boldsymbol{s},\sigma) = \frac{1}{2\pi\sigma^2}\exp\left(-\frac{(\Delta\boldsymbol{g}-\Delta\boldsymbol{s})^2}{2\sigma^2}\right) \tag{2.53}$$

$$P(\Delta\boldsymbol{s}|\sigma,\{\Delta\boldsymbol{p}_\mu\}) = \frac{1}{2\pi\frac{\sigma^2}{M}}\exp\left(-\frac{(\Delta\boldsymbol{s}-\frac{1}{M}\sum_{\mu=1}^{M}\Delta\boldsymbol{p}_\mu)^2}{2\frac{\sigma^2}{M}}\right) \tag{2.54}$$

$$P(\sigma|\{\Delta\boldsymbol{p}_\mu\}) \propto \frac{1}{(2\pi\sigma^2)^{M-1}}\exp\left(-\frac{\frac{1}{M}\sum_{\mu=1}^{M}(\Delta\boldsymbol{p}_\mu-\frac{1}{M}\sum_{\eta=1}^{M}\Delta\boldsymbol{p}_\eta)^2}{2\frac{\sigma^2}{M}}\right) \tag{2.55}$$

The parameter

$$\sigma_{data} = \sqrt{\frac{1}{M}\sum_{\mu=1}^{M}(\Delta\boldsymbol{p}_\mu-\frac{1}{M}\sum_{\eta=1}^{M}\Delta\boldsymbol{p}_\eta)^2} \tag{2.56}$$

now refers to the motion in two spatial dimensions, whereas the parameter σ refers to the distribution width in one spatial dimension. A parameter value $\sigma_{data} = \sqrt{2}\cdot 0.2$ corresponds to an estimated distribution width of 0.2 in each spatial dimension. For the simulations in this section we chose $\sigma_{data} = \sqrt{2}\times 0.2$.

Figure 2.7b shows the optimal fluence profiles that account for an uncertain σ (black solid line) for the parameters $N = 30$ and $M = 5$. For comparison the corresponding results

from sections 2.5 and 2.4 are shown, i.e. the optimal fluence profile that accounts for random and systematic errors (dashed line) and the profile that only accounts for random errors (dotted line). All profiles are characterized by a moderate peak at the edge of the tumor that is due to the random error. The first planning strategy that considers random errors only leads to the least expanded fluence profile ($\Phi_{random}(x)$). The second planning strategy that incorporates systematic errors leads to a more expanded profile ($\Phi_{sys}(x)$). The third method that in addition allows for an uncertain σ again expands the fluence profile ($\Phi_{bayes}(x)$). This can be understood by regarding the dashed line in figure 2.12b that shows the posterior probability distribution for σ. When only $M = 5$ measurements are performed, the value for σ that actually describes the movement of this patient could be significantly larger than $\sigma_{data}/\sqrt{2}$. This in turn makes larger systematic errors and larger random errors possible and hence requires a larger volume to be irradiated.

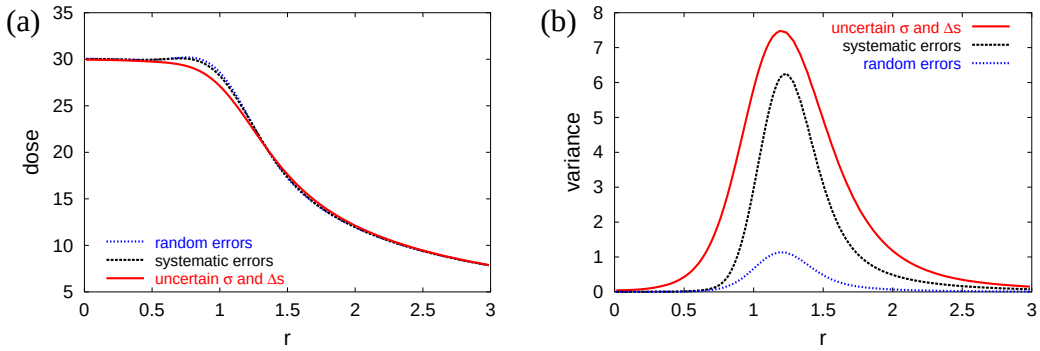

Figure 2.9: (a) expectation values $\langle D_c \rangle$ for the fluence profile $\Phi_{random}(x)$ while taking into account different uncertainties according to sections 2.4, 2.5 and 2.6, respectively (b) corresponding values of the variance $\langle D_c^2 \rangle - \langle D_c \rangle^2$

Accounting only for random errors during the optimization leads to an underdosage of the tumor edge for many patients. Figure 2.9a shows three times the expectation value of the dose distribution obtained for the same fluence profile $\Phi_{random}(x)$ but using the three different methods to calculate the expectation values. Figure 2.9b shows the corresponding variances. The dotted lines represent the planned dose, i.e. expectation value and variance obtained by consideration of random errors alone (equations 2.34-2.38). The dashed lines show the expectation value and the variance when systematic errors are considered (equations 2.40-2.46). This leads to a minor effect concerning the expectation value, however the variance is significantly underestimated when only random errors are included. The solid line corresponds to the third method that additionally allows for uncertainties in the distribution width. Uncertainties in σ result in a distinct flattening of the expectation value and a further increase of the variance. The flattened expectation value indicates that on average the tumor edge is significantly underdosed. In other words, when a large number of patients from that population are irradiated with that fluence profile, most patients will

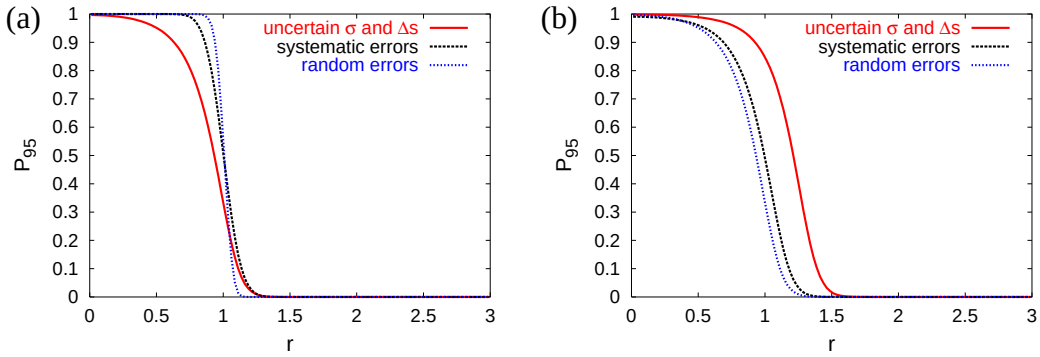

Figure 2.10: Both pictures show the probability P_{95} that a point at radial coordinate r recieves a cumulative dose higher than 95% of the prescribed tumor dose ($N = 30$) (a) for the fluence profile $\Phi_{random}(x)$ while taking into account different uncertainties according to sections 2.4, 2.5 and 2.6, respectively (b) for the three different fluence profiles in figure 2.7b while taking into account uncertainties in both parameters σ and $\Delta\boldsymbol{s}$

show an underdosage on parts of the tumor edge. To clarify the risk of underdosing, one can also look at the probability that at a given point the delivered dose exceeds a certain threshold. Figure 2.10a shows the probability P_{95} that at a point with radial coordinate r the delivered cumulative dose exceeds 95% of the prescribed tumor dose. Again all lines correspond to the same fluence profile $\Phi_{random}(x)$, but different uncertainties during treatment are considered. The planned dose seems to guarantee a satisfying target coverage (dotted line). However, when systemetic errors (dashed line) and additional uncertainties in the distribution width (solid line) are taken into account, the probability that the edge of the target receives the desired dose becomes very low. The calculation of the probability P_{95} is discussed in appendix A.3.

The planning strategy defined in equations 2.48 to 2.55 accounts for uncertainties in both parameters $\Delta\boldsymbol{s}$ and σ already in the optimization process. Figure 2.10b shows the probability P_{95} that the dose at a given point r exceeds 95% of the prescribed tumor dose for the three different fluence profiles in figure 2.7b. All P_{95} curves were calculated by allowing for systematic errors and an uncertain σ (equations 2.48 to 2.55). Figure 2.11 shows the corresponding expectation values of the dose and the variance. The planning strategy defined in this section automatically shifts the dose gradient between tumor and normal tissue towards the normal tissue (figure 2.11a) and therefore leads to a better dose coverage of the tumor (figure 2.10b).

Figure 2.11b allows for a comparison of the total variance for the three planning procedures. The total variance of the dose in the adjacent healthy tissue cannot be reduced too much, although the planning strategy defined in this section minimizes the variance due to an uncertain σ and $\Delta\boldsymbol{s}$ in the optimization process, which is not the case for the planning

strategies in sections 2.4 and 2.5. The variance at the edge of the tumor is an intrinsic consequence of the movement and the steep dose gradient at the edge of the tumor. Therefore the variance in the healthy tissue can only to a limited extent be reduced by shaping the fluence profile.

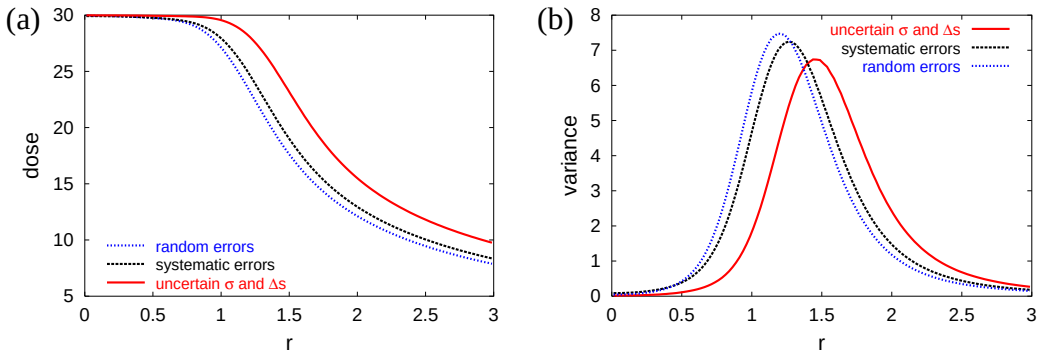

Figure 2.11: (a) expectation values $\langle D_c \rangle$ for the three different fluence profiles in figure 2.7b while taking into account uncertainties in both parameters σ and $\Delta \boldsymbol{s}$ (equations 2.48-2.52) (b) corresponding values of the total variance $\langle D_c^2 \rangle - \langle D_c \rangle^2$

2.6.1 Inclusion of population based knowledge

The concept of Bayesian inference provides a method to interpolate between patient specific data on organ motion and knowledge that was gathered for a larger population of patients. We now demonstrate the impact of prior knowledge on inverse planning. We substitute the probability distribution in equation 2.55 by

$$P(\sigma|\{\Delta \boldsymbol{p}_\mu\}) \propto \frac{\sigma^{(\alpha-1)}}{\left(2\pi\sigma^2\right)^{M-1}} \exp\left(-\lambda\sigma\right) \exp\left(-\frac{\sigma_{data}^2}{2\frac{\sigma^2}{M}}\right) \tag{2.57}$$

where α and λ are given by equation 2.21. We choose the parameters $\sigma_{data} = \sqrt{2} \times 0.2$, $\sigma_{pop} = 0.15$, $\sigma_{var} = 0.075$, $N = 30$ and $M = 5$. This corresponds to the situation that the 5 measurements for the patient give rise to a larger organ mobility when compared to the average patient. Figure 2.12b compares the posterior distributions for σ with and without prior. Figure 2.12a shows the corresponding optimal fluence profiles. The profile that was optimized by incorporating the prior knowledge is less expanded and leads to an irradiation of a smaller volume compared to the fluence profile optimized without incorporating prior knowledge. This can easily be understood by considering the posterior distributions in figure 2.12b. When prior knowledge is used, large values of σ become much more unlikely. Figure 2.13 shows the probability P_{95} that the dose at a point at radial coordinate r exceeds 95% of the prescribed dose. The curves where calculated by using the fluence profiles in figure 2.12a together with the corresponding posterior distributions in figure 2.12b. The

optimization leads to a similar expected target coverage in both cases. In this example the inclusion of population based knowledge justifies the reduction of the irradiated volume and hence allows for a better sparing of the adjacent healthy tissue.

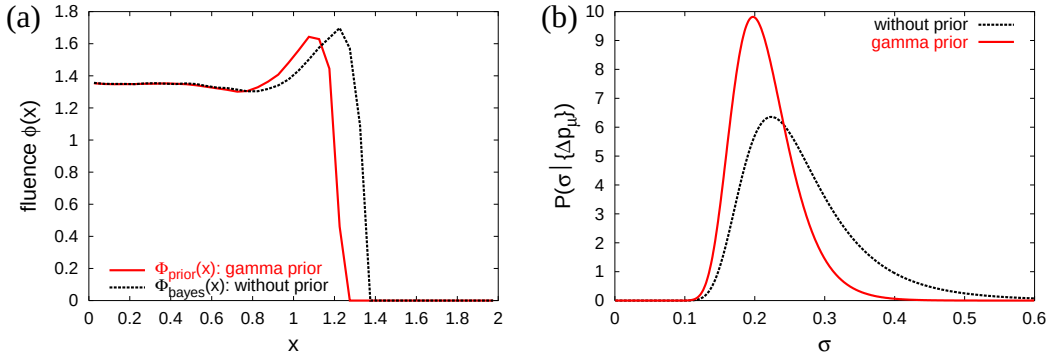

Figure 2.12: Comparison between optimization incorporating and not incorporating prior knowledge. (a) Optimal fluence profiles resulting from inverse planning using the different posterior distributions for σ as displayed in figure 2.12b. (b) Posterior distributions for σ according to equations 2.55 and 2.57 for parameters $\sigma_{data} = \sqrt{2} \times 0.2$, $\sigma_{pop} = 0.15$, $\sigma_{var} = 0.075$ and $M = 5$.

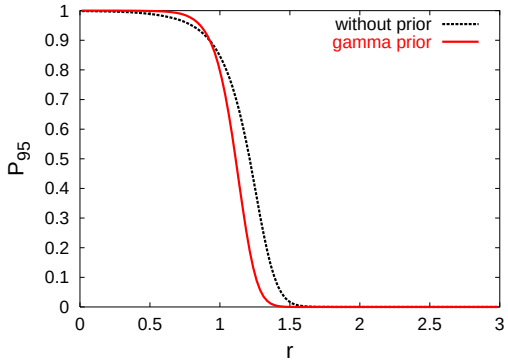

Figure 2.13: Comparison between optimization incorporating and not incorporating prior knowledge. The curves show the P_{95} probabilities for the fluence profiles in figure 2.12a. To calculate these curves uncertainties in $\Delta \boldsymbol{s}$ and σ were allowed and the posterior distributions in figure 2.12b were used. Parameters: $\sigma_{data} = \sqrt{2} \times 0.2$, $\sigma_{pop} = 0.15$, $\sigma_{var} = 0.075$ and $M = 5$.

2.7 Adapting fluence profiles

In this section, we consider again the simplified case that the magnitude of motion σ is fixed and only random errors and systematic errors are considered. In section 2.5 we assumed that the same fluence profile is applied in every fraction. However, the evaluation of the objective function 2.33 does not depend on the assumption that in all fractions the same fluence profile is used. In principle it is possible to allow for a different fluence profile in each fraction. If the systematic error is equal for all fractions, the global minimum of 2.33 corresponds indeed to a treatment plan with a fluence profile that is equal for all fractions, as can be shown analytically. However, if the systematic error is reduced during treatment, the situation changes. Let us consider the case that one position of the patient $\Delta\boldsymbol{p}_0$ is measured before treatment and until fraction M another $M-1$ measurements of the positions $\Delta\boldsymbol{p}_\mu$ are performed. We now allow for two different fluence profiles, one for the first $M-1$ fractions and the other for the remaining $N-M+1$ fractions. The strategy for the adaptation of the treatment plan is as follows: For the first fraction the best estimate for the isocenter is $\Delta\boldsymbol{p}_0$. This position is kept for the first $M-1$ fractions. In fraction M the fluence profile is changed and the isocenter is shifted to $\frac{1}{M}\sum_{\mu=0}^{M-1}\Delta\boldsymbol{p}_\mu$. This position is kept for the remaining fractions.
Let us assume that the "true" mean position of the patient is 0 and that $\Delta\boldsymbol{p}_0$ is the "planning CT measurement" of the tumor position. We place the isocenter for irradiation at $\Delta\boldsymbol{p}_0$ which means that the systematic error for the first $M-1$ fractions is $\Delta\boldsymbol{s}_b = -\Delta\boldsymbol{p}_0$. The probability for $\Delta\boldsymbol{s}_b$ equals the probability to measure $\Delta\boldsymbol{p}_0$, i.e

$$P\left(\Delta\boldsymbol{s}_b|\sigma\right) = \frac{1}{2\pi\sigma^2}\exp\left(-\frac{\Delta\boldsymbol{s}_b^2}{2\sigma^2}\right) \tag{2.58}$$

In the meantime, we measure another $M-1$ positions $\Delta\boldsymbol{p}_\mu$ of the patient and place the isocenter at $\frac{1}{M}\sum_{\mu=0}^{M-1}\Delta\boldsymbol{p}_\mu$. The systematic error is hence $\Delta\boldsymbol{s}_e = -\frac{1}{M}\sum_{\mu=0}^{M-1}\Delta\boldsymbol{p}_\mu$ for the remaining fractions and its distribution is

$$P\left(\Delta\boldsymbol{s}_e|\sigma\right) = \frac{1}{2\pi\frac{1}{M}\sigma^2}\exp\left(-\frac{\Delta\boldsymbol{s}_e^2}{2\frac{1}{M}\sigma^2}\right) \tag{2.59}$$

In this special case, both fluence profiles can be optimized prior to treatment because the actual values of the position measurements $\Delta\boldsymbol{p}_\mu$ are only needed for shifting the isocenter in fraction M but not for inverse planning. For the optimization of the fluence profiles, the information that the distribution width of the systematic error is reduced by a factor $1/\sqrt{M}$ is needed, but this is independent of the actual values of $\boldsymbol{p}_\mu$ which are not known at that time.

We want to minimize objective function 2.33 under the assumption of different systematic errors and different fluence profiles for both parts of the treatment. In this case, the expectation value of the cumulative dose can be written as

$$\langle D_c\rangle = (M-1)\langle D_b\rangle + (N-M+1)\langle D_e\rangle \tag{2.60}$$

where the expectation values

$$\langle D_b \rangle = \int\int D_b(\boldsymbol{r}|\Delta\boldsymbol{g}) P(\Delta\boldsymbol{g}|\Delta\boldsymbol{s}_b,\sigma) P(\Delta\boldsymbol{s}_b|\sigma)\, d\Delta\boldsymbol{g}\, d\Delta\boldsymbol{s}_b \tag{2.61}$$

$$\langle D_e \rangle = \int\int D_e(\boldsymbol{r}|\Delta\boldsymbol{g}) P(\Delta\boldsymbol{g}|\Delta\boldsymbol{s}_e,\sigma) P(\Delta\boldsymbol{s}_e|\sigma)\, d\Delta\boldsymbol{g}\, d\Delta\boldsymbol{s}_e \tag{2.62}$$

describe the expectation value of the dose per fraction for the first $M-1$ fractions and the remaining $N-M+1$ fractions, respectively. The expectation value of the cumulative dose is thus $M-1$ times the expectation value of the dose per fraction in the first part of the treatment plus $N-M+1$ times the expectation value of the dose per fraction in the second part of the treatment. $D_b(\boldsymbol{r}|\Delta\boldsymbol{g})$ and $D_e(\boldsymbol{r}|\Delta\boldsymbol{g})$ refer to the dose calculation using the two fluence profiles ϕ_b and ϕ_e, respectively. The probability distributions in equations 2.45, 2.58 and 2.59 apply. Further details for the evaluation of the expectation values can be found in the appendix of [1]. The expectation value $\langle D_c^2 \rangle$ can be rewritten as

$$\begin{aligned}\langle D_c^2 \rangle &= (M-1)\langle D_b^2 \rangle + (N-M+1)\langle D_e^2 \rangle \\ &\quad +(M-1)(M-2)\langle D_b D_b \rangle \\ &\quad +(N-M+1)(N-M)\langle D_e D_e \rangle \\ &\quad +2(N-M+1)(M-1)\langle D_b D_e \rangle\end{aligned} \tag{2.63}$$

with the following definitions of expectation values:

$$\langle D_b^2 \rangle = \int\int D_b^2(\boldsymbol{r}|\Delta\boldsymbol{g}) P(\Delta\boldsymbol{g}|\Delta\boldsymbol{s}_b,\sigma) P(\Delta\boldsymbol{s}_b|\sigma)\, d\Delta\boldsymbol{g}\, d\Delta\boldsymbol{s}_b \tag{2.64}$$

$$\langle D_e^2 \rangle = \int\int D_e^2(\boldsymbol{r}|\Delta\boldsymbol{g}) P(\Delta\boldsymbol{g}|\Delta\boldsymbol{s}_e,\sigma) P(\Delta\boldsymbol{s}_e|\sigma)\, d\Delta\boldsymbol{g}\, d\Delta\boldsymbol{s}_e \tag{2.65}$$

$$\begin{aligned}\langle D_b D_b \rangle &= \int\int\int D_b(\boldsymbol{r}|\Delta\boldsymbol{g}_\mu) D_b(\boldsymbol{r}|\Delta\boldsymbol{g}_\eta) \\ &\quad \times P(\Delta\boldsymbol{g}_\mu|\Delta\boldsymbol{s}_b,\sigma) P(\Delta\boldsymbol{g}_\eta|\Delta\boldsymbol{s}_b,\sigma) P(\Delta\boldsymbol{s}_b|\sigma)\, d\Delta\boldsymbol{g}_\mu\, d\Delta\boldsymbol{g}_\eta\, d\Delta\boldsymbol{s}_b\end{aligned} \tag{2.66}$$

$$\begin{aligned}\langle D_e D_e \rangle &= \int\int\int D_e(\boldsymbol{r}|\Delta\boldsymbol{g}_\mu) D_e(\boldsymbol{r}|\Delta\boldsymbol{g}_\eta) \\ &\quad \times P(\Delta\boldsymbol{g}_\mu|\Delta\boldsymbol{s}_e,\sigma) P(\Delta\boldsymbol{g}_\eta|\Delta\boldsymbol{s}_e,\sigma) P(\Delta\boldsymbol{s}_e|\sigma)\, d\Delta\boldsymbol{g}_\mu\, d\Delta\boldsymbol{g}_\eta\, d\Delta\boldsymbol{s}_e\end{aligned} \tag{2.67}$$

$$\begin{aligned}\langle D_b D_e \rangle &= \int\int\int\int D_b(\boldsymbol{r}|\Delta\boldsymbol{g}_\mu) D_e(\boldsymbol{r}|\Delta\boldsymbol{g}_\eta) P(\Delta\boldsymbol{g}_\mu|\Delta\boldsymbol{s}_b,\sigma) P(\Delta\boldsymbol{g}_\eta|\Delta\boldsymbol{s}_e,\sigma) \\ &\quad \times P(\Delta\boldsymbol{s}_b|\sigma) P(\Delta\boldsymbol{s}_e|\Delta\boldsymbol{s}_b,\sigma)\, d\Delta\boldsymbol{g}_\mu\, d\Delta\boldsymbol{g}_\eta\, d\Delta\boldsymbol{s}_b d\Delta\boldsymbol{s}_e\end{aligned} \tag{2.68}$$

To calculate the expectation value $\langle D_b D_e \rangle$ we need the conditional probability $P(\Delta\boldsymbol{s}_e|\Delta\boldsymbol{s}_b,\sigma)$ for a systematic error $\Delta\boldsymbol{s}_e$ in a fraction $\eta \geq M$ given a systematic error $\Delta\boldsymbol{s}_b$ in fraction $\mu < M$. Since the measurement $\Delta\boldsymbol{p}_0$ influences both systematic errors, $\Delta\boldsymbol{s}_b$ and $\Delta\boldsymbol{s}_e$ are not statistically independent. To derive $P(\Delta\boldsymbol{s}_e|\Delta\boldsymbol{s}_b,\sigma)$ note that $\Delta\boldsymbol{s}_e = -\frac{1}{M}[-\Delta\boldsymbol{s}_b + \sum_{\mu=1}^{M-1} \Delta\boldsymbol{p}_\mu]$. Defining $\Delta\tilde{\boldsymbol{s}} = -\frac{1}{M-1}\sum_{\mu=1}^{M-1} \Delta\boldsymbol{p}_\mu$ we can rewrite $\Delta\tilde{\boldsymbol{s}} = \frac{M}{M-1}[\Delta\boldsymbol{s}_e - \frac{1}{M}\Delta\boldsymbol{s}_b]$. The probability distribution for $\Delta\tilde{\boldsymbol{s}}$ is given by

$$P(\Delta\tilde{\boldsymbol{s}}|\sigma) = \frac{1}{2\pi\frac{1}{M-1}\sigma^2} \exp\left(-\frac{\Delta\tilde{\boldsymbol{s}}^2}{2\frac{1}{M-1}\sigma^2}\right)$$

We can now interpret the probability $P(\Delta\tilde{\boldsymbol{s}}|\sigma)$ as the conditional probability $P(\Delta\boldsymbol{s}_e|\Delta\boldsymbol{s}_b,\sigma)$, i.e. $P(\Delta\tilde{\boldsymbol{s}}|\sigma)d\Delta\tilde{\boldsymbol{s}} = P(\Delta\boldsymbol{s}_e|\Delta\boldsymbol{s}_b,\sigma)d\Delta\boldsymbol{s}_e$. This gives

$$\begin{aligned} P(\Delta\boldsymbol{s}_e|\Delta\boldsymbol{s}_b,\sigma) &= \det\left(\frac{d\Delta\tilde{\boldsymbol{s}}}{d\Delta\boldsymbol{s}_e}\right)\frac{1}{2\pi\frac{1}{M-1}\sigma^2}\exp\left(-\frac{\left(\frac{M}{M-1}\right)^2\left(\Delta\boldsymbol{s}_e-\frac{1}{M}\Delta\boldsymbol{s}_b\right)^2}{2\frac{1}{M-1}\sigma^2}\right) \\ &= \frac{1}{2\pi\frac{M-1}{M^2}\sigma^2}\exp\left(-\frac{\left(\Delta\boldsymbol{s}_e-\frac{1}{M}\Delta\boldsymbol{s}_b\right)^2}{2\frac{M-1}{M^2}\sigma^2}\right) \end{aligned} \tag{2.69}$$

In the evaluation of $\langle D_c\rangle$ and $\langle D_c^2\rangle$ it is assumed that the systematic errors $\Delta\boldsymbol{s}_e$ and $\Delta\boldsymbol{s}_b$ are statistically independent of the random errors $\Delta\boldsymbol{g}_\mu - \Delta\boldsymbol{s}_\mu$. This describes the situation that all M measurements of the position, which are used to estimate the mean position, are independent of the actual treatment positions, i.e. the measurements are performed at arbitrary instants of time before fraction M. This assumption would not hold if the $M-1$ position measurements were identical to the treatment positions in fraction 1 to $M-1$. In this case $\Delta\boldsymbol{s}_e$ would depend on $\Delta\boldsymbol{g}_\mu$ for $\mu < M$ and the evaluation of the expectation values $\langle D_c\rangle$ and $\langle D_c^2\rangle$ would be different.

Figure 2.14a shows the fluence profiles that minimize objective function 2.33 for $M = 5$ and $N = 30$. The optimization results in a dramatic dose reduction for the first $M-1$ fractions where the mean position of the patient is poorly known. This is compensated for by increasing the dose per fraction for the remaining fractions where the mean position is more clearly defined.

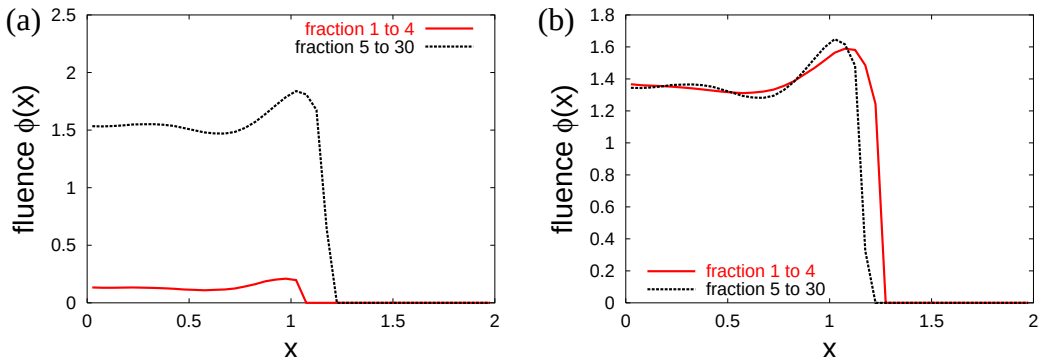

Figure 2.14: Adaptive inverse planning: (a) fluence profiles that minimize objective function 2.33 allowing for two different fluence profiles for both parts of the treatment (b) fluence profiles for both periods of the treatment that minimize the modified objective function 2.70

This result arises from the objective function that only considers the physical dose but not the biological effect. In other words, optimising the cumulative physical dose alone is not consistent with the well established fractionation scheme in the framework of an adaptive

treatment planning. One could try to solve this problem by introducing a more biologically motivated objective function based on cell survival models. However, we restrict ourselves to the dose domain. We do not only want the total dose to be close to the prescribed total dose but also the dose per fraction shall approximately be the same for all fractions. We therefore consider the following heuristic modification of the first term in objective function 2.33:

$$\begin{aligned} E &= \int_0^R \alpha(r) \left[N \sum_{\mu=1}^{N} \left[\langle D_\mu \rangle (r) - D_{pres}(r) \right]^2 + \left[\left\langle D_c^2 \right\rangle (r) - \langle D_c \rangle^2 (r) \right] \right] r dr \\ &= \int_0^R \alpha(r) N(M-1) [\langle D_b \rangle (r) - D_{pres}(r)]^2 r dr \\ &\quad + \int_0^R \alpha(r) N(N-M+1) [\langle D_e \rangle (r) - D_{pres}(r)]^2 r dr \\ &\quad + \int_0^R \alpha(r) \left[\left\langle D_c^2 \right\rangle (r) - \langle D_c \rangle^2 (r) \right] r dr \end{aligned} \tag{2.70}$$

This modified objective function combines the objective of a minimal variance of the total dose and the demand that the expectation value of the dose per fraction is close to the prescribed dose per fraction for every single fraction. As a boundary condition the modified objective function 2.70 reduces to objective function 2.33 if the fluence profile is required to be equal for all fractions. Figure 2.14b depicts the optimal fluence profiles according to 2.70 for $M = 5$ and $N = 30$. The result is now consistent with the fractionation scheme and corresponds to what one would intuitively expect. The fluence profile for the early fractions is more expanded than the one for later fractions, since the systematic error is larger for the first part of the treatment. However, the fluence profile for fraction 1 to 4 is less expanded compared to the fluence profile in 2.7a for $M = 1$, although in both cases the same systematic error is expected. In addition, the profile is quite different from the result one would obtain if objective function 2.47 was evaluated for a total number of $N = 4$ fractions. In this case the fluence profile would be much smoother. In summary: To determine the optimal fluence profile for fraction 1 to 4 one has to take into account that the treatment is continued for another 26 fractions with a reduced systematic error.

2.7.1 Comparison to section 2.5

Finally, we would like to compare the adaptive strategy described above to the planning concept in section 2.5, i.e. we compare three different scenarios:

1) adapting the isocenter and the fluence profile in fraction 5
(fluence profiles in figure 2.14b),

2) preparing only a single measurement of the position
(fluence profile in figure 2.7a for $M = 1$) and

3) preparing all 5 measurements before treatment
(fluence profile in figure 2.7a for $M = 5$).

Figure 2.15 shows the expectation values of the total dose und their variances for the three different scenarios and $N = 30$. As expected the reduction of the systematic error by preparing more than one measurement of the position significantly improves the dose distribution. However, preparing all measurements before the first fraction does not lead to a major benefit compared to the adaptive strategy. Both planning procedures end up with almost the same expectation value of the dose and the same variance. This can be interpreted as a positive result since the adaptive strategy will be more convenient for an implementation in a clinical environment. The additional measurements of the position (corresponding to the additional CT scans of the patient) can be performed at arbitrary times before fraction M (and not necessarily before treatment planning) without major deterioration of the dose distribution.

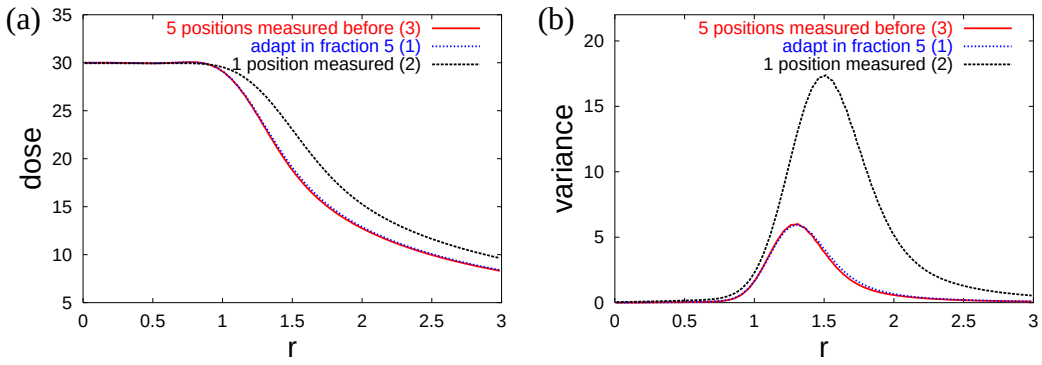

Figure 2.15: Comparison of the planning conceps in section 2.5 and 2.7: (a) expectation values of the dose for three different treatment procedures (b) corresponding variances of the dose

2.7.2 Further comments

Different papers tried to determine the optimal point in time when to adjust the treatment plan for a single adaptation strategy. Bortfeld *et al* [29] minimized the overall expectation value of the systematic error and concluded that an adaptation in fraction 5 is optimal for typical cases. Birkner *et al* [23] considered an adaptive planning strategy for prostate cases that starts with a conventional $1cm$ uniform CTV-to-PTV extension for the first $M - 1$ fractions. In fraction M a new treatment plan is optimized based on a probability distribution of patient geometries that is predicted from the M CT scans. They also came to the conclusion that $M = 5$ is an adequate number of images, since for a later adaptation the improved treatment plan affects a smaller number of fractions. Yan *et al* [14] defined a new planning target volume (PTV) for fraction M to N on the basis of the convex hull of the

daily CTVs in the first $M-1$ fractions. They also found that $M = 5$ is adequate to significantly reduce the additionally required safety margin to fulfil a certain dosimetric criterion.

Our described concept optimizes both fluence profiles prior to the process of gathering image data. This is possible in this particular case because the actual values of the position measurement are not explicitely needed for treatment planning. In general this is not possible. Generally, one would like to update the knowledge about the magnitude of motion σ, which is based on population based knowledge when only the planning CT exists. For the second fluence profile one would like to incorporate the patient specific parameter σ_{data} which requires the actual values of $\Delta\boldsymbol{p}_\mu$. Therefore, a second optimization step before fraction M may be required.
In this section the measurements $\Delta\boldsymbol{p}_\mu$ are used to shift the isocenter. Realistically, probabilistic treatment planning will possibly not deal with setup errors which can be corrected by a shift of the patient, but with non-rigid internal organ motion. In this case one may not want to correct for the systematic error by shifting the patient but by adapting the fluence profiles.
In summary, this section demonstrated an adaptive inverse planning approach by rigorously evaluating quadratic objective functions based on expectation value and variance of the dose. This was done for idealized assumptions, i.e. a rigid translation of the patient and a known magnitude of motion, which allowed us to analyze generic features of the approach. The application to real clinical situations is, however, not straightforward.

Chapter 3

Application to prostate cancer

This section deals with the application of probabilistic treatment planning to prostate cancer. The movement of the prostate is considered as interfractional motion. The concept developed in chapter 2 is now transferred to clinical data. Probabilistic treatment planning was implemented into a research version of the inverse planning tool "KonRad" developed at the german cancer research center [30, 31]. Since the major conceptual ideas have been discussed in chapter 2, the focus of this chapter is the presentation of results for clinical data.

3.1 Preliminaries

We consider IMRT treatments with a $6MV$ linear accelerator with an internal multi leaf collimator (MLC). The resolution of beamlets (bixels) is $(10\ mm)^2$ at the isocenter plane, the resolution of volume elements (voxels) is $(2.6\ mm)^3$. We assume that several CT scans of the patient exist, one planning CT scan and several verification images. For all results presented in this chapter we consider the same patient and an identical irradiation geometry. We optimize a treatment plan with 7 coplanar beams with equidistant angular separation at 0°, 52°, 103°, 154°, 206°, 257° and 309°.

In the presence of internal organ movements and deformations we distinguish two coordinate systems:

1) The static coordinate system: This coordinate system is fixed in the treatment room. When the patient is deformed, a certain volume element of tissue is changing its coordinate in the static coordinate system, i.e. it is moving with respect to the static coordinate system.

2) The anatomy-based coordinate system: This coordinate system is attached to the deforming tissue. The anatomy-based coordinate system is warped with respect to the static coordinate system when the patient is deformed. A certain volume element

of tissue always remains at the same position with respect to the anatomy-based coordinate system.

The planning CT scan will represent a reference image, i.e. for the planning CT both coordinate systems are identical. To display a dose distribution in the anatomy-based coordinate system we adopt the planning CT. The warping of the anatomy-based coordinate system with respect to the static coordinate system will not explicitely be considered or parameterized. However, it formulates the idea behind the concept.
The dose distribution in the static coordinate system will in general change when the patient changes his geometry. In this paper, we will neglect changes of the dose distribution in the static coordinate system. The validity of this approximation depends on the clinical indication and the type of radiation. E.g. the approximation will be poor and invalid if the treatment of lung tumors with proton beams is considered. However, for treating prostate patients with photons the approximation seems to be reasonable. Air cavities in the rectum cause the largest modifications of the dose distribution in the static coordinate system.

At the german cancer research center (DKFZ) prostate patients can be immobilized using body casts made of self-hardening bandages [32, 33]. Therefore, the outer patient contour is considered equal for all fractions. A laser system is used for patient positioning. In addition, the Siemens CT-on-Rails system located within the treatment room can be used for online correction of setup errors. In summary: we finally want to deal with movements of the prostate that are purely due to internal tissue movements and deformations. The tissue deformation in turn mainly arises from changes in the filling of rectum and bladder.

We use the Gaussian motion model derived in section 2.1 to model the interfractional movements of the prostate. Chapter 2 considered rigid translations of the entire patient and the geometric state of the patient could be parameterized by the random variables $\Delta \boldsymbol{g}$, $\Delta \boldsymbol{s}$ and σ. For the prostate, we finally want to be able to deal with internal deformations of the tissue. This can be realized by assuming a seperate Gaussian motion model for each individual voxel. The movement of each individual voxel is described by a Gaussian distribution parameterized by the mean position of the voxel and a voxel-dependent covariance matrix to describe the random motion of the voxel in three spatial dimensions. The Gaussian model is not only applied for simplicity purposes but can be "derived" from an extremum principle. In terms of information theory, the Gaussian distribution satisfies Jaynes principle of the unbiased guess, also referred to as the maximum entropy principle [26]. This means the Gaussian distribution minimizes the Shannon information under the assumption that the requested distribution can be described by an average value and a mean deviation from the average value. Hence, the application of a different type of probability distribution would have to be justified by detailed experimental data.

As mentioned in section 1.4, the quadratic objective function 1.11 can be evaluated by considering each voxel seperately. The expectation value and the variance of the dose in a moving voxel only depend on the movement of this individual voxel. They do not depend

on the movement of any neighboring voxel [1]. Therefore, correlations between the movement of different voxels do not need to be considered. In fact, the movement of different voxels is of cause highly correlated. This means, the probability distribution for finding a certain patient geometry, i.e. a set of positions for all voxels $\{\boldsymbol{r}_i\}$, does not factorise:

$$P_G(\boldsymbol{r}_1, \boldsymbol{r}_2, \boldsymbol{r}_3, \dots) \neq P_1(\boldsymbol{r}_1)P_2(\boldsymbol{r}_2)P_3(\boldsymbol{r}_3)\dots \tag{3.1}$$

For the calculation of expectation value and variance that does not cause problems since only the marginal probability distributions

$$P_i(\boldsymbol{r}_i) = \int \cdots \int P_G(\boldsymbol{r}_1, \boldsymbol{r}_2, \boldsymbol{r}_3, \dots) d\boldsymbol{r}_1 \dots d\boldsymbol{r}_{i-1} d\boldsymbol{r}_{i+1} \dots \tag{3.2}$$

occur, where $P_i(\boldsymbol{r}_i)$ is assumed to be Gaussian. When non-local objective functions, e.g. a non-linear EUD or TCP based objective functions shall be applied, the current implementation had to be modified. In this case it may be necessary to parameterize the probability distribution of patient geometries as a whole instead of looking at the movement of individual voxels. An approach to parameterize tissue deformations based on a principal component analysis (PCA) of volume element displacements was presented [34, 35]. It is a feature of the quadratic objective function that it can be evaluated without consideration of the patient geometry as a whole.

3.2 Accounting for random errors

In this section, we consider the simplified case which neglects systematic errors and uncertainties in the magnitude of motion. Only random errors are considered. Section 3.2.1 describes the implementation of the motion model into the inverse planning programm and the evaluation of the objective function. Sections 3.2.2 to 3.2.7 provide the results obtained. The content of this section has been published as a paper [3].

3.2.1 Implementation of probabilistic optimization for random errors

We describe the evaluation of the expectation value of the dose, the variance and the objective function. Integrals to calculate expectation values are transformed into sums which are evaluated on the relatively course voxel grid, leading to an approximation of the Gaussian motion model. From a practical point of view, the integration of the variance term into the gradient optimization may be the most interesting part.

[1] This requires the approximation that the dose distribution in the static coordinate system is constant

The expectation value of the dose distribution

The dose distribution in the static coordinate system is determined by the fluence maps alone. Dose calculation is performed on the planning CT scan. To calculate the expectation value of the dose distribution in the anatomy-based coordinate system it is sufficient to consider every volume element (voxel) independently. Let i denote the index of a voxel in the anatomy-based coordinate system. The voxel i is moving within the static dose distribution during the course of treatment. The expectation value of the dose in the moving voxel i is approximately given by

$$\langle D_i \rangle = \sum_j D_j^{stat} P_{ij} \tag{3.3}$$

D_j^{stat} denotes the value of the static dose distribution in the static voxel j and P_{ij} is the probability for finding the moving voxel i at the position of the static voxel j. We assume that voxels move according to a Gaussian distribution. The probability for finding the voxel i at position $\boldsymbol{r}$ in the static coordinate system is given by

$$P_i(\boldsymbol{r}) = \frac{\sqrt{\det \boldsymbol{C}_i^{-1}}}{(\sqrt{2\pi})^3} \exp\left(-\frac{1}{2}(\boldsymbol{S}_i - \boldsymbol{r})^T \boldsymbol{C}_i^{-1} (\boldsymbol{S}_i - \boldsymbol{r})\right) \tag{3.4}$$

$\boldsymbol{S}_i$ denotes the estimated mean position of the moving voxel i in the static coordinate system and $\boldsymbol{C}_i^{-1}$ denotes the inverse of the covariance matrix $\boldsymbol{C}_i$ of the displacements of the voxel i. The probability P_{ij} is hence determined by

$$P_{ij} = \frac{1}{Z_i} \exp\left(-\frac{1}{2}(\boldsymbol{S}_i - \boldsymbol{r}_j)^T \boldsymbol{C}_i^{-1} (\boldsymbol{S}_i - \boldsymbol{r}_j)\right) \tag{3.5}$$

with the normalization constant $Z_i = \sum_j \exp\left(-\frac{1}{2}(\boldsymbol{S}_i - \boldsymbol{r}_j)^T \boldsymbol{C}_i^{-1} (\boldsymbol{S}_i - \boldsymbol{r}_j)\right)$. The vector $\boldsymbol{r}_j$ denotes the central position of the static voxel j.

Estimating motion model parameters

To evaluate equation (3.5) one has to estimate the 3-dimensional vectors $\boldsymbol{S}_i$ for the mean position of every moving voxel and 6 components of the covariance matrix $\boldsymbol{C}_i$. For a reasonable application, these parameters have to be estimated from patient specific measurements, i.e. the estimation should be based on the planning CT and the verification CT scans of the patient. An elastic image registration algorithm could be used to map the additional CT scans onto the planning CT. The algorithm provides measured positions $\boldsymbol{p}_i^\mu$ for all moving voxels. These positions are used to estimate the mean position of every voxel as

$$\boldsymbol{S}_i = \frac{1}{M} \sum_{\mu=1}^{M} \boldsymbol{p}_i^\mu \tag{3.6}$$

where M is the number of CT scans including the planning CT. The estimate of the covariance matrix is given by

$$\boldsymbol{C}_i = \frac{1}{M-1}\sum_{\mu=1}^{M}(\boldsymbol{p}_i^{\mu} - \boldsymbol{S}_i)\cdot(\boldsymbol{p}_i^{\mu} - \boldsymbol{S}_i)^T \tag{3.7}$$

where $(\boldsymbol{p}_i^{\mu} - \boldsymbol{S}_i)\cdot(\boldsymbol{p}_i^{\mu} - \boldsymbol{S}_i)^T$ is the matrix product of a three dimensional column vector and a row vector which yields a 3×3-matrix. Due to ongoing work on elastic image registration algorithms in our department, we have not yet implemented this approach. In this thesis, we choose constant values for the covariance matrix for all voxels in order to emphasize the generic features of the inverse planning concept. However, the current implementation allows for voxel dependent covariance matrices and is not in principle limited to constant movements for all voxels. For the results presented in section 3.2.3 to 3.2.5 we assume a standard deviation of 8mm in AP-direction and 5mm in both CC- and LR-direction. The mean position of a voxel is assumed to be identical to the position in the planning CT. In section 3.2.6 we additionally consider the cases of very large and rather small motion amplitudes.

The variance of the dose distribution

The expectation value of the dose in the anatomy-based coordinate system will not be realized after the actual treatment. The dose distribution is uncertain, i.e. the expectation value of the dose in each moving voxel is associated with a standard deviation. The variance of the dose is due to the sparse sampling of the probability distribution for the random error during a finite number of fractions. The variance of the dose in the moving voxel i is given by

$$V_i = \frac{1}{N}\left(\langle D_i^2\rangle - \langle D_i\rangle^2\right) \tag{3.8}$$

where N is the number of fractions and

$$\langle D_i^2\rangle = \sum_j (D_j^{stat})^2 P_{ij} \tag{3.9}$$

Equation 3.8 defines the variance of the expected cumulative dose after the treatment of N fractions. The standard deviation of the dose in vovel i that will be displayed on various pictures in sections 3.2.3 to 3.2.6 is defined as the square root of the variance, i.e.

$$SD_i = \sqrt{V_i} = \sqrt{\frac{1}{N}\left(\langle D_i^2\rangle - \langle D_i\rangle^2\right)} \tag{3.10}$$

The objective function

For the optimization of the fluence maps we adopt the following quadratic objective function:

$$\begin{aligned} E &= \sum_{i \in CTV} \alpha_{CTV} \left[\left(\langle D_i \rangle - D_{CTV} \right)^2 + V_i \right] \\ &\quad + \sum_n \left[\sum_{i \in OAR_n} \alpha_n \left(\langle D_i \rangle - D_n^{max} \right)_+^2 \right] \end{aligned} \tag{3.11}$$

where $(\langle D_i \rangle - D_n^{max})_+ = (\langle D_i \rangle - D_n^{max})$ for $\langle D_i \rangle > D_n^{max}$ and $(\langle D_i \rangle - D_n^{max})_+ = 0$ for $\langle D_i \rangle < D_n^{max}$. D_{CTV} is the dose prescribed to the tumor, D_n^{max} is a maximum dose for the organ at risk (OAR) with index n and α_{CTV} and α_n are penalty factors for the CTV and organs at risk, respectively. Contoured organs at risk are rectum, bladder and the pelvic bones. The unclassified tissue that surrounds the CTV and the contoured organs at risk is also treated as an organ at risk.
The first term in objective function 3.11 aims to securely deliver a homogeneous dose to the CTV. It represents the sum of the variance of the dose and the quadratic difference of expectation value and prescribed dose. The second term aims to minimize the dose in the adjacent organs at risk. In the limit $N \to \infty$ the variance term in the objective function 3.11 vanishes. This corresponds to optimizing the expectation value of the dose in the anatomy-based coordinate system alone. The variance term is incorporated only for the CTV but not for the OARs. There are different motivations for that. First, the dose delivered to the OARs should be as low as possible. One does not want to ensure that a certain dose is delivered to the OARs. Second, the variance in the healthy tissue adjacent to the tumor is an intrinsic consequence of the large dose gradients which are desired at the edge of the tumor. It cannot be reduced significantly anyhow. Section 6.1 outlines the evaluation of a modification of objective function 3.11.

Evaluation of the objective function

We discuss the numerical methods used to evaluate and minimize the objective function 3.11. For the dose calculation, we adopt a dose contribution matrix concept, i.e. the dose contribution of a beamlet to a voxel for unit fluence is precalculated and stored as a matrix element. We consider the static dose distribution first: Let $G_{j\alpha}^{stat}$ be the dose contribution of the beamlet α to the static voxel j so that

$$D_j^{stat} = \sum_\alpha G_{j\alpha}^{stat} \Phi_\alpha \tag{3.12}$$

holds, where Φ_α is the fluence of beamlet α. The expectation value of the dose in the anatomy-based coordinate system can be calculated by precalculating an effective dose contribution matrix $G_{i\alpha}$ according to

$$G_{i\alpha} := \sum_j G_{j\alpha}^{stat} P_{ij} \tag{3.13}$$

so that

$$\langle D_i \rangle = \sum_\alpha G_{i\alpha} \Phi_\alpha \tag{3.14}$$

holds.

Taking into account the variance in the optimization is the most challenging part. The variance of the dose in the anatomy-based coordinate system can be expressed as a function of the beamlet weights by defining a variance contribution tensor $Q_{i\alpha\beta}$. From

$$\begin{aligned} V_i &= \frac{1}{N}\left(\langle D_i^2 \rangle - \langle D_i \rangle^2\right) \\ &= \frac{1}{N}\left[\left(\sum_j (D_j^{stat})^2 P_{ij}\right) - \left(\sum_\alpha G_{i\alpha}\Phi_\alpha\right)^2\right] \\ &= \frac{1}{N}\left[\left(\sum_j \left[(\sum_\alpha G_{j\alpha}^{stat}\Phi_\alpha)(\sum_\beta G_{j\beta}^{stat}\Phi_\beta)P_{ij}\right]\right) - \left(\sum_\alpha G_{i\alpha}\Phi_\alpha\right)\left(\sum_\beta G_{i\beta}\Phi_\beta\right)\right] \end{aligned} \tag{3.15}$$

we obtain

$$V_i = \frac{1}{N}\sum_{\alpha,\beta} Q_{i\alpha\beta}\Phi_\beta\Phi_\alpha \tag{3.16}$$

with the definition

$$Q_{i\alpha\beta} = \sum_j \left(G_{j\alpha}^{stat} G_{j\beta}^{stat} P_{ij}\right) - G_{i\alpha}G_{i\beta} \tag{3.17}$$

The variance contribution tensor $Q_{i\alpha\beta}$ stores the variance contribution of a beamlet pair to a voxel for unit fluence. The dose itself is a linear function of the fluence but the variance is a quadratic function of the dose. Therefore, the evaluation of $\langle D_i^2 \rangle$ leads to a coupling of two beamlets.
The objective function (3.11) can now be written in the form

$$\begin{aligned} E &= \sum_{i\in CTV} \alpha_{CTV}\left[\left(\sum_\alpha G_{i\alpha}\Phi_\alpha - D_{CTV}\right)^2 + \frac{1}{N}\sum_{\alpha,\beta} Q_{i\alpha\beta}\Phi_\alpha\Phi_\beta\right] \\ &\quad + \sum_n \left[\sum_{i\in OAR_n} \alpha_n \left(\sum_\alpha G_{i\alpha}\Phi_\alpha - D_n^{max}\right)_+^2\right] \end{aligned} \tag{3.18}$$

The objective function is a quadratic function of the beamlet weights Φ_α and the minimization problem can be solved by standard gradient methods.
The number of elements in the variance contribution tensor is in the order of "Number of voxels" times "Number of bixels squared". Due to limitations of RAM storage capacity and computation time we do not store the variance contribution tensor for all voxels. We restrict ourselves to 5% of the CTV voxels that are randomly extracted. The contribution

to the variance term in the objective function is then multiplied by a factor of 20. The required RAM storage capacity for the prostate case discussed in this chapter is in the order of $1GB$. The fraction of CTV voxels which is incorporated into the variance term was increased to up to 20%. Naturally, the sampling of the CTV voxels in the variance term has some impact on the optimization result. However, deviations between two static dose distributions occurred mainly in the outer regions and were small within the CTV where the dose kernels of many beamlets intersect. The optimization results presented in this chapter can be considered representative.

Treatment plan evaluation

The evaluation of a treatment plan, even in the absence of organ motion, is inherently a difficult task. In the presence of organ movements, the evaluation of a treatment plan becomes much more complex. In the static case without motion, one has to evaluate a single 3D dose distribution. Probabilistic treatment planning to account for random errors as presented in this section yields three 3D distributions:

1) The expectation value of the dose distribution in the anatomy-based coordinate system.

2) The standard deviation of the dose distribution in the anatomy-based coordinate system.

3) The static dose distribution in the static coordinate system.

Basically, one would like to consider the dose distribution in the anatomy-based coordinate system that will actually be delivered to the patient. It is an intrinsic consequence of the statistical nature of the problem that we do not precisely know this distribution. It has to by assessed by appropriate surrogates. Each of the three distributions listed above provides some information on how the dose distribution that will actually be delivered may look like.
First of all, one may evaluate the expectation value of the dose distribution in the anatomy-based coordinate system since this represents the best estimate of the dose that will be delivered to the patient. However, it is of limited use to look at the expectation value only. An optimal expectation value is beneficial only when the related variance is small. Otherwise, the actually delivered dose may differ significantly from the expectation value. Therefore, one should also look at the standard deviation of the dose. Finally, the static dose distribution assesses some kind of worst case scenario. The static dose distribution displays the dose that would be delivered if the patient was always in the same configuration than in the planning CT. In the optimization process only the dose in the anatomy-based coordinate system is considered explicitly. The optimization results in fluence maps that yield a homogeneous expectation value of the dose in the CTV under the assumption that internal organ motion is present. In general, this leads to an inhomogeneous static dose distribution.

Additional remarks

The dose-volume histogram (DVH) is a global property of a dose distribution. To calculate the "expectation value of the DVH", one has to consider the geometry of the patient as a whole. Therefore, the expectation value of the dose distribution and the variance distribution do not contain the information about the expected DVH. One can easily calculate the DVH of the expectation value of the dose in the anatomy-based coordinate system and the DVH of the static dose distribution. In addition, one can calculate a standard-deviation-volume histogram (SDVH) of the standard deviation distribution in analogy to the classical DVH. These histograms can be used to evaluate the obtained treatment plan but they will not provide the "expectation value of the DVH".

3.2.2 Treatment planning for prostate patients

In the following subsections 3.2.3-3.2.5 we demonstrate the results of probabilistic treatment planning accounting for random errors when applied to prostate patients. We assume uncorrelated movements of 8 mm standard deviation in AP-direction and 5 mm in both CC-direction and LR-direction for all voxels in the region of interest near the prostate. The mean position of all voxels is assumed to be identical to the position in the planning CT. The variance and hence the objective function (3.11) depends on the number of fractions N. Therefore, we obtain different treatment plans for different numbers of fractions. We compare three different cases: $N = 1$, $N = 30$ and the limit $N \to \infty$ which corresponds to the optimization of the expectation value alone without consideration of the dose variance. All treatment plans shown in section 3.2 are optimized for the same set of optimization parameters, i.e. penalty factors and maximum dose constraints are kept the same. Only the parameter N is varied.

3.2.3 Results: $N = 30$

Figure 3.1 shows the obtained treatment plan that was optimized for $N = 30$ fractions. Figure 3.1a and 3.1b show the expectation value of the dose in the anatomy-based coordinate system for a transversal slice and the central slice in sagittal view, respectively. Due to the movement, dose gradients at the edge of the tumor are less steep when compared to conventional treatment planning based on a static geometry. The expectation value of the dose can be interpreted as the best prediction for the dose that will be delivered to a moving voxel.
However, after the actual treatment of 30 fractions the expectation value of the dose will not be realized. Figure 3.1c and 3.1d show the standard deviation of the dose due to a finite number of fractions for a treatment course consisting of 30 fractions. The standard deviation is large where steep dose gradients occur. Therefore, the largest values appear at the edge of the tumor and the adjacent healthy tissue. The largest value corresponds to approximately 7% of the prescribed tumor dose. However, figure 3.1c and 3.1d provide only a lower boundary for the standard deviation since uncertainties in the knowledge of

the model parameters $\Delta \boldsymbol{s}_i$ and $\boldsymbol{\sigma}_i$ are not considered. In analogy to the dose-volume histogram, figure 3.2a shows the standard-deviation-volume-histogram (SDVH). The dashed line corresponds to figure 3.1c and 3.1d, i.e. $N = 30$. The median standard deviation in the CTV is in the order of 2% of the dose prescribed to the tumor. For a large population of identical patients, the standard deviation can be interpreted as the average variation of the dose in moving voxels among different patients of the population. For the individual patient, the standard deviation can be interpreted as the uncertainty of the dose prediction provided by the expectation value.
Figure 3.1e and 3.1f show the corresponding static dose distribution. This dose distribution would be delivered if the patient was not moving during the actual course of treatment, although assumed in the treatment planning process. The static dose distribution is inhomogeneous within the CTV. Within 30 fractions, these inhomogeneities are partly averaged out when the prostate is in different locations in different fractions. Figure 3.3a shows a dose profile in AP-direction in the lower part of the prostate. In this region, the static dose distribution is characterized by a dose peak at the edge of the CTV near the transition to the rectum. The amplitude of the peak is in the order of 120% of the prescribed tumor dose. The dose peak helps to deliver the prescribed dose to the CTV without shifting the dose gradient of the static dose distribution too much towards the rectum. To avoid overdosage inside the CTV, the peak is followed by a dose valley of approximately 90% of the prescribed dose. The modulation pattern of the static dose distribution is determined by the magnitude of motion and the geometry of the CTV, i.e. the shape and location of inhomogeneities is essentially determined by the first term in objective function 3.11 that minimizes the difference of expected and prescribed dose. The amplitude of the inhomogeneities is mainly determined by the variance term since large inhomogeneities cause large dose variances in the CTV. The variance term automatically limits the amplitude of modulation. The DVH of the static dose distribution provides averaged information on the magnitude of modulation. Figure 3.2b shows the DVH of the static dose distribution for the CTV (dashed line). The amplitude of dose peaks goes up to approximately 125% of the prescribed dose. The smooth drop-off of between approximately 90% and 115% marks the dose range of prevalent modulations. In contrast, a steep drop-off near 100% would indicate the absence of modulations.
Due to the static dose modulations, the dose delivered to a certain element of tumor tissue will not be the same in each fraction. This changes the established fractionation scheme, however, the related biological effect is not discussed in this thesis. The biological effect of the non-uniform fractionation could e.g. be assessed in the framework of the linear-quadratic cell survival model by approximating the expectation value of the equivalent uniform fraction dose as the sum of the expectation value of the physical dose and a variance-dependent perturbation [36].

3.2.4 Results: $N = 1$

Figure 3.4 shows the 3D distributions for a treatment plan that was optimized for a single fraction, i.e. $N = 1$ was used as a parameter value in the objective function 3.11 applied

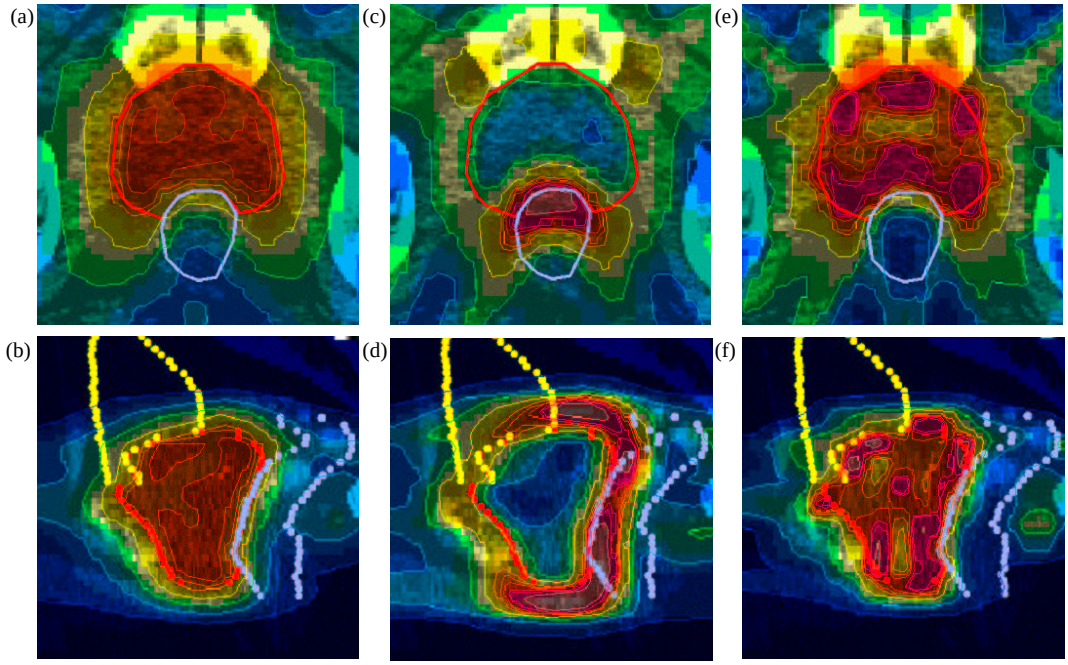

Figure 3.1: 3D distributions for a treatment plan optimized for 30 fractions (a-b) expectation value of the dose (c-d) standard deviation of the dose (e-f) static dose distribution (dose legend: see figure 3.8a)

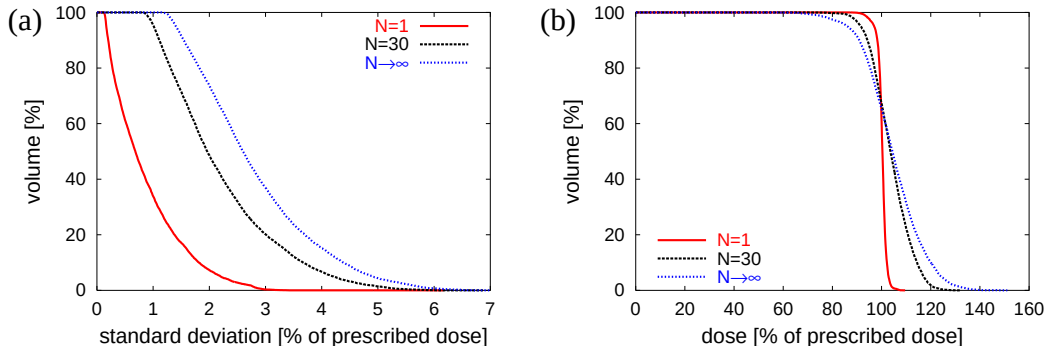

Figure 3.2: (a) Standard-deviation-volume-histogram (SDVH) of the CTV for the treatment plans optimized for $N = 1$, $N = 30$ and $N \to \infty$ (b) Dose-volume-histogram of the static dose distribution for the CTV for the treatment plans optimized for $N = 1$, $N = 30$ and $N \to \infty$

for the optimization. However, realistically the patient will still be irradiated with 30 fractions. Therefore, the standard deviation in figure 3.4c and 3.4d is normalized to 30 fractions to facilitate a comparison with figure 3.1, i.e. after the optimization we recalculate the standard deviation based on the static dose distribution while setting $N = 30$ in

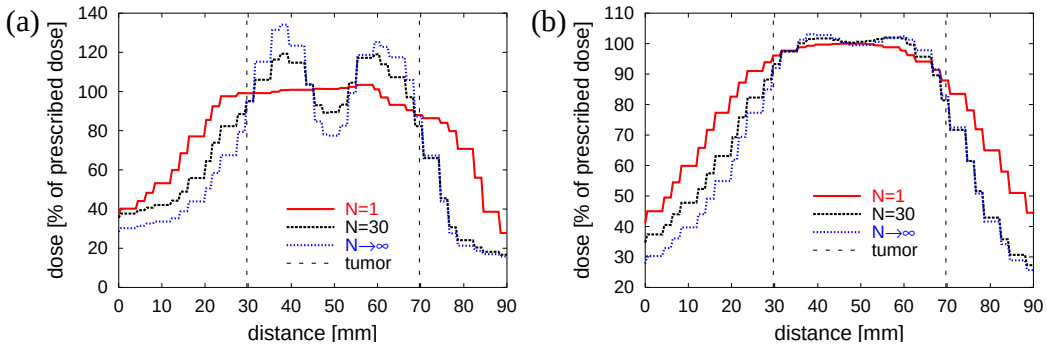

Figure 3.3: Profiles in AP-direction for the treatment plans optimized for $N = 1$, $N = 30$ and $N \to \infty$ located in the central slice in sagital view and the transversal slice shown in figure 3.1a: (a) for the static dose distribution (b) for the distribution of the expectation value of the dose

equation 3.10. We start with a discussion of the static dose distribution in figure 3.4e and 3.4f. The characteristic dose inhomogeneities in figure 3.1e and 3.1f have disappeared. Instead, the static dose distribution represents a safety margin like solution. The widely homogeneous high dose region is expanded towards the normal tissue, especially at the transition to the unclassified normal tissue. However, a decrease of the penalty factor for the rectum would also shift the dose gradient towards the rectum. For a single fraction, initial dose inhomogeneities could never be compensated for by later fractions. This is measured by the variance term in the objective function that hence effectively suppresses dose modulations. The homogeneity of the static dose distribution is also clarified by the dose profile in AP-direction in figure 3.3a (solid line). The absence of modulation of the static dose distribution reduces the standard deviation of the dose in the anatomy-based coordinate system (figure 3.4c-d). This can also be seen in the standard-deviation-volume-histogram in figure 3.2a (solid line). For roughly 70% of the CTV, the standard deviation due to a finite number of 30 fractions is no greater than 1% of the prescribed dose. The dose delivered to the CTV is well predictable which clearly is a favorable feature. However, the downside of the lower standard deviation is a worsening of the expectation value of the dose. Dose gradients at the edge of the tumor are smoother, leading to a worse target coverage and a worse sparing of healthy tissues. This can be seen from the isodose lines in figure 3.4a and 3.4b when carefully compared to 3.1a and 3.1b. The observation is supported by figures 3.3b and 3.5. Figure 3.3b shows a dose profile of the expectation value of the dose in AP-direction. The dose gradients are significantly flattened for the treatment plan optimized for $N = 1$ (solid line) when compared to the treatment plan optimized for $N = 30$ (dashed line). Figure 3.5 shows the dose-volume-histogram of the expectation value of the dose. Comparing the DVH for $N = 1$ and $N = 30$ in particular shows the increase in dose delivered to the rectum.

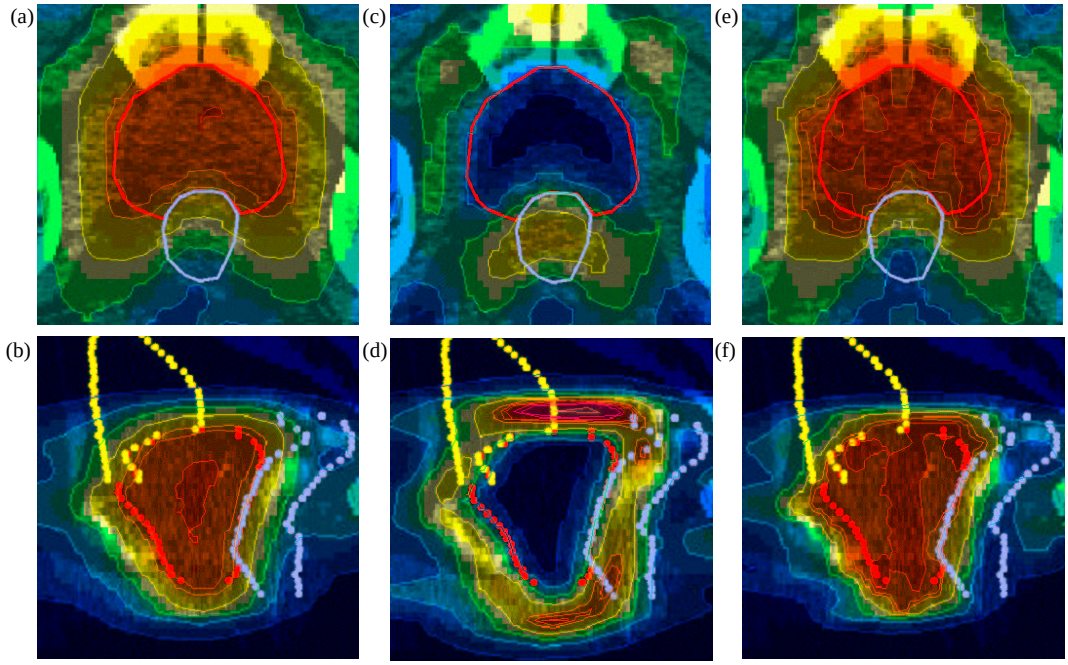

Figure 3.4: 3D distributions for a treatment plan optimized for one fraction (a-b) expectation value of the dose (c-d) standard deviation of the dose (e-f) static dose distribution (dose legend: see figure 3.8a)

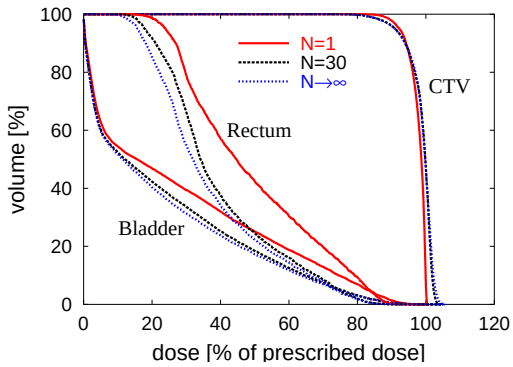

Figure 3.5: Dose-volume-histogram (DVH) of the expectation value of the dose distribution for the treatment plans optimized for $N = 1$, $N = 30$ and $N \to \infty$

3.2.5 Results: $N \to \infty$

Figure 3.6 shows the 3D distributions for a treatment plan that was optimized while the variance term was omitted in the objective function. This corresponds to the limit $N \to \infty$. The standard deviation in figure 3.6b is, however, normalized to 30 fractions. The static dose distribution (figure 3.6c) shows that the amplitude of modulation is increased when

compared to the optimization for $N = 30$. This becomes obvious also in the static dose profile in AP-direction in figure 3.3 (dotted line). Dose peaks rise up to 135 % of the prescribed dose, valleys go down below 80 %. This increase in modulation increases the standard deviation of the dose (see figure 3.6b in comparison with 3.1d and 3.4d). The standard-deviation-volume-histogram in figure 3.2a clearly shows the increase of the median standard deviation in the CTV. On the other hand, the expectation value of the dose distribution is improved. When compared to the optimization for $N = 30$ fractions, dose gradients at the transition between CTV and healthy tissue become slightly steeper (see the expectation value dose profile in figure 3.3b). The DVH of the expectation value (figure 3.5) indicates better sparing of the rectum for similar target coverage. However, the improvement is rather small and the increase of the variance of the dose makes the assumed benefit of the improved expectation value quite questionable.

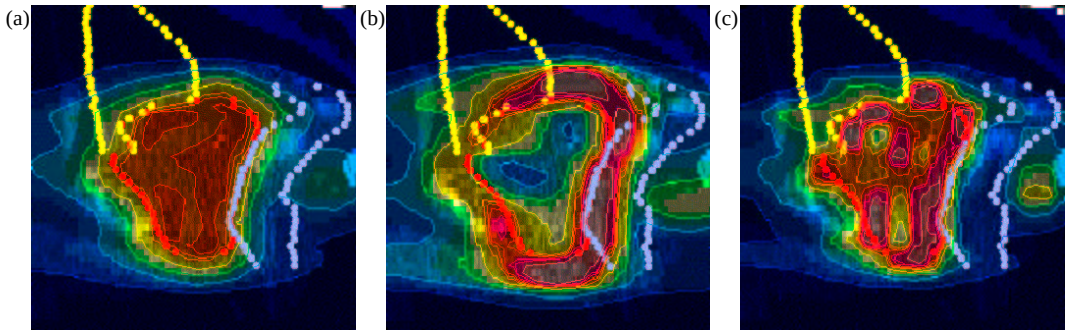

Figure 3.6: 3D distributions for a treatment plan where only the expectation value is optimized (limit $N \to \infty$) (a) expectation value of the dose (b) standard deviation of the dose (c) static dose distribution (dose legend: see figure 3.8a)

3.2.6 Results: small and large organ movements

For illustrative purpose we also discuss the two extreme cases of very large amplitudes of organ movements and rather small amplidudes of motion. For the large movement scenario we adopt standard deviations for voxel displacements of 10 mm in AP-direction and 8 mm in both CC- and LR-direction. Figure 3.7 compares the static dose distributions for treatment plans optimized for $N = 30$ (3.7a,c,e) and $N \to \infty$ (3.7b,d,f). It turns out that the magnitude of inhomogeneities is much higher now for $N \to \infty$ when compared to $N = 30$. The amplitude of the most pronounced dose peak exceeds 200% of the prescribed tumor dose. Dose valleys go down below 50% of the prescribed dose. Figure 3.9a shows the respective DVH of the static dose distributions. The increase in modulation causes larger standard deviations of the dose as depicted in the standard-deviation-volume-histogram in figure 3.9b and the 3D distributions in figures 3.7c-d. For organ movements of 8 mm and 5 mm motion amplitude as discussed in sections 3.2.3-3.2.5, such large modulations of the static dose distribution did not occur. When comparing the static dose distributions in

figure 3.1f and 3.6c, the difference is rather moderate, i.e. the variance term in objective function 3.11 has a limited impact on the optimization result. This changes if large organ movements are considered. In this case, the treatment plans optimized for $N = 30$ and $N \to \infty$ differ dramatically. For such large movements, the optimization of the expectation value alone would clearly be insufficient since it produces inhomogeneities in the static dose distribution that would not be fully compensated for by later fractions.
For the small movement case we adopt standard deviations for voxel displacements of 3 mm in AP-direction and 2 mm in both CC- and LR-direction. Figures 3.8b and 3.8c compare the static dose distributions for treatment plans optimized for $N = 30$ and $N \to \infty$. There are only minor differences between the two static dose distributions. The treatment plans optimized for $N = 30$ and $N \to \infty$ are almost identical, i.e. the variance term in the objective function has a negligible impact on the optimization result for such values of N. Figure 3.9a shows the DVH of the static dose distributions. The DVH of the treatment plan optimized for $N = 30$ can not be distinguished from the DVH of the treatment plan optimized for $N \to \infty$. Since the static dose distributions are almost identical, the expectation values and the standard deviations of the respective treatment plans are almost the same as well. Figure 3.9b shows the standard-deviation-volume-histogram, where there is again no visible difference between the treatment plans optimized for $N = 30$ and $N \to \infty$. In summary, we observe that treatment plans optimized for $N = 30$ and $N \to \infty$ differ strongly for large amplitudes of organ motion, but for small movements both treatment plans are almost identical. We suppose that this effect can to some extent be explained by the resolution of beamlets which was $(10\ mm)^2$ in this study. The length scale on which modulations in the static dose distribution have to occur is determined by the magnitude of movements. The required distance of a dose peak from a dose valley is in the order of the standard deviation of the voxel displacements so that initial inhomogeneities can be compensated for by later fractions. With a beamlet resolution of $(10\ mm)^2$, dose modulations can not be shaped sufficiently precise as required for small movements even though 7 beams are assumed for treatment planning. Hence, large inhomogeneities are not formed in the optimization, independent of the variance term in the objective function. We hypothesize that the optimization process would be more sensitive to the parameter N if a smaller beamlet resolution was applied, even for relatively small amplitudes of motion. At the current stage, we could not verify this hypothesis by simulations due to limitations of RAM storage capacity. For sufficiently small movements, the ability to form modulations of the static dose distribution is of course limited due to lateral scattering of photons.

3.2.7 Discussion

Section 3.2.3 to 3.2.6 intend to emphasize the generic features of probabilistic treatment planning as an off-line strategy to incorporate organ movements in inverse planning. With the objectives of sparing healthy tissues from dose burden while the dose coverage of the tumor is not compromised, the optimization concept leads to inhomogeneous dose distributions in the static coordinate system. If the internal organ movements during the treatment

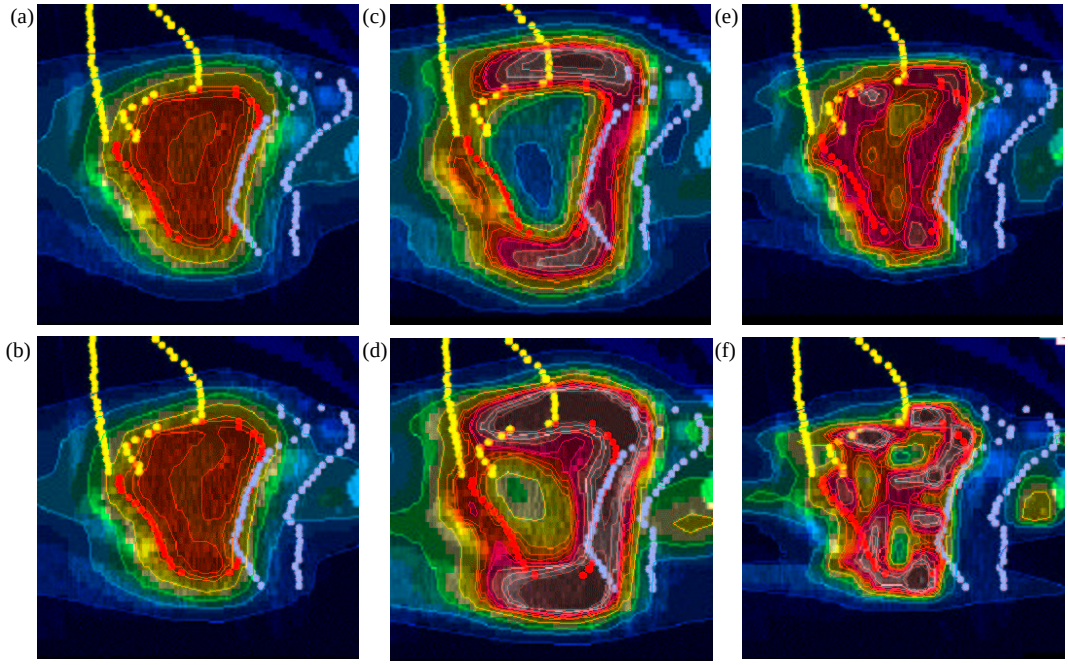

Figure 3.7: 3D distributions for a treatment plan incorporating large tumor motion: (a,c,e) optimized for $N = 30$ (b,d,f) optimized for $N \to \infty$ (a-b) expectation value of the dose (c-d) standard deviation of the dose (e-f) static dose distribution (dose legend: see figure 3.8a)

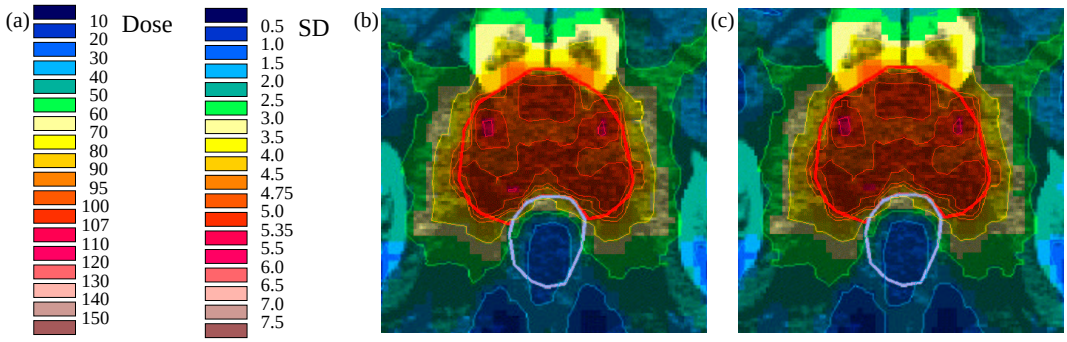

Figure 3.8: (a) color coding for dose and standard deviation (in % of prescribed dose) (b-c) static dose distributions for a treatment plan incorporating small tumor motion (b) optimized for $N = 30$ (c) optimized for $N \to \infty$

course occur as predicted at the time of treatment planning, these dose inhomogeneities will be smoothed out. Consequently, a more or less homogeneous dose distribution in the anatomy-based coordinate system will be delivered to the patient, characterized by the expectation value of the dose. In reality, the expectation value of the dose will not be

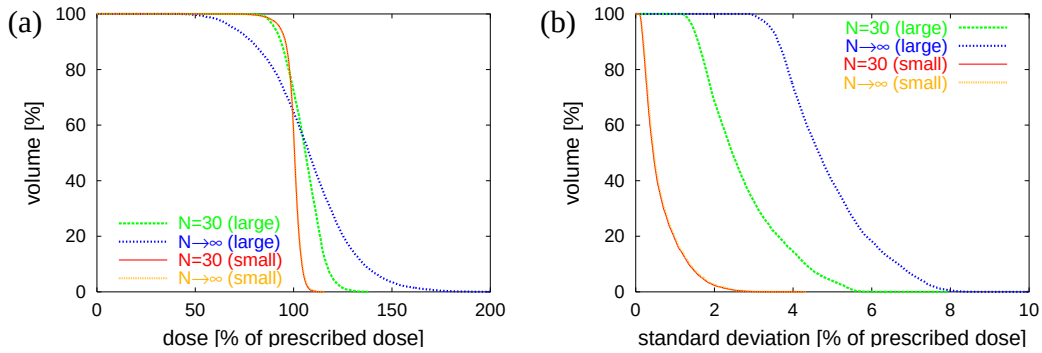

Figure 3.9: (a) Dose-volume-histograms of the static dose distribution for the CTV for treatment plans incorporating large/small movements, optimized for $N = 30$ and $N \to \infty$ (b) corresponding standard-deviation-volume-histogram (SDVH) of the CTV

realized. We have characterized the uncertainty of the treatment plan by the standard deviation of the dose distribution. The standard deviation within the CTV is closely related to the magnitude of modulation of the static dose distribution. The parameter N, the number of fractions, can be used to control the standard deviation of the dose during the optimization process, which in turn controls the modulation of the static dose distribution. Modulations of the static dose distribution potentially allow for a better sparing of healthy tissue since they lead to steeper dose gradients in the expectation value of the dose. On the other hand, these modulations bear risks. When organ movements during the actual treatment are significantly smaller than assumed at the time of treatment planning, the delivered dose distribution in the patient may be strongly inhomogeneous. In the limit that no movements occur, the static dose distribution will be delivered to the patient. The treatment planner has to find a reasonable trade-off between risk and potential benefit. By including the variance of the dose into the objective function, we, in principle, define the optimal trade-off mathematically when N is the actual number of fractions. From a mathematical point of view, the optimal treatment plan is simply defined by the minimum of the objective function. However, optimizing the expectation value of a quadratic objective function corresponds to optimizing the average treatment outcome. This is not necessarily appropriate to avoid worst case scenarios, i.e. bad cumulative dose distributions for some patients. From this point of view, the parameter N could be considered as a regularization parameter which is used to control the trade-off between potential benefit and risk - although this does not represent the initial intention.
For small amplitudes of internal prostate movements in the order of 2-3 mm standard deviation, the inverse planning concept based on probability distributions is less sensitive to the parameter N when a beamlet resolution of $(10\ mm)^2$ is applied. This may indicate that the variance term in objective function (3.11) is less important for most patients and that an optimization of the expectation value of the dose may be sufficient. However, we hypothesize that the situation may change if IMRT was planned for a multi leaf col-

limator with smaller leaf width. In this case, modulations of the static dose distribution could be shaped more precisely and may strongly depend on N even for relatively small movements. In addition, the inclusion of the variance in the objective function allows for generalizations, i.e. uncertainties in the magnitude of motion and systematic errors can be incorporated (sections 3.3-3.6).
In chapter 2.4 we analyzed probabilistic treatment planning to incorporate random errors for an idealized geometry. The prostate patient study in this section has now reinforced the major results of the previous chapter.

3.3 Dose calculation in the presence of systematic errors and an uncertain magnitude of motion

This section describes the inclusion of systematic errors and an uncertain magnitude of motion into the calculation of the expected dose and its variance. Two seperate tools have been developed or modified for this purpose. In order to incorporate these additional uncertainties into the optimization of the treatment plan, the inverse planning tool KonRad was extended. In addition, an external program was implemented which calculates expected dose and variance based on the static dose distribution of a previously optimized treatment plan. This tool is independent of the optimization of the treatment plan. The implementation of this program was achieved by a diploma thesis at DKFZ [9].

3.3.1 A simulation and visualization tool for assessing dose uncertainties

We briefly describe the mathematical basis and the output of the simulation tool. The mathematical basis is mainly governed by section 2.1 and this section will only recall the results but not their derivation. One aim of the simulation tool is the calculation of expected dose and variance which is done by simulating a large number of treatment scenarios. Mathematically, this corresponds to a Monte Carlo integration of the respective integrals.

The incorporation of uncertainties in the magnitude of motion was implemented for uncorrelated movements in the three spatial dimensions, i.e. the covariance matrix $\boldsymbol{C}_i$ is assumed to be diagonal for each voxel:

$$\boldsymbol{C}_i = \begin{pmatrix} \sigma_{xi}^2 & 0 & 0 \\ 0 & \sigma_{yi}^2 & 0 \\ 0 & 0 & \sigma_{zi}^2 \end{pmatrix} \tag{3.19}$$

The expectation value of the cumulative dose in the moving coordinate system is given by

$$\begin{aligned}\langle D_i \rangle &= \int \cdots \int \left(\frac{1}{N} \sum_{\mu=1}^{N} D^{stat}(\boldsymbol{r}_\mu) \right) \prod_{\mu=1}^{N} P(\boldsymbol{r}_\mu | \Delta \boldsymbol{s}_i, \boldsymbol{\sigma}_i) \\ &\quad \times P(\Delta \boldsymbol{s}_i | \boldsymbol{\sigma}_i, \boldsymbol{S}_i) P(\boldsymbol{\sigma}_i | \boldsymbol{\Sigma}_i) \prod_{\mu=1}^{N} d\boldsymbol{r}_\mu d\Delta \boldsymbol{s}_i d\boldsymbol{\sigma}_i \end{aligned} \tag{3.20}$$

The dose $D^{stat}(\boldsymbol{r})$ refers to the dose value of the static dose field at position $\boldsymbol{r} = (x, y, z)^T$. The static dose distribution is assumed to be constant within a static voxel, i.e. no interpolation between neighboring voxels was implemented. The three dimensional vector $\boldsymbol{S}_i = (S_{xi}, S_{yi}, S_{zi})^T$ denotes the estimated mean position of the voxel i and the three components of $\boldsymbol{\Sigma}_i$ denote the estimated distribution widths of the Gaussian based on the patient data. $\Delta \boldsymbol{s}_i$ is the systematic error, the deviation of the estimated mean position $\boldsymbol{S}_i$ from the real mean position. The components of $\boldsymbol{\sigma}_i$ denote the magnitudes of motion in the three directions realized by the patient. The distributions for $\boldsymbol{r}_\mu$, $\Delta \boldsymbol{s}_i$ and $\boldsymbol{\sigma}_i$ factorize with respect to the three spatial coordinates:

$$P(\boldsymbol{r}_\mu | \Delta \boldsymbol{s}_i, \boldsymbol{\sigma}_i) = P(x_\mu | \Delta s_{xi}, \sigma_{xi}) P(y_\mu | \Delta s_{yi}, \sigma_{yi}) P(z_\mu | \Delta s_{zi}, \sigma_{zi}) \tag{3.21}$$

$$P(\Delta \boldsymbol{s}_i | \boldsymbol{\sigma}_i, \boldsymbol{S}_i) = P(\Delta s_{xi} | \sigma_{xi}, S_{xi}) P(\Delta s_{yi} | \sigma_{yi}, S_{yi}) P(\Delta s_{zi} | \sigma_{zi}, S_{zi}) \tag{3.22}$$

$$P(\boldsymbol{\sigma}_i | \boldsymbol{\Sigma}_i) = P(\sigma_{xi} | \Sigma_{xi}) P(\sigma_{yi} | \Sigma_{yi}) P(\sigma_{zi} | \Sigma_{zi}) \tag{3.23}$$

The probability distributions for each spatial coordinate are derived in section 2.1 and are only repeated here:

$$P(x_\mu | \Delta s_{xi}, \sigma_{xi}) = \frac{1}{2\pi\sigma_{xi}^2} \exp\left(-\frac{(x_\mu - \Delta s_{xi})^2}{2\sigma_{xi}^2} \right) \tag{3.24}$$

$$P(\Delta s_{xi} | \sigma_{xi}, S_{xi}) = \frac{1}{2\pi\frac{\sigma_{xi}^2}{M}} \exp\left(-\frac{(\Delta s_{xi} - S_{xi})^2}{2\frac{\sigma_{xi}^2}{M}} \right) \tag{3.25}$$

$$P(\sigma_{xi} | \Sigma_{xi}) \propto \frac{1}{(2\pi\sigma_{xi}^2)^{M-1}} \exp\left(-\frac{\Sigma_{xi}^2}{2\frac{\sigma_{xi}^2}{M}} \right) \tag{3.26}$$

The variance of the cumulative dose is given by

$$V_i = \left(\langle D_i^2 \rangle - \langle D_i \rangle^2 \right) \tag{3.27}$$

where

$$\begin{aligned}\langle D_i^2 \rangle &= \int \cdots \int \left(\frac{1}{N} \sum_{\mu=1}^{N} D^{stat}(\boldsymbol{r}_\mu) \right)^2 \prod_{\mu=1}^{N} P(\boldsymbol{r}_\mu | \Delta \boldsymbol{s}_i, \boldsymbol{\sigma}_i) \\ &\quad \times P(\Delta \boldsymbol{s}_i | \boldsymbol{\sigma}_i, \boldsymbol{S}_i) P(\boldsymbol{\sigma}_i | \boldsymbol{\Sigma}_i) \prod_{\mu=1}^{N} d\boldsymbol{r}_\mu d\Delta \boldsymbol{s}_i d\boldsymbol{\sigma}_i \end{aligned} \tag{3.28}$$

The integrals in equations 3.20 and 3.28 can be evaluated by Monte Carlo simulation. The steps of such a simulation are as follows:

1. Randomly select the three components of the distribution width $\boldsymbol{\sigma}_i$ from the distribution 3.26 with the appropriate values of $\boldsymbol{\Sigma}_i$ for each spatial direction.

2. Randomly select the three components of the systematic error $\Delta \boldsymbol{s}_i$ from the distribution 3.25 with the appropriate values of $\boldsymbol{S}_i$ for each spatial direction and the values of $\boldsymbol{\sigma}_i$ chosen in the first step.

3. Randomly select a set of N positions $\boldsymbol{r}_\mu$ from the distribution 3.24 with the appropriate values of $\Delta \boldsymbol{s}$ and $\boldsymbol{\sigma}$ chosen in the first and second step.

4. Calculate the cumulative dose

$$D_{in} = \sum_{\mu=1}^{N} \frac{1}{N} D^{stat}(\boldsymbol{r}_\mu) \tag{3.29}$$

   and the cumulative dose squared

$$D_{in}^2 = \left(\sum_{\mu=1}^{N} \frac{1}{N} D^{stat}(\boldsymbol{r}_\mu) \right)^2 \tag{3.30}$$

   where the index n refers to the number of the simulation.

After the simulation of a large number of treatments n_{sim}, the expectation value of the dose can be estimated as

$$\langle D_i \rangle \approx \frac{1}{n_{sim}} \sum_{n=1}^{n_{sim}} D_{in} \tag{3.31}$$

and the variance can be estimated as

$$V_i \approx \left(\frac{1}{n_{sim}} \sum_{n=1}^{n_{sim}} D_{in}^2 \right) - \left(\frac{1}{n_{sim}} \sum_{n=1}^{n_{sim}} D_{in} \right)^2 \tag{3.32}$$

The simulation procedure allows for the output of additional surrogates to assess the dose delivered to a voxel. For example one can estimate the probability that the dose delivered to a voxel is within a predefined dose interval. For example, the probability that the dose delivered to voxel i is within a 5% tolerance interval around the prescribed dose D^{pres} is approximately given by

$$P_i^{95-105} \approx \frac{1}{n_{sim}} \sum_{n=1}^{n_{sim}} \Theta(1.05 D_{CTV} - D_{in}) \Theta(D_{in} - 0.95 D_{CTV}) \tag{3.33}$$

with the Heavyside step function Θ.
The simulation tool allows for an analysis of the impact of the different uncertainties, i.e.

random errors, systematic errors and uncertain magnitude of motion. When uncertainties in the magnitude of motion are neglected, the first step in the simulation procedure is omitted and the same values for the distribution widths are applied in each treatment simulation. Formally, this corresponds to replacing the probability distribution $P(\boldsymbol{\sigma}_i|\boldsymbol{\Sigma}_i)$ by a Dirac δ-function located at the desired value of $\boldsymbol{\sigma}_i$.

3.3.2 Implementation into the optimization tool KonRad

Most aspects of the optimization are similar or identical to the methods introduced in section 3.2.1 for random errors. We still use objective function 3.11 for the optimization of the fluence maps. The only difference is that the expected dose $\langle D \rangle$ and the variance V now involve systematic errors and uncertainties in the magnitude of motion according to the definitions in equation 3.20 and 3.27/3.28, respectively. The expectation value of the dose and the variance can be written as a function of the beamlet weights using a dose contribution matrix and the variance contribution tensor.
Exemplarily, the calculation of the variance contribution tensor is described here. The variance V_i in voxel i is

$$V_i = \frac{1}{N} \sum_{\alpha,\beta} Q_{i\alpha\beta} \Phi_\beta \Phi_\alpha \tag{3.34}$$

The tensor element $Q_{i\alpha\beta}$ is calculated according to

$$\begin{aligned} Q_{i\alpha\beta} \;=\; & \left[\int \cdots \int \left(\frac{1}{N} \sum_{\mu=1}^{N} G_\alpha^{stat}(\boldsymbol{r}_\mu) \right) \left(\frac{1}{N} \sum_{\mu=1}^{N} G_\beta^{stat}(\boldsymbol{r}_\mu) \right) \prod_{\mu=1}^{N} P(\boldsymbol{r}_\mu|\Delta\boldsymbol{s}_i, \boldsymbol{\sigma}_i) \right. \\ & \left. \times\, P(\Delta\boldsymbol{s}_i|\boldsymbol{\sigma}_i, \boldsymbol{S}_i) P(\boldsymbol{\sigma}_i|\boldsymbol{\Sigma}_i) \prod_{\mu=1}^{N} d\boldsymbol{r}_\mu d\Delta\boldsymbol{s}_i d\boldsymbol{\sigma}_i \right] - G_{i\alpha} G_{i\beta} \end{aligned} \tag{3.35}$$

where the effective dose contribution matrix element $G_{i\alpha}$ is given by

$$\begin{aligned} G_{i\alpha} \;=\; & \int \cdots \int \left(\frac{1}{N} \sum_{\mu=1}^{N} G_\alpha^{stat}(\boldsymbol{r}_\mu) \right) \prod_{\mu=1}^{N} P(\boldsymbol{r}_\mu|\Delta\boldsymbol{s}_i, \boldsymbol{\sigma}_i) \\ & \times P(\Delta\boldsymbol{s}_i|\boldsymbol{\sigma}_i, \boldsymbol{S}_i) P(\boldsymbol{\sigma}_i|\boldsymbol{\Sigma}_i) \prod_{\mu=1}^{N} d\boldsymbol{r}_\mu d\Delta\boldsymbol{s}_i d\boldsymbol{\sigma}_i \end{aligned} \tag{3.36}$$

$G_\alpha^{stat}(\boldsymbol{r}_\mu)$ is the dose contribution of beamlet α to the point $\boldsymbol{r}_\mu$ in the static coordinate system. The integrals in 3.35 are evaluated by Monte Carlo calculation for the dose distributions of all pairs of beamlets α and β using the procedure described in section 3.3.1.

3.4 Difficulties in treatment plan evaluation and visualization

Before we analyze the impact of different uncertainties on the result of treatment plan optimization in section 3.5 and 3.6, we focus on the problem of treatment plan evaluation in general. It was already discussed in section 3.2 that the dose distribution is a random variable and treatment plan evaluation thus complicated. The difficulty is enlarged when additionally systematic errors and an uncertain magnitude of motion are taken into account.

We consider a treatment plan that was optimized by incorporating uncertainties in the magnitude of motion ($P(\boldsymbol{\sigma}|\boldsymbol{\Sigma})$), systematic errors ($P(\Delta\boldsymbol{s}|\boldsymbol{\sigma}, \boldsymbol{S})$) and random errors ($P(\boldsymbol{r}_\mu|\Delta\boldsymbol{s}, \boldsymbol{\sigma})$). It is assumed that $M = 5$ CT scans are performed prior to treatment and that the following set of motion model parameters was estimated from these images for all voxels i:

$$\boldsymbol{\Sigma}_i = \frac{M-1}{M} \begin{pmatrix} 3mm \\ 4mm \\ 3mm \end{pmatrix} \tag{3.37}$$

where the x-coordinate corresponds to the LR-direction, the y-coordinate to the AP-direction and the z-coordinate to the CC-direction. The factor $\frac{M-1}{M}$ is introduced in order to make 3 mm and 4 mm the unbiased estimates of the standard deviation of voxel displacements whereas $\boldsymbol{\Sigma}_i$ refers to the maximum likelihood estimate (2.1.2). The estimated mean position $\boldsymbol{S}_i$ is assumed to be identical to the position in the planning CT for all voxels. The treatment plan is optimized for $N = 30$ fractions.

Figure 3.10a shows the static dose distribution of the optimized treatment plan. As expected, the static dose distribution shows some moderate dose peaks at the edge of the tumor. The highest dose peaks are approximately 110% of the prescribed dose. In figure 3.10b, the modulation pattern of the static dose field is illustrated in more detail. It shows the difference of the static dose and the prescribed dose in each voxel. The static dose distribution is important to understand the generic features of the probabilistic treatment planning approach. However, it is per definition not the dose distribution we expect to be realized in the patient. In the context of treatment plan evaluation we are primarily interested in assessing the dose that is finally delivered to the patient. We can look at the expectation value of the dose (figure 3.10c) which provides the best estimate of the delivered dose for each voxel. The overall expectation value of the dose is relatively difficult to interpret because the expected dose can never be realized at all voxels simultaneously. The expectation value involves averaging over the systematic error and different magnitudes of motion. This averaging process occurs only for a population of patients but not for the individual patient. The spatial 3D distribution of dose expectation values is therefore not a good surrogate for the delivered dose distribution as a whole. It has to be interpreted for each voxel separately. Since we know that the expectation value is not realized, we can

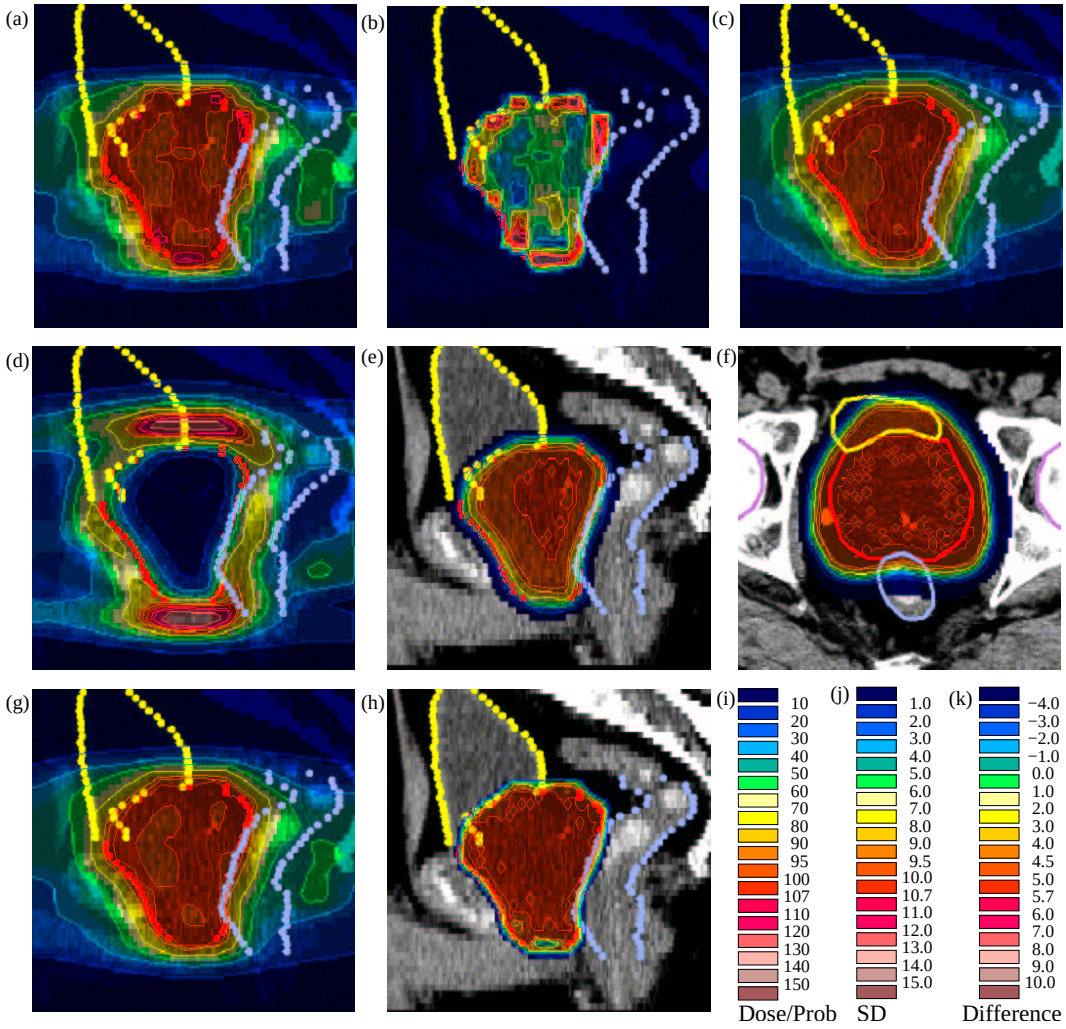

Figure 3.10: 3D distributions for treatment plan evaluation in the presence of interfractional organ movements: (a) static dose distribution (b) difference of static dose and prescribed dose (c) overall expectation value of the dose (d) overall standard deviation of the dose (e) probability that a voxel receives a dose within a 5% tolerance interval around the prescribed dose (f) probability that a voxel receives a dose above 75% of the prescribed dose (g) expectation value of the dose for a certain realization of the motion model parameters (h) probability that a voxel receives a dose within a 5% tolerance interval around the prescribed dose given a certain realization of the motion model parameters (i,j,k) color coding for dose/probability, standard deviation and dose difference, respectively (in percent of the prescribed dose)

in addition look at the overall uncertainty of this dose prediction, too, i.e. the standard deviation in figure 3.10d. The dose uncertainty is relatively small in the inner region of the CTV (in the order of 1-2% of the prescribed dose). At the edge of the CTV, the standard

deviation is approximately 5% of the prescribed dose. The largest values occur in the adjacent healthy tissue above and below the CTV, with peaks of 10-15% of the prescribed dose.
One aspect of treatment plan evaluation is to ensure a sufficient target coverage. To assess the target coverage, the treatment planner has to combine the information of the expectation value and the standard deviation. When the expected dose in a voxel is close to the prescribed dose and the standard deviation of the dose is small, this voxel will very likely receive a sufficient dose. Figure 3.10e shows the probability that a voxel receives a dose within a 5% tolerance interval around the prescribed dose. Such an illustration allows for directly assessing the probability of sufficient target coverage. It may be a valuable tool for treatment plan evaluation. Similar pictures can be used to estimate the risk for overdosing an organ at risk. Figure 3.10f shows the probability that a voxel receives a dose above 75% of the prescribed dose.
Figure 3.10g shows the expectation value of the dose for a certain realization of the motion model parameters. We choose $\Delta \boldsymbol{s} = 0$ and $\boldsymbol{\sigma} = \frac{M}{M-1}\boldsymbol{\Sigma}$. Thus, the blurring of the static dose distribution is due to the random error only. Figure 3.10g is therefore a better surrogate for the 3D dose distribution which may approximately be realized (in contrast to the overall expectation value in figure 3.10c). However, it does not contain the information about the systematic error. Figure 3.10h shows the probability that a voxel receives a dose within a 5% tolerance interval around the prescribed dose given the realization of the motion model parameters $\Delta \boldsymbol{s} = 0$ and $\boldsymbol{\sigma} = \frac{M}{M-1}\boldsymbol{\Sigma}$. It can, for example, be observed that voxels in the most caudal part of the prostate will probably be overdosed. Figure 3.10h shows, that the probability for delivering a dose within the 5% tolerance interval is quite low and combination with figure 3.10b one can conclude that these voxels will mostly be overdosed. This information is not that obvious in figure 3.10e which involves the averaging over the systematic error and different magnitudes of motion.
In summary it can be stated that a large variety of pictures can be used to assess the dose distribution delivered to the patient. None of them seems to be perfect or even sufficient all alone. At the current stage, it is not clear which type of illustration will turn out most useful in a clinical environment.

3.5 The impact of systematic errors on the optimized treatment plan

In this section, we focus on the impact of systematic errors on treatment plan optimization and neglect uncertainties in the magnitude of motion. We assume motion amplitudes of 4 mm in AP direction and 3 mm in both LR and CC direction for all voxels and optimize a treatment plan for $N = 30$ fractions. We optimize treatment plans for different systematic errors und compare the three cases $M = 1$ (only a single CT scan), $M = 5$ (5 CT scans provided) and $M \to \infty$ (no systematic error). All parameters of the optimization are kept constant, except the number of CT scans M.

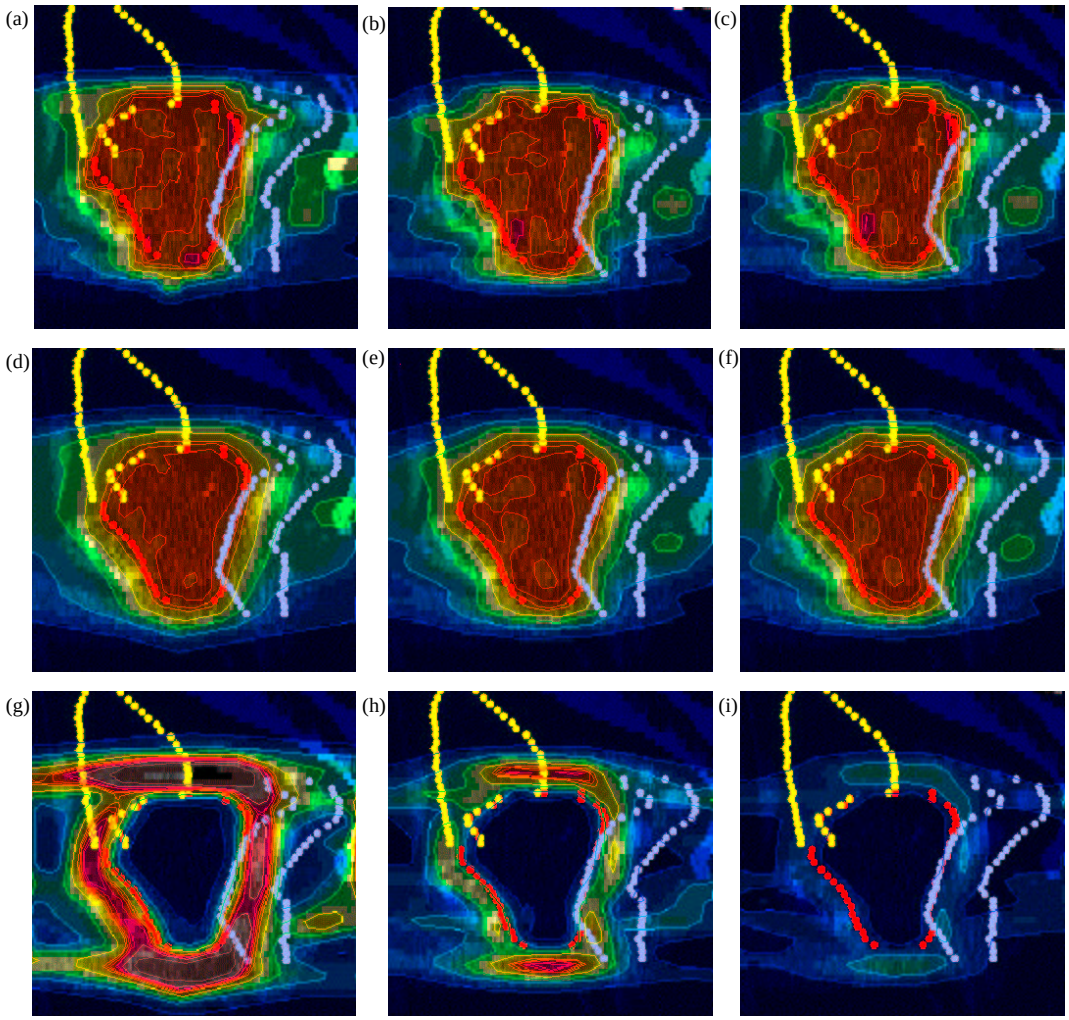

Figure 3.11: 3D distributions for treatment plans incorporating different systematic errors. The columns show the treatment plans optimized for $M = 1$ (a,d,g), $M = 5$ (b,e,h) and $M \to \infty$ (c,f,i). The three rows show the static dose distribution (a,b,c), the expectation value of the dose (d,e,f) and the standard deviation of the dose (g,h,i), respectively. For the color coding, the legends in figures 3.12c-d apply.

Figure 3.11 shows the treatment plans optimized for $M = 1$, $M = 5$ and $M \to \infty$. The pictures in the upper row show the static dose distributions. In the static dose distribution for $M = 1$ (figure 3.11a), the high dose region is more expanded compared to $M = 5$ (figure 3.11b) and $M \to \infty$ (figure 3.11c). This is also emphasized in figure 3.12a which shows the difference of the static dose distributions for $M = 1$ and $M = 5$. In the transition region between CTV and healthy tissue, the dose for $M = 1$ is up to 25% of the prescribed dose higher compared to $M = 5$. Figure 3.12b shows the difference of the static dose fields for

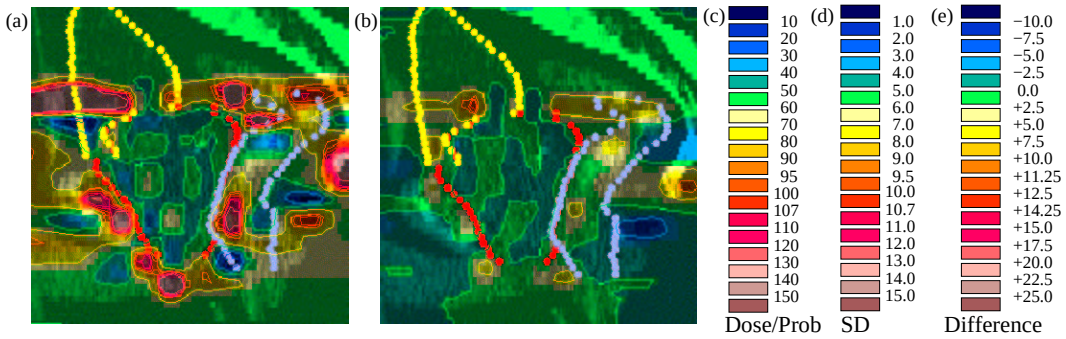

Figure 3.12: (a) Difference of the static dose distributions optimized for $M = 1$ (figure 3.11a) and $M = 5$ (figure 3.11b) (b) Difference of the static dose distributions optimized for $M = 5$ (figure 3.11b) and $M \to \infty$ (figure 3.11c) (c) color coding for dose distributions (d) color coding for the standard deviation (e) color coding for the dose difference plots

$M = 5$ and $M \to \infty$. The high dose region is more expanded for $M = 5$ compared to the case where systematic errors are eliminated. However, the difference between $M = 1$ and $M = 5$ is significantly larger compared to the difference between $M = 5$ and $M \to \infty$. This result is confirmed in figure 3.13a which shows profiles of the static dose distributions in AP direction in the lower part of the prostate.

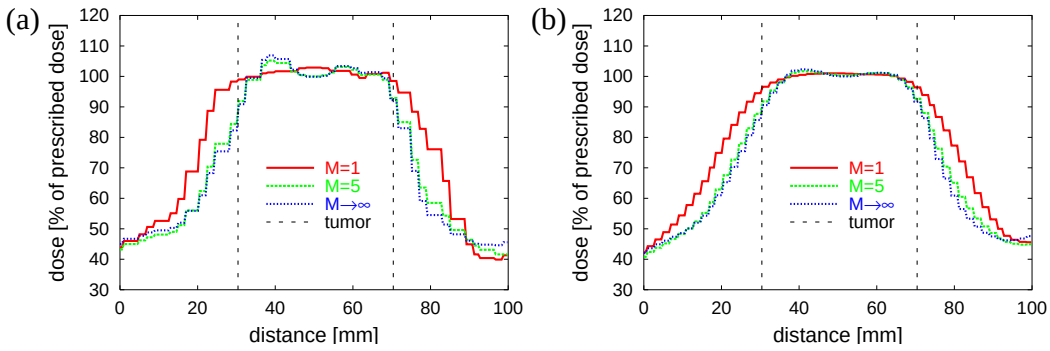

Figure 3.13: Dose profiles in AP direction for different systematic errors (located in the central slice in sagittal view in the lower part of the prostate) (a) for the static dose distributions in figure 3.11a-c (b) for the expectation value of the dose distributions in figure 3.11d-f

Figures 3.11d-f show the corresponding 3D distributions of expectation values of the dose in each voxel. Corresponding dose profiles in AP direction are depicted in figure 3.13b. The distributions of expectation values reflect the more expanded high dose region for large systematic errors. In order to make the expected dose close to the prescribed dose

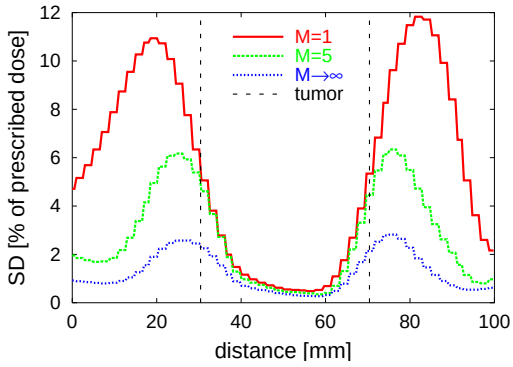

Figure 3.14: Profiles for the standard deviation of the dose in figures 3.11g-i (located in the central slice in sagittal view in the lower part of the prostate)

for voxels at the edge of the tumor, the irradiated area has to be expanded significantly for the large systematic error ($M = 1$). Figures 3.11g-i show the standard deviations of the dose. Generally, the optimization shapes the static dose distribution in such a way that the dose uncertainty is small within the CTV. The large systematic error for $M = 1$ causes a relatively large region in the adjacent healthy tissue where the dose is not very well predictable and different dose values may be realized. The enlarged region of uncertain dose values is also illustrated in figure 3.14 which shows profiles of the standard deviation in AP direction.

3.6 The impact of different sources of uncertainty on the optimized treatment plan

In this section, we analyse the impact of the three sources of uncertainty (magnitude of motion, systematic errors, random errors) on the optimized treatment plan. We compare the three different cases:

1. Incorporating all three sources of uncertainty into the optimization
2. Incorporating systematic errors and random errors:
   constant $\boldsymbol{\sigma}$: $P(\boldsymbol{\sigma}|\boldsymbol{\Sigma}) = \delta(\boldsymbol{\sigma} - \frac{M}{M-1}\boldsymbol{\Sigma})$
3. Incorporating only random errors:
   constant $\boldsymbol{\sigma}$: $P(\boldsymbol{\sigma}|\boldsymbol{\Sigma}) = \delta(\boldsymbol{\sigma} - \frac{M}{M-1}\boldsymbol{\Sigma})$
   no systematic error: $P(\Delta\boldsymbol{s}|\boldsymbol{\sigma}, \boldsymbol{S}) = \delta(\Delta\boldsymbol{s} - \boldsymbol{S})$

We consider the same parameter set as in section 3.4, i.e. $N = 30$ fractions, $M = 5$ CT scans, estimated amplitudes of motion of 4mm in AP and 3mm in LR/CC direction. No prior knowledge about the amplitude of motion is incorporated.

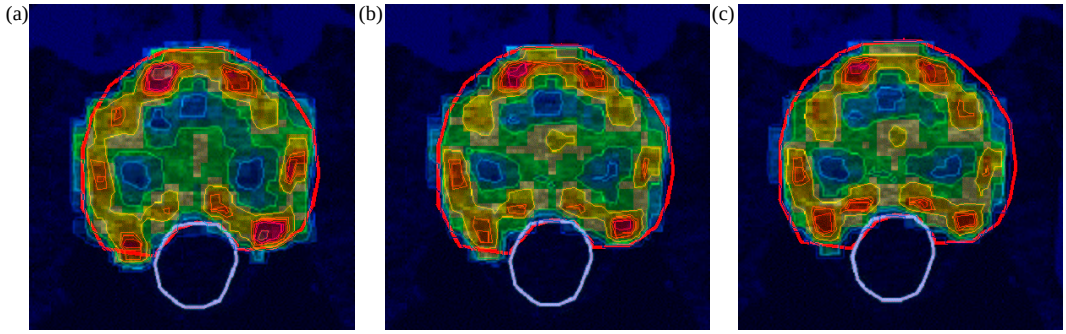

Figure 3.15: Modulation pattern of the static dose distributions for the three treatment plans. The difference of static dose and prescribed dose is shown (the color code legend in figure 3.10k applies): (a) for the treatment plan incorporating random errors, systematic errors and an uncertain magnitude of motion (figure 3.10a) (b) for the treatment plan incorporating random errors and systematic errors (figure 3.11b) (c) for the treatment plan incorporating only random errors (figure 3.10c)

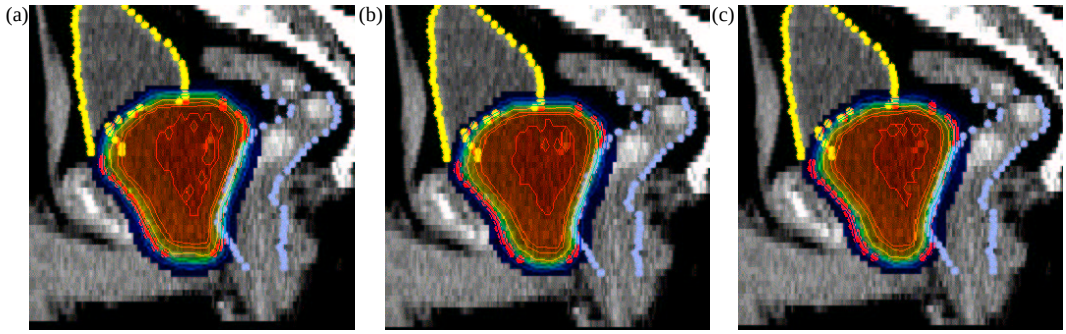

Figure 3.16: Probability that a voxel receives a dose within a 5% tolerance interval around the prescribed dose, taking into account all three types of uncertainties (a) for the treatment plan incorporating random errors, systematic errors and an uncertain magnitude of motion (figure 3.10a) (b) for the treatment plan incorporating random errors and systematic errors during the optimization (figure 3.11b) (c) for the treatment plan incorporating only random errors (figure 3.10c). The color code legend in figure 3.10i applies.

The respective static dose distributions were already presented in figures 3.10a, 3.11b and 3.11c. In figure 3.15a-c the differences of the static dose distributions and the prescribed dose are depicted. It is observed that the modulation pattern of the static dose distribution is similar for all three treatment plans. The major difference between the three treatment plans is that the high dose region is more expanded into the healthy tissue when more uncertainties are taken into account. It is intuitive that the inclusion of systematic errors should not change the modulation pattern too much. For the individual patient, the averaging process that levels out the static dose inhomogeneities is only due to the random

error which remains the same. Figure 3.17 shows dose profiles in AP direction for the static dose distributions and the expectation values of the dose. These profiles show the expansion of the irradiated volume around the prostate when additional sources of uncertainty are considered.
When systematic errors or uncertainties in the magnitude of motion are neglected during the optimization process, this may result in an insufficient target coverage. Figure 3.16a-c shows the probability that a voxel receives a dose within a 5% tolerance interval around the prescribed dose for the three treatment plans. For the retrospective calculation of these probabilities, all three types of uncertainties were incorporated (in contrast to the treatment planning process). Figure 3.16c shows the risk of underdosing the edge of the CTV when only random errors are taken into account during the optimization. Figure 3.18 shows the corresponding profiles in AP direction.

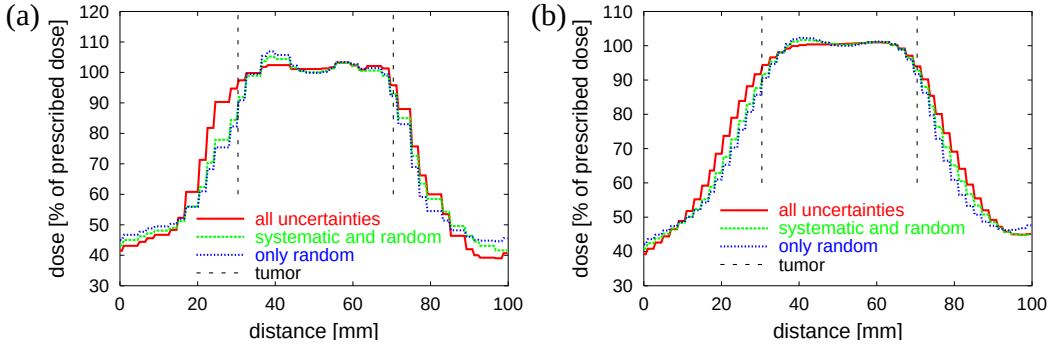

Figure 3.17: Dose profiles (located in the central slice in sagittal view in the lower part of the prostate) for the treatment plans incorporating a different amount of uncertainty (a) of the static dose distributions in figures 3.10a, 3.11b and 3.11c (b) of the expectation values of the dose distribution in 5% tolerance probabilities in figures 3.10c, 3.11e and 3.11f

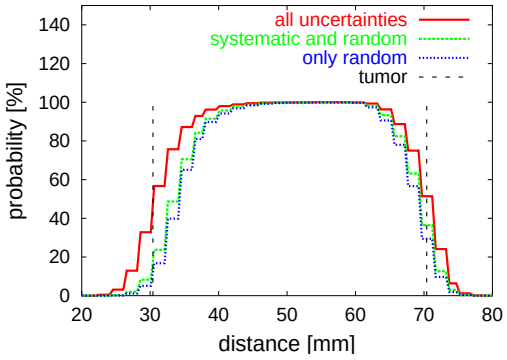

Figure 3.18: Profiles (located in the central slice in sagittal view in the lower part of the prostate) of the 5% tolerance probabilities in figure 3.16

Chapter 4

Dealing with respiratory motion

This section deals with the application of probabilistic treatment planning to respiratory motion as for the case of lung tumors. It is again the aim to determine the dose distribution that minimizes the expectation value of the quadratic objective function 1.12. The major difficulty in the context of respiratory motion is the evaluation of the variance term. For inter-fractional motion, the variance of the dose is independent of the dose delivery process. It is determined by the static dose distribution but independent of the way the static dose distribution is realized in practice. For respiratory motion, temporal aspects of the dose delivery process come into play. In this chapter a motion model is introduced which is applied to model respiratory motion. Like for inter-fractional motion, an idealized geometry is considered first in order to demonstrate the mathematical formalism and generic features of the approach. In chapter 5, the concepts developed in this chapter are transferred to a clinical lung case.

4.1 The idealized geometry

In order to develop a concept to incorporate respiratory motion in IMRT optimization, a one-dimensional geometry is considered. A one-dimensional line of tissue is assumed to move as a rigid object within a static dose field. Similar to the approximation in chapter 3, the static dose field is assumed to be unaffected by the movement of the tissue. Dose distributions are again described in two coordinate systems, the static coordinate system and the tissue-fixed coordinate system. Both coordinate systems can be transformed into each other by a time-dependent rigid translation. The trajectory of a tissue point r within the static coordinate system is described by some function $r'(r,t)$ specified by the motion model in section 4.2. r' refers to a point in the static coordinate system. Section 4.3 considers the motion of the tissue in the static dose field shown in figure 4.1a. The situation may model the movement of a tumor in the dose field of an open beam, where the direction of motion is perpendicular to the beam direction. The static dose distribution was generated by convolving a step function that is 1.0 in the interval $[0.0, 2.0]$ and 0.0 elsewhere with a Gaussian distribution of width 0.2 in order to model the penumbra of the beam.

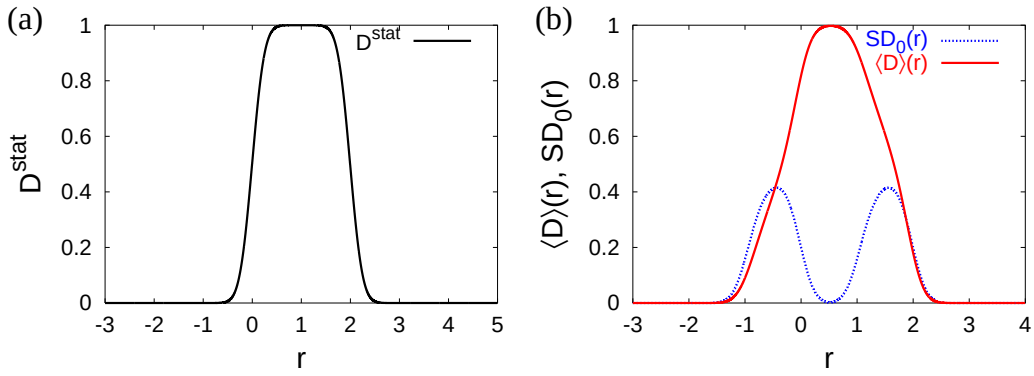

Figure 4.1: (a) Dose distribution of an open field in the static coordinate system (b) Expectation value of the dose in the tissue fixed coordinate system

4.2 The respiratory motion model

For this study, it is assumed that the tumor trajectory resulting from respiratory motion can be parameterized by a model proposed by Lujan *et al* [37]. Let r be a point in the moving tumor and let r' be a point in the static coordinate system. The trajectory of a volume element at point r in the static coordinate system is described by

$$r'(r,t) = r_0 + r + A\cos^{2n}\left(\pi\frac{(t+\varphi)}{T}\right) \tag{4.1}$$

where t is the time, A is the amplitude, r_0 is the exhale position, T is the period of motion, φ is the starting phase and n is an integer parameter that determines the shape of the motion trajectory. Figure 4.2a shows the trajectory of a tissue element at $r = 0$ for different values of n and the parameters $A = 1$, $r_0 = 0$, $\varphi = 0$ and $T = 3.0$. For $n = 1$ the motion is symmetric with respect to the exhale and the inhale state. For $n \geq 2$ the tumor spends more time in exhale position than in inhale position.
If the tissue is irradiated in the time interval $[0, \tau]$ with a beam that produces the static dose rate field $\dot{D}^{stat}(r')$, the dose

$$D(r|\tau, A, r_0, \varphi) = \int_0^\tau \dot{D}^{stat}\left(r'(r,t)\right) dt \tag{4.2}$$

is delivered to the moving tissue. Assuming that the dose rate is constant in time at each point r' in space, this yields

$$D(r|\tau, A, r_0, \varphi) = \frac{1}{\tau}\int_0^\tau D^{stat}\left(r'(r,t)\right) dt \tag{4.3}$$

when $D^{stat}\left(r'(r,t)\right) = \tau\dot{D}^{stat}\left(r'(r,t)\right)$ is the total static dose delivered during time τ. The delivered dose depends on the parameters of the motion model. Realistically, these parameters are not known exactly. To a first approximation, the starting phase φ is random

and uniformly distributed. The exhale position r_0 and the amplitude A may have some average values but they also fluctuate since the breathing is usually irregular. Hence, the delivered dose is uncertain.
In order to quantify the expected dose and the associated uncertainty, the following assumptions are applied:

1) During the irradiation of a single field, tissue moves according to equation 4.1 with a particular realization of the parameters A, r_0 and φ.

2) The starting phase φ is randomly distributed according to a uniform distribution, i.e.

$$P(\varphi) = \frac{1}{T} \qquad (\varphi \in [0, T]) \tag{4.4}$$

3) The amplitude A is randomly distributed according to a Gaussian distribution with mean $\langle A \rangle$ and width σ_A, i.e.

$$P(A) = \frac{1}{\sqrt{2\pi}\sigma_A} \exp\left(\frac{(A - \langle A \rangle)^2}{2\sigma_A^2}\right) \tag{4.5}$$

4) The exhale position r_0 is also randomly distributed according to a Gaussian distribution with mean $\langle r_0 \rangle$ and width σ_{r_0}, i.e.

$$P(r_0) = \frac{1}{\sqrt{2\pi}\sigma_{r_0}} \exp\left(\frac{(r_0 - \langle r_0 \rangle)^2}{2\sigma_{r_0}^2}\right) \tag{4.6}$$

The breathing period T which generally would be variable as well is considered as a constant for now. This issue will be further discussed in section 4.3.3. The random variables amplitude A and exhale position r_0 are assumed to be statistically independent. Due to the first assumption, the motion model is not designed to model the tumor trajectory for long periods of time. However, the irradiation of a single field is usually relatively short.

4.3 Uncertainties due to a finite irradiation time

First, the simplified case is considered where the amplitude and the exhale position are known exactly. In this case, the dose uncertainty is only due to the finite irradiation time τ. Because the irradiation time is finite and will usually not be a multiple of the period T, the delivered dose depends on the starting phase φ.

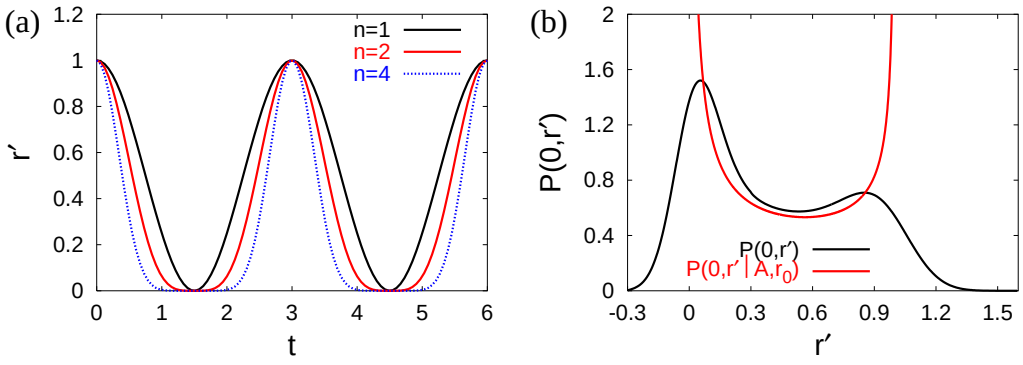

Figure 4.2: (a) Trajectories of a tissue element according to the motion model in equation 4.1 for different values of n (b) Probability density to find the tissue point $r = 0$ at position r': (red) for fixed amplitude and exhale position (black) including amplitude/exhale uncertainties

4.3.1 The expectation value of the dose

In a first step, the expectation value of the dose $\langle D|A, r_0\rangle$ given the parameters A, r_0 and τ is defined:

$$\begin{aligned}\langle D|A, r_0\rangle(r) &= \int_0^T D(r|\tau, A, r_0, \varphi)P(\varphi)d\varphi \\ &= \int_0^T \frac{1}{\tau}\int_0^\tau D^{stat}(r'(r, t, A, r_0, \varphi))P(\varphi)dtd\varphi \\ &= \frac{1}{\tau}\int_0^\tau \frac{1}{T}\int_0^T D^{stat}(r'(r, t, A, r_0, \varphi))d\varphi dt\end{aligned} \tag{4.7}$$

The integration over φ yields an expression that is independent of t since the function r' is periodic in φ and t and the integration range is a full period. We thus obtain

$$\langle D|A, r_0\rangle(r) = \frac{1}{T}\int_0^T D^{stat}(r'(r, t, A, r_0, \varphi))d\varphi$$

The integration over the starting phase can be transformed into an integration over the spatial coordinate r'. Equation 4.1 yields

$$t(r') = \frac{T}{\pi}\arccos\left[\left(\frac{r' - r_0 - r}{A}\right)^{\frac{1}{2n}}\right] - \varphi \tag{4.8}$$

and the derivative with respect to r'

$$\frac{dt}{dr'}(r') = -\frac{T}{2\pi nA}\frac{1}{\sqrt{1 - \sqrt[n]{\frac{r' - r_0 - r}{A}}}}\left(\frac{r' - r_0 - r}{A}\right)^{\left(\frac{1}{2n}-1\right)} \tag{4.9}$$

The expectation value of the dose becomes

$$\langle D|A,r_0\rangle(r) = \int_{r+r_0+A}^{r+r_0} D^{stat}(r')P(r,r'|A,r_0)dr' \tag{4.10}$$

where $P(r,r'|A,r_0)$ can be interpreted as the probability density for finding the point r at position r'. Equation 4.9 yields

$$P(r,r'|A,r_0) = \begin{cases} \frac{1}{\pi n A}\left[\left(\frac{r'-r_0-r}{A}\right)^{\left(\frac{2n-1}{2n}\right)}\sqrt{1-\sqrt[n]{\frac{r'-r_0-r}{A}}}\right]^{-1} & (r' \in [r+r_0, r+r_0+A]) \\ 0 & otherwise \end{cases} \tag{4.11}$$

Figure 4.2b (red line) shows the probability density $P(r,r'|A,r_0)$ for parameters $A = 1$, $r_0 = 0$ and $n = 2$. The distribution is sharply peaked at the exhale position and the inhale position which results from the feature that the velocity of the tissue element is zero at the turning points.
The expectation value would be realized in the limit $\tau \to \infty$, i.e. the irradiation time is long compared to the breathing period. The expectation value would also be realized if the irradiation time is a multiple of the breathing period. In all other cases the delivered dose differs from the expectation value. Figure 4.1b shows the expectation value of the dose for the motion parameters $A = 1$, $r_0 = 0$ and the static dose field in figure 4.1a.

4.3.2 The variance due to a finite irradiation time

In order to quantify the uncertainty of the expected dose, the variance is calculated. The variance is defined as

$$V(r,\tau|A,r_0) = \left\langle \left(D(r|A,r_0) - \langle D|A,r_0\rangle\right)^2 \right\rangle = \langle D^2|A,r_0\rangle(r,\tau) - \langle D|A,r_0\rangle^2(r) \tag{4.12}$$

where the brackets refer to the integration over the starting phase φ. Since the expectation value of the dose is realized when the irradiation time is a multiple of the breathing period, the total irradiation time τ is devided into two parts according to

$$\tau = kT + \tilde{t} \tag{4.13}$$

where $\tilde{t} \in [0, T]$. Hence, kT represents the completed breathing cycles that fit into τ and $\tilde{t}$ is the remainder. Evaluating $\langle D^2|A, r_0\rangle(r, \tau)$ yields

$$\begin{aligned}
\langle D^2|A, r_0\rangle(r, \tau) &= \int_0^T D^2(r|A, r_0, \tau, \varphi)P(\varphi)d\varphi \\
&= \frac{1}{T}\int_0^T \left[\frac{kT}{\tau}\langle D|A, r_0\rangle(r) + \frac{\tilde{t}}{\tau}D(r|A, r_0, \tilde{t}, \varphi)\right]^2 d\varphi \\
&= \frac{1}{T}\int_0^T \left(\frac{kT}{\tau}\right)^2 \langle D|A, r_0\rangle^2(r)d\varphi \\
&\quad + \frac{1}{T}\int_0^T 2\frac{kT\tilde{t}}{\tau^2}\langle D|A, r_0\rangle(r)D(r|A, r_0, \tilde{t}, \varphi)d\varphi \\
&\quad + \frac{1}{T}\int_0^T \left(\frac{\tilde{t}}{\tau}\right)^2 D^2(r|A, r_0, \tilde{t}, \varphi)d\varphi \\
&= \frac{(kT)^2 + 2\tilde{t}kT}{\tau^2}\langle D|A, r_0\rangle^2(r) + \left(\frac{\tilde{t}}{\tau}\right)^2 \langle D^2|A, r_0\rangle(r, \tilde{t}) \qquad (4.14)
\end{aligned}$$

with

$$\begin{aligned}
\langle D^2|A, r_0\rangle(r, \tilde{t}) &= \frac{1}{T}\int_0^T D^2(r|A, r_0, \tilde{t}, \varphi)d\varphi \\
&= \frac{1}{T}\int_0^T \left[\frac{1}{\tilde{t}}\int_0^{\tilde{t}} D^{stat}(r'(r, t, A, r_0, \varphi))dt\right]^2 d\varphi \qquad (4.15)
\end{aligned}$$

The variance is thus given by

$$V(r, \tau|A, r_0) = \left(\frac{\tilde{t}}{\tau}\right)^2 \left[\langle D^2|A, r_0\rangle(r, \tilde{t}) - \langle D|A, r_0\rangle^2(r)\right] \qquad (4.16)$$

and the standard deviation is given by the square root of the variance:

$$SD(r, \tau|A, r_0) = \frac{\tilde{t}}{\tau}\sqrt{\langle D^2|A, r_0\rangle(r, \tilde{t}) - \langle D|A, r_0\rangle^2(r)} \qquad (4.17)$$

Lets name the term $\left[\langle D^2|A, r_0\rangle(r, \tilde{t}) - \langle D|A, r_0\rangle^2(r)\right]$ in equation 4.16 the *characteristic variance function*. The characteristic variance function does not depend on the total irradiation time τ but only on the remainder $\tilde{t}$. Hence, if the characteristic variance function is calculated for the time interval $[0, T]$ for each point r of the moving tissue, the dose variance can be reconstructed from that for all times τ.
Figure 4.3a shows the square root of the characteristic variance function for different points. The results were generated by solving the integrals in equation 4.15 numerically for the static dose field in figure 4.1a and $A = 1.0$. For $\tilde{t} \to T$ the characteristic variance function approaches zero since the expectation value is realized. The limit $\tilde{t} \to 0$ corresponds to the

hypothetical case of an infinitesimally short irradiation time. Figure 4.3a shows the standard deviation for larger values of τ according to equation 4.17. The standard deviation as a function of irradiation time equals zero for $\tau = kT$.
The dashed blue line in figure 4.1b shows the spatial dependence of the standard deviation for an infinitesimal irradiation time $\tau \to 0$. As expected, the largest dose uncertainties occur at steep dose gradients.

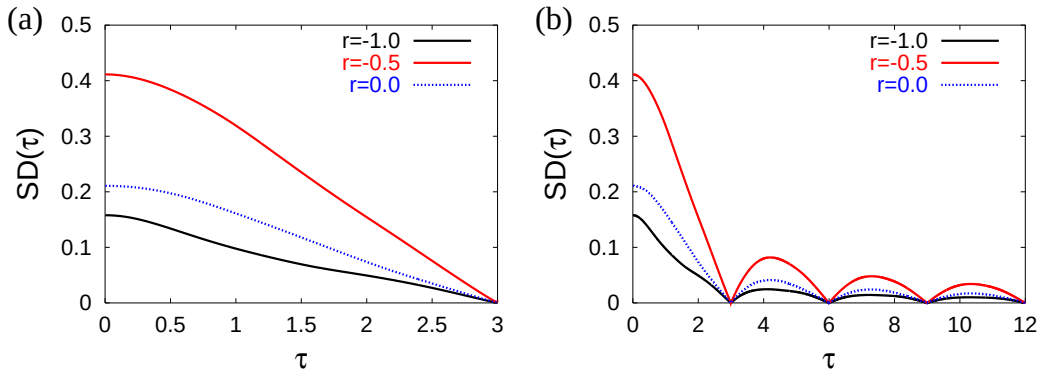

Figure 4.3: (a) Square root of the characteristic variance function for different points r (b) Standard deviation of the dose as a function of irradiation time τ for different points r

4.3.3 Approximation of the standard deviation

The calculation of the characteristic variance function is computationally extensive and unhandy. Particularly with regard to the application in probabilistic treatment planning, an approximation of the standard deviation of the dose is desirable. Fortunately, the extreme points of the characteristic variance function can be calculated relatively easily. On one side, $V(r, T|A, r_0) = 0$ holds. On the other side, the variance for an infinitesimal irradiation time $V_0(r|A, r_0)$ can be calculated according to

$$\begin{aligned}
V_0(r|A,r_0) &= V(r,0|A,r_0) = \lim_{d\tau\to 0}\left(\langle D^2|A,r_0\rangle(r,d\tau) - \langle D|A,r_0\rangle^2(r)\right) \\
&= \lim_{d\tau\to 0}\left(\frac{1}{T}\int_0^T D^2(r|A,r_0,d\tau,\varphi)d\varphi - \langle D|A,r_0\rangle^2(r)\right) \\
&= \lim_{d\tau\to 0}\left(\frac{1}{T}\int_0^T \left[\frac{1}{d\tau}\int_0^{d\tau} D^{stat}(r'(r,t,A,r_0,\varphi))dt\right]^2 d\varphi - \langle D|A,r_0\rangle^2(r)\right) \\
&= \frac{1}{T}\int_0^T \left[D^{stat}(r'(r,0,A,r_0,\varphi))\right]^2 d\varphi - \langle D|A,r_0\rangle^2(r) \\
&= \int_{r+r_0}^{r+r_0+A} \left[D^{stat}(r')\right]^2 P(r,r'|A,r_0)dr' - \langle D|A,r_0\rangle^2(r)
\end{aligned} \tag{4.18}$$

V_0 assesses both the magnitude of the variance and its spatial dependence. Looking at figure 4.3 suggests that the square root of the characteristic variance function can be approximated as a linear function:

$$SD(r,\tilde{t}|A,r_0) \approx SD_0(r|A,r_0)\left(1-\frac{\tilde{t}}{T}\right) \tag{4.19}$$

This linear approximation neglects details of the characteristic variance function, but it should provide a reasonable estimate. The red line in figure 4.4a shows the time-dependence of the standard deviation that results from the linear approximation in equation 4.19.

Realistically, the breathing period will be subject to variations. Hence, the application of the variance term in its current form would be questionable. Especially, the zeros of the variance function at times $\tau = kT$ seem unrealistic. One way of dealing with the problem is to use the envelope of the variance function instead of the variance function itself. For $\tilde{t} = T/2$ the standard deviation in linear approximation is $SD(r,\tau|A,r_0) = SD_0(r|A,r_0)T/(4\tau)$ with $(\tau = (k+1/2)T)$. Since $\tilde{t}(1-\tilde{t}/T) \leq T/4$ $(\tilde{t} \in [0,T])$, the function $SD_0(r|A,r_0)T/(4\tau)$ is the envelope of the standard deviation (blue dashed line in figure 4.4a). Since that would result in a singularity at $\tau = 0$ we define

$$SD(r,\tau|A,r_0) = \begin{cases} SD_0(r|A,r_0)\left(1-\frac{\tau}{T}\right) & (\tau < \frac{T}{2}) \\ \left(\frac{SD_0(r|A,r_0)T}{4}\right)\frac{1}{\tau} & (\tau > \frac{T}{2}) \end{cases} \tag{4.20}$$

as an upper bound for the standard deviation in linear approximation of the characteristic function.

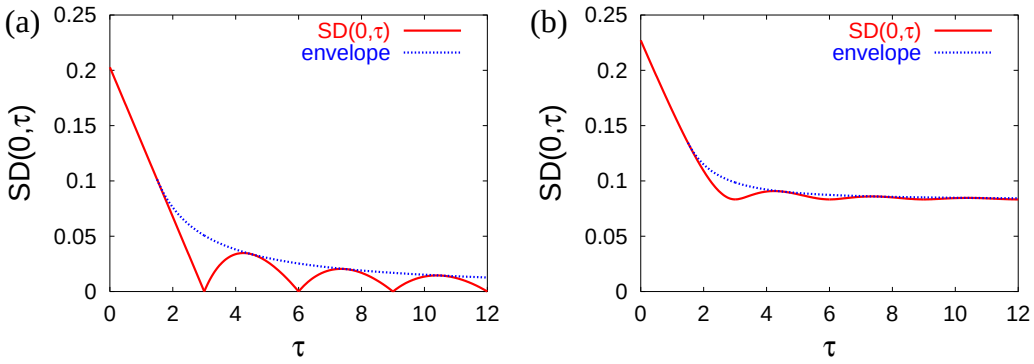

Figure 4.4: Standard deviation as a function of the irradiation time in linear approximation of the characteristic function (a) for fixed amplitude/exhale position (b) including amplitude/exhale uncertainties

4.4 Uncertainties due to variations in amplitude and exhale position

In section 4.3 amplitude and exhale position were considered fixed parameters. In this section, the calculation of expectation value and variance is generalized to uncertainties in the amplitude of motion and the exhale position. Uncertainties in both parameters are modeled by Gaussian distributions as described in section 4.2.

4.4.1 The expectation value of the dose

In the presence of amplitude and exhale position uncertainties, the expectation value of the dose is given by

$$\langle D \rangle(r) = \int\int\int_0^T D(r|A, r_0, \tau, \varphi) P(\varphi) P(A) P(r_0) d\varphi dA dr_0 \tag{4.21}$$

where the realized dose $D(r|A, r_0, \tau, \varphi)$ is still given by equation 4.3. Transforming the integration over φ into an integration over r' yields

$$\langle D \rangle(r) = \int\int\int D^{stat}(r') P(r'|r, A, r_0) P(A) P(r_0) dr' dA dr_0 \tag{4.22}$$

where $P(r'|r, A, r_0)$ is given by equation 4.11. Since $D^{stat}(r')$ only depends on the spatial coordinate r', this can be rearranged to give

$$\langle D \rangle(r) = \int D^{stat}(r') P(r'|r) dr' \tag{4.23}$$

where

$$P(r'|r) = \int\int P(r'|r, A, r_0) P(A) P(r_0) dA dr_0 \tag{4.24}$$

is the total probability density for finding the tissue point r at position r'. The black line in figure 4.2b shows the total probability for the parameters $\langle A \rangle = 1$, $\sigma_A = 0.1$, $\langle r_0 \rangle = 0$ and $\sigma_{r_0} = 0.1$.
Figure 4.5a shows the overall expectation value of the dose for the same parameters. The difference when compared to calculating the expectation values for fixed parameters $A = \langle A \rangle$ and $r_0 = \langle r_0 \rangle$ (figure 4.1b) is relatively small. For the irradiation of a single field, the expecation value in equation 4.21 would never be realized at all points simultaneously. It involves averaging over different amplitudes and exhale positions which would only occur if the same field was irradiated in infinitely many fractions.

4.4.2 The variance of the dose

The variance of the dose is defined as

$$V(r,\tau) = \langle D^2 \rangle(r,\tau) - \langle D \rangle^2(r) \tag{4.25}$$

where the expectation value is given by equation 4.21. Evaluating

$$\langle D^2 \rangle(r,\tau) = \int\int\int_0^T D^2(r|A,r_0,\tau,\varphi) P(\varphi) P(A) P(r_0) d\varphi dA dr_0 \tag{4.26}$$

yields

$$\begin{aligned} \langle D^2 \rangle(r,\tau) &= \int\int \left(\frac{k^2 T^2 + 2kT\tilde{t}}{\tau^2} \right) \langle D|A,r_0 \rangle^2(r) P(A) P(r_0) dA dr_0 \\ &+ \int\int \frac{1}{T} \int_0^T \frac{1}{\tau^2} \left[\int_0^{\tilde{t}} D^{stat}(r'(r,t,A,r_0,\varphi)) dt \right]^2 d\varphi P(A) P(r_0) dA dr_0 \end{aligned}$$

Substituting this into the variance term yields

$$V(r,\tau) = \underbrace{\int\int \langle D|A,r_0 \rangle^2(r) P(A) P(r_0) dA dr_0 - \langle D \rangle^2(r)}_{V_A(r)} \tag{4.27}$$

$$+ \underbrace{\left(\frac{\tilde{t}}{\tau} \right)^2 \int\int \left[\langle D^2|A,r_0 \rangle(r,\tilde{t}) - \langle D|A,r_0 \rangle^2(r) \right] P(A) P(r_0) dA dr_0}_{V_\varphi(r,\tau)} \tag{4.28}$$

The second variance term $V_\varphi(r,\tau)$ describes the dose uncertainty due to a finite irradiation time. The first term $V_A(r)$ describes the uncertainty due to variations in the amplitude and the exhale position. The starting phase contribution $V_\varphi(r,\tau)$ vanishes in the limit of large irradiation times $\tau \to \infty$. The amplitude contribution $V_A(r)$ is independent of τ since the motion model assumes that A and r_0 are constant during the irradiation of a single field.

4.4.3 Approximation of the standard deviation

Again, the variance for an infinitesimal short irradiation time can be calculated easily. Evaluating the variance for the limit $\tau \to 0$ yields

$$V_0(r) = V(r,0) = \int \left[D^{stat}(r') \right]^2 P(r,r') dr' - \langle D \rangle^2(r) \tag{4.29}$$

In order to simplify the calculation of the variance due to a finite irradiation time, it is again assumed that the square root of the characteristic variance function can be approximated

by a linear function, i.e.

$$\begin{aligned} V_\varphi(r,\tau) &= \left(\frac{\tilde{t}}{\tau}\right)^2 \int\int \left[\langle D^2|A,r_0\rangle(r,\tilde{t}) - \langle D|A,r_0\rangle^2(r)\right] P(A)P(r_0)dAdr_0 \\ &\approx \left(\frac{\tilde{t}}{\tau}\right)^2 (V_0(r) - V_A(r)) \left(1 - \frac{\tilde{t}}{T}\right)^2 \end{aligned} \tag{4.30}$$

The red line in figure 4.4 shows the time dependence of the total standard deviation $SD(r,\tau) = \sqrt{V(r,\tau)}$ as a function of τ for the point $r = 0$ in linear approximation. For short irradiation times the uncertainty is dominated by the starting phase contribution $V_\varphi(r,\tau)$, whereas for large irradiation times the standard deviation converges towards $\sqrt{V_A(r)}$. The blue line shows the corresponding envelope.

The red line and the blue line in figure 4.5a show $\sqrt{V_A(r)}$ and $\sqrt{V_\varphi(r,0)}$ as a function of the position r, respectively. For an infinitesimal treatment time, the uncertainty is dominated by the starting phase dependence of the delivered dose. The red and blue lines in figure 4.5b show the spatial dependence of the variances $V_A(r)$ and $V_\varphi(r,\tau)$ for $\tau = 1.5T$, respectively. For the standard motion parameters chosen here, both variance contributions are of similar importance if the irradiation time is one and a half breathing cycles. This would obviously change for other parameters of σ_A and σ_{r_0}.

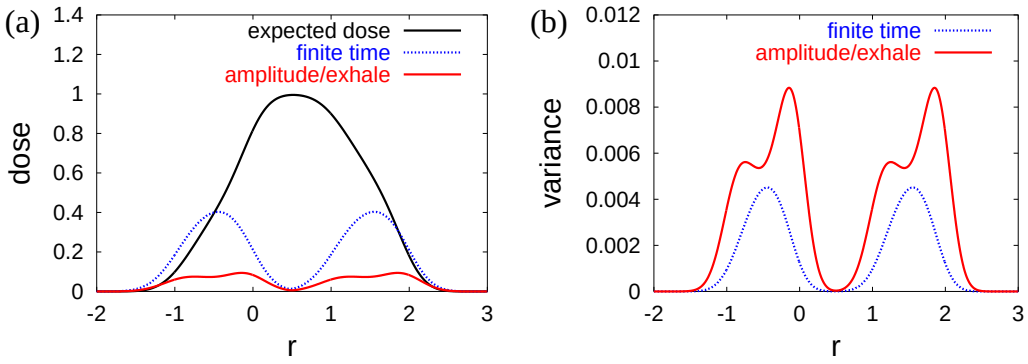

Figure 4.5: (a) expectation value of the dose (black), standard deviation due to a finite irradiation time (blue) and standard deviation due to amplitude/exhale uncertainties (red) (b) relative importance of the variance contributions $V_A(r)$ (red) and $V_\varphi(r,\tau)$ (blue) for $\tau = 1.5T$

4.5 Incorporating respiratory motion into treatment plan optimization

In this section, respiratory motion shall be incorporated in inverse planning by means of probabilistic treatment planning. It is the aim to minimize the expectation value of

the quadratic objective function 1.12 using the expressions for the expectation value of the dose and the variance derived in section 4.3 and 4.4. Generally, an IMRT treatment plan consists of multiple beams. For step-and-shoot IMRT delivered using a multi leaf collimator, each beam consists of multiple segments. Sections 4.3 and 4.4 quantified dose uncertainties for the irradiation of a single field and the generalization to multiple fields is not straightforward. This issue will be discussed further in the context of application to clinical data in section 5.1. For the idealized geometry considered in this chapter, a simplified optimization problem is considered. Instead of optimizing fluence values for multiple fields, the dose distribution in the static coordinate system is optimized. It is assumed that the static dose distribution is realized at all times during the irradiation in the time interval $[0, \tau]$, i.e. it is not decomposed into multiple fields which are delivered one after another. The optimization determines the optimal static dose distribution $D^{stat}(r')$, so that the dose distribution in the tissue, that moves within the static dose distribution, becomes optimal in the sense of minimizing objective function 1.12. The model is therefore oversimplified for two major reasons. First, because the temporal aspects of the dose delivery process are not included. And second, the optimized static dose distribution can usually not be realized by external fields. The purpose of this investigation should be understood as follows: The model should provide some general understanding and some guidelines on what to expect when applying probabilistic treatment planning to respiratory motion.
We consider a tumor of size 2.0 that is surrounded by a healthy tissue of size 2.0 on either side. For the optimization of the static dose field, we apply the quadratic objective function

$$E = \int_{-2}^{4} \alpha(r) \left[\left(\langle D \rangle(r) - D^{pres}(r) \right)^2 + \left(\langle D^2 \rangle(r) - \langle D \rangle^2(r) \right) \right] dr \tag{4.31}$$

with standard parameters

$$D^{pres}(r) = \begin{cases} 1 & (r \in [0,2]) \\ 0 & otherwise \end{cases} \tag{4.32}$$

$$\alpha(r) = \begin{cases} 1 & (r \in [0,2]) \\ 0.01 & otherwise \end{cases} \tag{4.33}$$

4.5.1 Incorporating a finite irradiation time

In a first step, amplitude A and exhale position r_0 are considered as fixed parameters, i.e. section 4.3 is applied to quantify the expected dose and the variance. For the expectation value of the dose, equation 4.10 is applied. For the variance, the square of the approximation of the standard deviation in equation 4.20 is used. The motion parameters are $A = 1$ and $r_0 = 0$.

Figure 4.6a shows the optimized static dose fields for different irradiation times τ. Let us first consider the realistic case $\tau = 2T$, i.e. the irradiation time is two times the breathing period (red solid line). In this case, the optimized static dose field shows a moderate peak

at $r' \approx 2$. This corresponds to the position where the right edge of the tumor is located at exhale. This allows for a dose reduction near $r' \approx 3$ where the right edge of the tumor is at inhale. The red line in figure 4.6b shows the corresponding expectation value of the dose in the moving tissue.

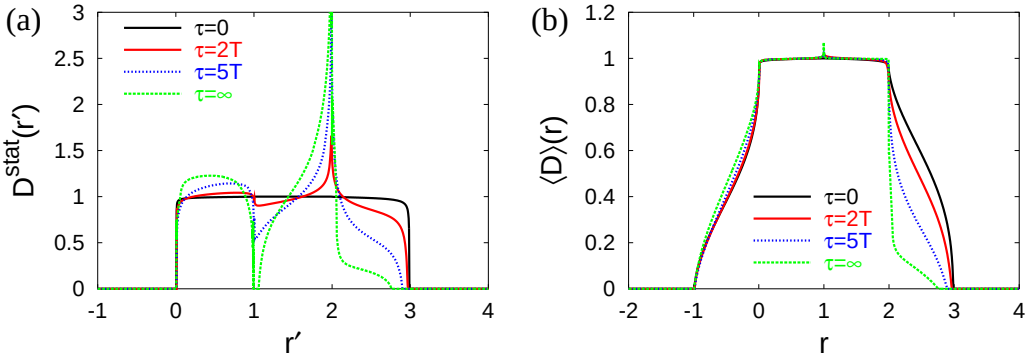

Figure 4.6: (a) optimized static dose field for different irradiation times (b) corresponding expectation values of the dose in the moving tissue

For the extreme case of an infinitesimal short irradiation time, a safety margin like dose field is reproduced (black solid line in figure 4.6a). The entire region where the tumor may be is irradiated with the prescribed dose (apart from the field edges where the dose is reduced due to penalizing the healthy tissue dose in the objective function). Comparing the expectation values in figure 4.6b shows that larger inhomogeneous static dose field allow for a better sparing of the healthy tissue on the right hand side of the tumor if the expectation value is realized.
The dashed green line in figure 4.6a shows the optimal static dose field for the hypothetical case of an infinitely long irradiation time $\tau \to \infty$. In this case, the variance term in the objective function vanishes and only the expectation value of the dose is optimized. The dose profile shows a very steep peak near $r' = 2$ and a substantially reduced dose is delivered to points between $r' = 2$ and $r' = 3$. The corresponding expectation value shows a significantly improved sparing of the healthy tissue that would be achieved if the expectation value was realized. For short treatment times, initial dose inhomogeneities that result from the steep peak would not be compensated for during the irradiation and the realized dose distribution in the moving tumor would show hot and cold spots.
Figure 4.7a shows the standard deviation of the dose for an infinitesimal treatment time for the different static dose fields in figure 4.6a. For the safety margin like solution ($\tau = 0$), the dose uncertainty is restricted to the healthy tissue outside the tumor since the tumor itself moves within an almost homogeneous dose field. Generating inhomogeneous static dose fields for $\tau > 0$ causes dose uncertainties within the tumor. The largest uncertainties are caused by the peak in the static dose field and therefore occur in the right half of the tumor. For the static dose profile optimized for $\tau = 2T$ (red lines), the standard deviation for infinitesimal irradiation time shows maximum values of $SD_0 \approx 0.4$ at the edge of the

tumor. If $\tau = 2T$ is the actual treatment time, the standard deviation is reduced by a factor of 8.0 according to equation 4.20. This yields a dose uncertainty of approximately 5% of the prescribed dose at the edge of the tumor, but significantly lower values for most parts inside the tumor.

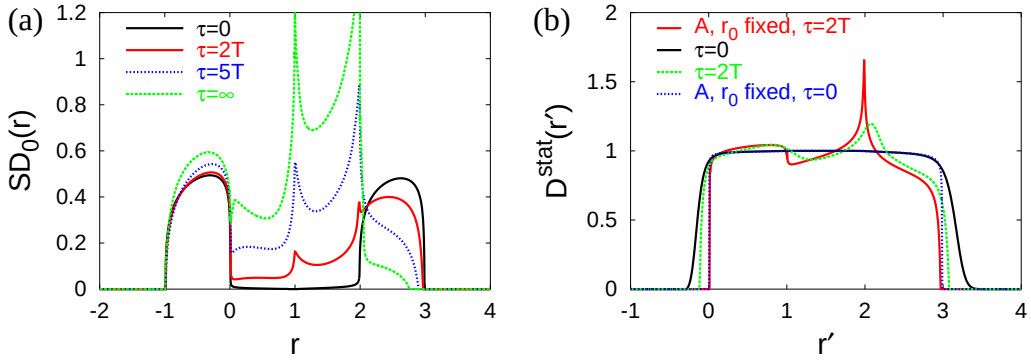

Figure 4.7: (a) Standard deviation $SD_0(r)$ for the different static dose fields in figure 4.6a (b) Static dose profiles optimized including uncertainties in amplitude and exhale position for different irradiation times

4.5.2 Incorporating uncertainties in the amplitude and exhale position

In the next step, uncertainties in amplitude and exhale position are included into the optimization of the static dose field. The following set of motion parameters is applied: $\langle A \rangle = 1$, $\langle r_0 \rangle = 0$, $\sigma_A = 0.1$ and $\sigma_{r_0} = 0.1$. This means, the motion is still dominated by the breathing itself and not by variations of exhale and inhale position, i.e. A is much larger than σ_A.

Figure 4.7b shows optimized static dose profiles for $\tau = 2T$ and $\tau = 0$. For comparison, the static dose fields from figure 4.6a are shown which are optimized for fixed values for A and r_0. Considering the case $\tau = 2T$ it is observed that the dose peak near $r' = 2$ is smoothed if A and r_0 are considered uncertain. The case $\tau = 0$ still reproduces a safety margin like solution. However, compared to figure 4.6a, the high dose region is extended on both sides in order to provide an additional margin for the uncertainty in amplitude and exhale position.

Let us now consider the extreme case of optimizing the expectation value of the dose alone. In this model, the patient would have to be irradiated in infinitely many fractions and the irradiation time would have to be infinitely long in order to realize the expectation value. This is of course unrealistic, but the investigation of this extreme case provides some further insight into the optimization problem. Figure 4.8a compares the optimization of the expectation value of the dose while including or not including uncertainties in amplitude

and exhale position. It shows the optimized static dose profiles. In both cases, the shape of the dose field is similar on a "large length scale". Both profiles show high doses near $r' = 2$ and low doses near $r' = 1$. In the presence of uncertainties of the parameters A and r_0, the profile is superimposed by a "high frequency modulation". These sharp hot and cold spots account for the interfractional changes of amplitude and exhale position. The same effect was observed in section 2.4. The variation of the exhale position practically corresponds to an interfractional random error. Obviously, a large number of fractions with different A and r_0 is required in order to level out initial dose inhomogeneities resulting from this modulation. For a realistic clinical situation such "high frequency modulations" in the static dose field could of course not be realized with external fields. However, this section analyzes general features of the optimization problem.

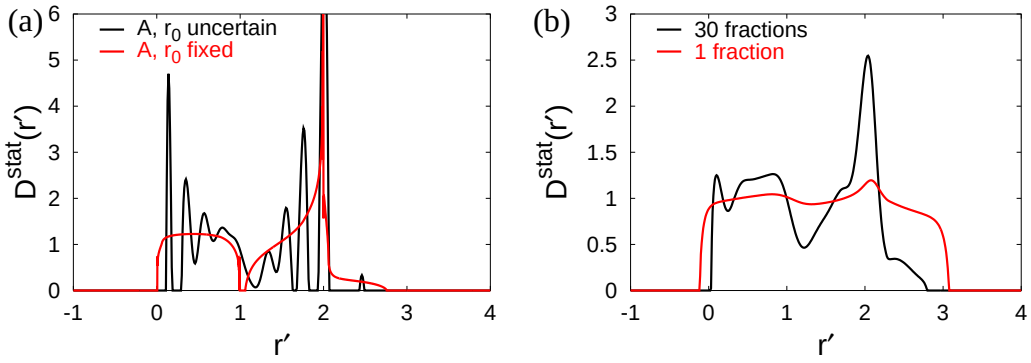

Figure 4.8: Optimized static dose fields (a) optimization of the expectation value of the dose without the variance term (b) comparison of the optimization for 30 fractions and 1 fraction

Let us consider a realistic number of N fractions. We assume that the random variables A, r_0 and φ are statistically independent for different fractions. In this case, the larger number of fractions simply leads to a factor $1/N$ in the variance term. The expected cumulative dose D_c after N fractions is $\langle D_c \rangle = N\langle D \rangle$ whereas the standard deviation of the cumulative dose is $SD_c = \sqrt{N}SD$.
Figure 4.8b shows the optimized static dose profile for 30 fractions in comparison to the optimization for one fraction for $\tau = 2T$. As expected, significantly larger inhomogeneities arise in the static dose profile when 30 fractions are assumed instead of a single one since remaining dose inhomogeneities within the tumor after the first fraction can be compensated for in later fractions.
Figure 4.9 shows the expectation value of the dose and its standard deviation for the static dose profiles in figure 4.8b. The standard deviation is normalized to 30 fractions for both plans in order to allow for a meaningful comparison. It can be seen that the increase in modulation of the static dose field potentially improves the sparing of healthy tissue. But at the same time, the uncertainty of the dose increases. Within the tumor, the standard deviation is significantly higher for the static dose field optimized for 30 fractions. Figure

4.10 shows the relative weight of the variance contributions $V_A(r)$ and $V_\varphi(r)$ for both plans.

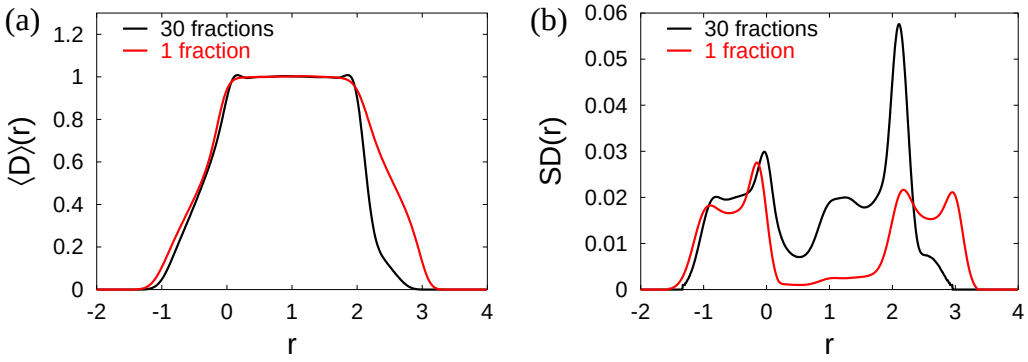

Figure 4.9: Comparison between the optimization for 30 fractions and 1 fraction (a) expectation value of the dose (b) standard deviation of the dose

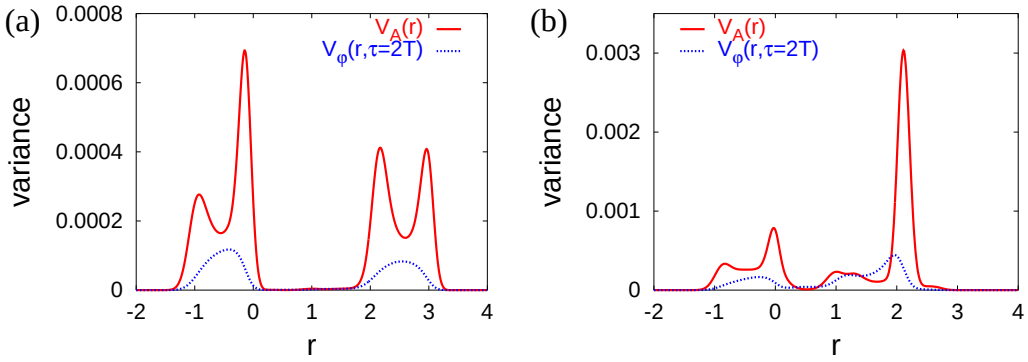

Figure 4.10: Relative importance of the two variance contributions: (a) optimized for a single fraction (b) optimized for 30 fractions

Chapter 5

Application to lung tumors

This chapter deals with probabilistic treatment planning for lung tumors. In chapter 4 a mathematical model to describe respiratory motion was introduced and equations to calculate the expectation value of the dose and its variance were derived. These concepts are now applied to clinical data. In the case of interfractional movements, the transition from the idealized model (chapter 2) to clinical data (chapter 3) was widely straightforward. This is not fully true for respiratory motion. As already mentioned in section 4.5, the variance of the delivered dose depends on temporal aspects of the dose delivery process and consequently on the application technique. In section 5.1, we generalize the variance calculation to multiple irradiation fields which are statistically independent with respect to the random variables of the motion model. Practically, this allows for a description of IMRT treatments delivered with compensators. Based on the variance calculation for compensator IMRT, an approximation of the variance for step-and-shoot IMRT is discussed, which represents one clinically relevant treatment technique. In section 5.2, aspects concerning the implementation are discussed. Section 5.3 presents results for a clinical case.

5.1 Estimation of the dose uncertainty for IMRT treatments

In section 4.3 and 4.4 we calculated the expectation value of the dose and the variance for the irradiation of a single field. We now generalize the respective equations to multiple fields. We consider the idealized geometry introduced in chapter 4.

5.1.1 Statistically independent random variables

We consider the irradiation of K fields that produce the static dose distributions $D_k^{stat}(r')$ during the irradiation times τ_k. Each field k is characterized by a set of random variables (φ_k, A_k, r_{0k}) which denote the starting phase, the amplitude and the exhale position for this field. In this section, we consider the simplified case that all random variables are

statistically independent, i.e.

$$P(\{\varphi_k, A_k, r_{0k}\}_{k=1}^K) = \prod_{k=1}^K P(\varphi_k)P(A_k)P(r_{0k}) \tag{5.1}$$

and that $P(\varphi_k)$, $P(A_k)$ and $P(r_{0k})$ are given by equations 4.4, 4.5 and 4.6, respectively. For the calculation of the expectation value of the cumulative dose, the correlation of the random variables is irrelevant, only the variance generally depends on the correlation.

The expectation value of the dose

The cumulative dose for all K fields is given by

$$D(r, \{\tau_k, \varphi_k, A_k, r_{0k}\}_{k=1}^K) = \sum_{k=1}^K \frac{1}{\tau_k} \int_0^{\tau_k} D_k^{stat}(r'(r, t, \varphi_k, A_k, r_{0k}))dt \tag{5.2}$$

and the expectation value of the cumulative dose turns out to be the sum of the dose expectation values of the individual fields, i.e.

$$\langle D\rangle(r) = \sum_{k=1}^K \langle D_k\rangle(r) \tag{5.3}$$

where

$$\begin{aligned} \langle D_k\rangle(r) &= \int\int\int_0^T \left[\frac{1}{\tau_k}\int_0^{\tau_k} D_k^{stat}(r'(r, t, A_k, r_{0k}, \varphi_k))dt\right] \\ &\quad \times P(\varphi_k)P(A_k)P(r_{0k})d\varphi_k dA_k dr_{0k} \end{aligned} \tag{5.4}$$

can be evaluated according to sections 4.3.1 and 4.4.1.

The variance of the dose

The variance of the cumulative dose is

$$V(r, \{\tau_k\}) = \langle D^2\rangle(r, \{\tau_k\}) - \langle D\rangle^2(r) \tag{5.5}$$

Evaluating $\langle D^2\rangle(r, \{\tau_k\})$ yields

$$\begin{aligned} \langle D^2\rangle(r, \{\tau_k\}) &= \sum_{k=1}^K \left[\int\int\int_0^T \frac{1}{\tau_k^2}\left[\int_0^{\tau_k} D_k^{stat}(r'(r, t, A_k, r_{0k}, \varphi_k))dt\right]^2\right. \\ &\quad \left. \times P(\varphi_k)P(A_k)P(r_{0k})d\varphi_k dA_k dr_{0k}\right] + \sum_{\substack{k,l=1 \\ k\neq l}}^K \langle D_k\rangle(r)\langle D_l\rangle(r) \end{aligned} \tag{5.6}$$

Equation 5.6 only holds for statistically independent random variables. The variance of the cumulative dose is hence the sum of the variances of the individual fields:

$$V(r,\{\tau_k\}) = \sum_{k=1}^{K}\left[\int\int\int_0^T \frac{1}{\tau^2}\left[\int_0^{\tau_k} D_k^{stat}(r'(r,t,A_k,r_{0k},\varphi_k))dt\right]^2 \times P(\varphi_k)P(A_k)P(r_{0k})d\varphi_k dA_k dr_{0k} - \langle D_k\rangle^2(r)\right] \quad (5.7)$$

5.1.2 Compensator based IMRT delivery

IMRT treatment plans can be realized using compensators. A compensator usually consists of a block of lead of variable thickness in order to realize the fluence modulation in the lateral direction to the beam. For compensator treatments, the irradiation consists of K intensity modulated fields when K is the number of beam directions. Each intensity modulated field is realized at once, i.e. a static dose rate field $\dot{D}_k^{stat}(r)$ is realized which is constant in time during the irradiation time τ_k (neglecting the pulsed time structure on a millisecond scale). The time interval between the start of irradiation for two successive fields is usually much larger than one breathing cycle. We may, therefore, assume that the random variables starting phase φ_k, amplitude A_k and exhale position r_{0k} are statistically independent for different fields. Therefore, the variance calculation for statistically independent random variables in section 5.1 may provide a reasonable description for compensator based IMRT. The irradiation time τ_k is mainly determined by the dose rate of the linac and the maximum weight of the fluence map.

5.1.3 Step-and-Shoot IMRT

For Step-and-Shoot IMRT, the situation is more difficult. An intensity modulated field is decomposed into a large number of segments. The irradiation time for a single segment is short, often shorter than one breathing cycle. In addition, the time between the irradiation of two successive segments is short, usually significantly shorter than the breathing period. Therefore, it would not be realistic to assume all segments to be statistically independent. The starting phase of one segment would clearly correlate with the starting phase of the previous segment.
An additional difficulty arises since the shapes of the segments are usually not known during the optimization. IMRT inverse planning tools usually perform a beamlet-based optimization. In the first step, a fluence map is optimized, which is, in a second step, decomposed into a set of segments using a sequencer. One appraoch to tackle this problem would be Direct Aperture Optimization (DAO) [38]. In this IMRT optimization approach for Step-and-Shoot dose delivery, the shape of a limited number of segments is optimized. The Direct Aperture Optimization problem is expected to be np-complete, i.e. the computational complexity increases exponentially with the number of apertures. It cannot be solved by standard gradient methods. Shepard *et al* [38] have used simulated annealing to

obtain clinically acceptable solutions, Li *et al* [39] applied genetic algorithms. Although this optimization approach would directly provide all segments that will be delivered, there would still be the problem that these segments are not independent.
We therefore investigate the possibility of using the beamlet-based optimized fluence maps to estimate the variance of the dose for Step-and-Shoot IMRT. It would be of particular interest to derive an upper bound for the variance for Step-and-Shoot IMRT based on the fluence maps, however, this has not been done so far. The following arguments in this section remain to some extent handwavy. We start with a discussion of the impact of correlations of random variables on the variance of the cumulative dose (subsection 5.1.4) and suggest an approximation of the variance for Step-and-Shoot IMRT in subsection 5.1.5.

5.1.4 The impact of correlations

We consider the irradiation of two segments that cause the static dose fields $D_1^{stat}(r')$ and $D_2^{stat}(r')$. We assume that the delivery time is equal for both segments. For simplicity, we assume the amplitude and the exhale position fixed so that only the starting phases φ_1 and φ_2 are random variables. We denote the delivered doses for the two fields by $D_1(r|\varphi_1)$ and $D_2(r|\varphi_2)$. Generally, φ_1 and φ_2 are correlated: $P(\varphi_1, \varphi_2) = P(\varphi_1)P(\varphi_2|\varphi_1)$. We consider two extrem cases:

1. $P(\varphi_1, \varphi_2) = P(\varphi_1)P(\varphi_2) = \frac{1}{T^2}$ (φ_1 and φ_2 are uncorrelated)

2. $P(\varphi_2|\varphi_1) = \delta(\varphi_2 - \varphi_1)$ and $P(\varphi_1) = \frac{1}{T}$ (φ_2 is already determined when φ_1 is chosen, i.e. $\varphi_2 = \varphi_1$)

In both cases we ensure that $\int P(\varphi_1, \varphi_2)d\varphi_1 = \int P(\varphi_1, \varphi_2)d\varphi_2 = \frac{1}{T}$ holds for the total probability. The second case is equivalent to compensator based IMRT delivery. If the irradiation starts at the same point in the breathing cycle for both fields, this is equivalent to delivering both fields at the same time.

We look at the cumulative dose $D(r|\varphi_1, \varphi_2) = D_1(r|\varphi_1) + D_2(r|\varphi_2)$ and calculate the expectation value and the variance according to the equations in section 4.3. We obtain

$$\begin{aligned} \langle D\rangle(r) &= \int_0^T \int_0^T (D_1(r|\varphi_1) + D_2(r|\varphi_2))P(\varphi_1, \varphi_2)d\varphi_1 d\varphi_2 \\ &= \langle D_1\rangle(r) + \langle D_2\rangle(r) \end{aligned} \tag{5.8}$$

and

$$\begin{aligned} \langle D^2\rangle(r) &= \int_0^T \int_0^T (D_1(r|\varphi_1) + D_2(r|\varphi_2))^2 P(\varphi_1, \varphi_2)d\varphi_1 d\varphi_2 \\ &= \langle D_1^2\rangle(r) + \langle D_2^2\rangle(r) + 2\int_0^T \int_0^T D_1(r|\varphi_1)D_2(r|\varphi_2)P(\varphi_1, \varphi_2)d\varphi_1 d\varphi_2 \end{aligned} \tag{5.9}$$

The variance of the cumulative dose is hence

$$\begin{aligned} V(r) &= V_1(r) + V_2(r) \\ &\quad +2\left[\int_0^T \int_0^T D_1(r|\varphi_1) D_2(r|\varphi_2) P(\varphi_1, \varphi_2) d\varphi_1 d\varphi_2 - \langle D_1\rangle(r)\langle D_2\rangle(r)\right] \end{aligned} \quad (5.10)$$

For uncorrelated random variables the non-diagonal term in the variance vanishes so that $V(r) = V_1(r) + V_2(r)$ (section 5.1.1).

Dose uncertainties occur near dose gradients. We therefore consider three different relative positions of the two segments so that the relative location of the gradients is different each time. Figure 5.1a shows the static dose distributions that may result from two segments. Figure 5.1b shows the corresponding expectation value of the cumulative dose and its variance for the parameters $A_{1,2} = 1$, $r_{01,2} = 0$, $n = 2$ and $\tau_{1,2} = 0.5T$. In this example, the dose gradients of the static dose fields are located at different places. As a consequence, the variance of the cumulative dose is approximately the same no matter whether the starting phases φ_1 and φ_2 are uncorrelated or identical. Figure 5.2 illustrates another example where the right edges of both fields coincide. In this case, the variance is approximately twice as large if the random variables are correlated. Figure 5.3 illustrates the opposite case, where the variance is much larger for uncorrelated random variables. In this example, the right edge of the first field coincides with the left edge of the second field. For $\varphi_2 = \varphi_1$, this corresponds to a single large field so that the variance in the center is almost zero. For uncorrelated random variables, a significant dose uncertainty arises in the center. In summary, the correlation between the two random variables can both increase or decrease the dose uncertainty.

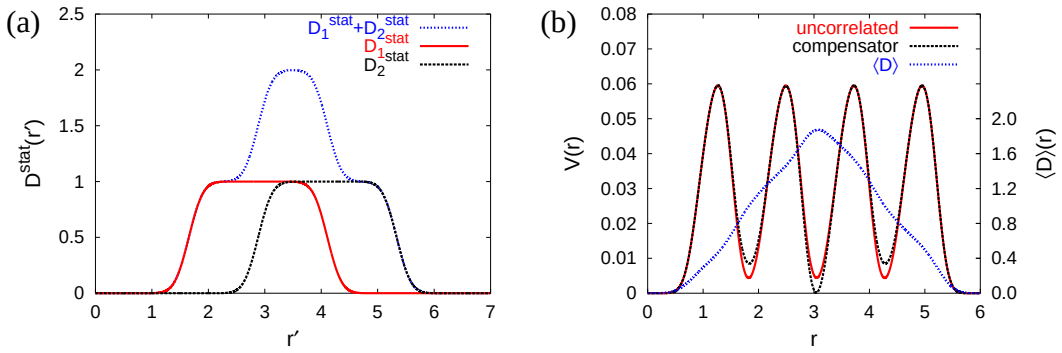

Figure 5.1: (a) Static dose distributions that may result from two segments. (b) corresponding expectation value of the cumulative dose and its variance for uncorrelated and coupled random variables

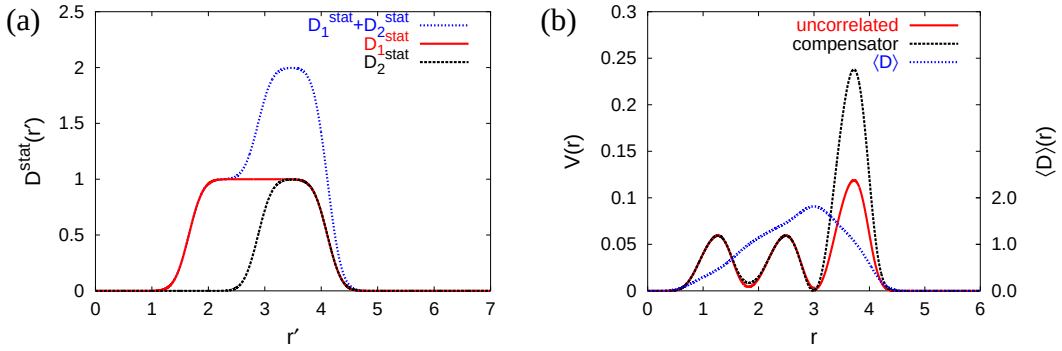

Figure 5.2: (a) Static dose distributions that may result from two segments. (b) corresponding expectation value of the cumulative dose and its variance for uncorrelated and coupled random variables

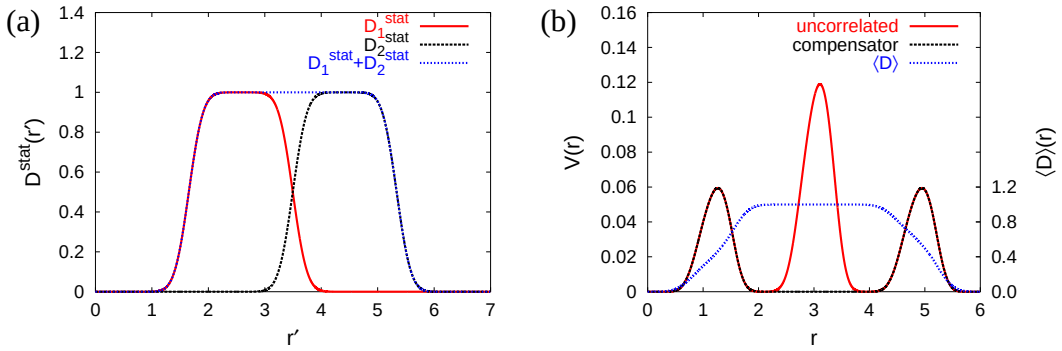

Figure 5.3: (a) Static dose distributions that may result from two segments. (b) corresponding expectation value of the cumulative dose and its variance for uncorrelated and coupled random variables

5.1.5 The variance of the dose for Step-and-Shoot IMRT

Generally, the variance of the cumulative dose distribution depends on the sequencing algorithm. We do not go into details of specific sequencing methods and adopt the assumptions made by Bortfeld *et al* [40]. We assume that the fluence map is discretized into F equidistant fluence levels. The discritized fluence map can be decomposed into deliverable MLC segments using the sliding window technique. An example for this decomposition is illustrated in figure 5.4.

Working hypothesis

Let F_k be the number of fluence levels of the discretized fluence map of beam k and let Φ_k^{max} be the maximum beamlet weight in the fluence map for beam k. The time to deliver

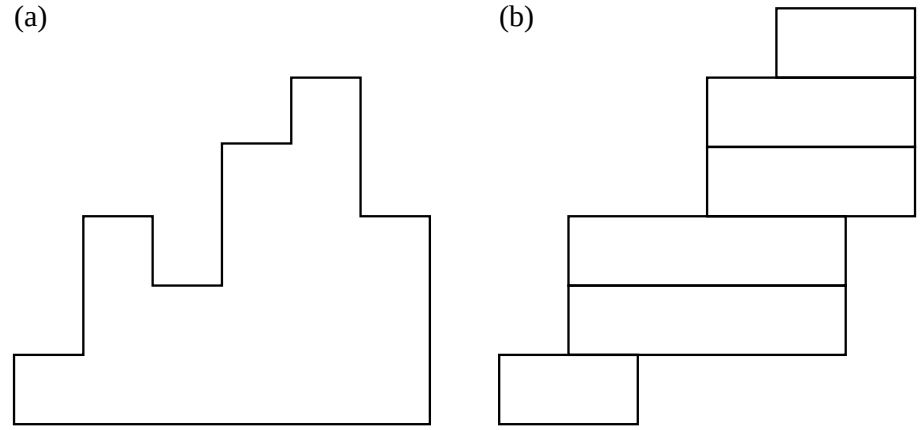

Figure 5.4: Illustration of the sequencing of a fluence profile using the sliding window technique (a) fluence profile in the direction of leaf travel (b) delivered segments

a segment with fluence weight Φ_k^{max}/F_k will approximately take the time τ_k/F_k where τ_k is the delivery time for compensator treatments. We claim that we can use the variance derived for compensator treatments as a rough estimate of the variance for Step-and-Shoot treatments if we replace the irradiation time τ_k by τ_k/F_k.

Arguments

The set of deliverable segments generated by the sequencer is of course closely related to the fluence map. In particular, the fluence map determines the location of dose gradients which are most important for the estimation of the dose uncertainty. The dose gradients in the fluence map reflect the locations of the field edges of the MLC segments. If the sequencing process is performed in a "reasonable way", the sequencer should avoid placing field edges at positions where there is no gradient in the fluence map. Looking at the sequencing example in figure 5.4 suggests that the variance of the cumulative dose will be overestimated in most cases. At most positions, the case illustrated in figure 5.2 occurs where the left or right field edges of two segments coincide. In this situation, the variance is overestimated by assuming compensator based delivery with a reduced irradiation time. If only the case illustrated in figure 5.1 occured, this approximation of the variance would perform well. The case illustrated in figure 5.3 where the variance is strongly underestimated should usually not occur. An overestimation of the variance makes the treatment plan more conservative, i.e. modulations of the static dose distribution are reduced and the treatment plan becomes more safety margin like (section 5.3). This may be desirable.

Realistically, the situation is more complex than the idealized examples in figures 5.1-5.3. The amplitude of motion may be larger than the penumbra of the field and the resolution of the beamlets. Step-and-Shoot IMRT is possibly not well described by neither of the two extreme cases discussed in section 5.1.4. The starting phases for different segments

are neither identical nor uncorrelated. Further investigation may be required to justify the suggested approximation of the variance for Step-and-Shoot IMRT. We are primarily interested in the variance term because it controls the robustness of the treatment plan in the optimization (section 5.3). A preferably accurate quantification of the dose uncertainty as an end in itself is not the primary interest.

5.2 Implementation

This section describes the implementation of probabilistic treatment planning for lung tumors into the inverse planning tool KonRad. The current implementation is provisional and not meant to be suitable for clinical application in its present form. It shall allow the presentation of generic results. We apply several limitations that shall be overcome in the future. Nonetheless, most of these limitations may not be relevant for the generic features of the resulting treatment plans presented in section 5.3.

1. We still apply the approximation that moving tissue elements move within a static dose distribution which is unaffected by the tissue deformation. This approximation was described in section 3.1. In the future, all phases of a 4D CT data set could be incorporated into the dose calculation.

2. Amplitude and exhale position are fixed. Only the uncertainty due to a finite irradiation time is considered. The starting phases φ_k are the only random variables.

3. We consider motion in CC-direction only and the amplitude A is assumed to be a multiple of the voxel resolution.

5.2.1 Calculation of the expectation value and the variance of the dose

We consider the moving voxel i. Let $\boldsymbol{S}_i = (S_{xi}, S_{yi}, S_{zi})^T$ denote the position of the center of the voxel in its exhale state. Let $\boldsymbol{r}_j = (x_j, y_j, z_j)^T$ denote the position of the center of the static voxel j. Since we deal with motion in CC-direction only, it is sufficient to consider the z-coordinate. The probability density for finding the voxel i at position $\boldsymbol{r} = (x, y, z)^T$ is given by $P(\boldsymbol{r}|\boldsymbol{S}_i) = \delta(S_{xi} - x)\delta(S_{yi} - y)P(z|S_{zi})$ where δ is the Dirac-Delta function and

$$P(z|S_{zi}) = \frac{1}{\pi n A}\left[\left(\frac{S_{zi} + \Delta z - z}{A}\right)^{\left(\frac{2n-1}{2n}\right)} \sqrt{1 - \sqrt[n]{\frac{S_{zi} + \Delta z - z}{A}}}\right]^{-1} \tag{5.11}$$

for $z \in [S_{zi} + \Delta z - A, S_{zi} + \Delta z]$ and $P(z|S_{zi}) = 0$ otherwise. Δz denotes the voxel resolution which is 2.6 mm in all spatial directions. The probability to find the center of the moving voxel i within the static voxel j is given by

$$P_{ij} = \int_{z_j - \frac{1}{2}\Delta z}^{z_j + \frac{1}{2}\Delta z} P(z|S_{zi})dz \tag{5.12}$$

We assume the dose distribution within one static voxel to be constant like we did in section 3.2.1 so that the expectation value of the dose for field k is given by

$$\langle D_k^i \rangle = \sum_j D_{kj}^{stat} P_{ij} \tag{5.13}$$

where D_{kj}^{stat} is the value of the static dose distribution of field k in voxel j. For the calculation of the variance, we assume that the random variables for the intensity modulated fields from different beams are statistically independent, so that the variance resulting from each field can be calculated independently. We apply the linear approximation of the characteristic standard deviation function introduced in section 4.3.3. The variance for the real irradiation time is approximated based on the variance that would arise for an infinitesimally short irradiation time. The variance for field k for an infinitesimal treatment time is

$$V_k^i(\tau_k \to 0) = \langle (D_k^i)^2 \rangle (\tau_k \to 0) - \langle D_k^i \rangle^2 \tag{5.14}$$

with

$$\langle (D_k^i)^2 \rangle (\tau_k \to 0) = \sum_j (D_{kj}^{stat})^2 P_{ij} \tag{5.15}$$

The standard deviation for the real irradiation time is calculated according to equation 4.20:

$$V_k^i(\tau_k) = \begin{cases} V_k^i(\tau_k \to 0) \left(1 - \frac{\tau_k}{T}\right)^2 & (\tau_k < \frac{T}{2}) \\ \left(\frac{V_k^i(\tau_k \to 0) T^2}{4^2}\right) \frac{1}{\tau_k^2} & (\tau_k > \frac{T}{2}) \end{cases} \tag{5.16}$$

The expectation value and the variance can be evaluated as a function of the beamlet weights using the concept of a dose contribution matrix and a variance contribution tensor as introduced in section 3.2.1. The expectation value of the total dose is the sum over the dose expectation values of the individual fields:

$$\langle D_i \rangle = \sum_{k=1}^{K} \langle D_k^i \rangle \tag{5.17}$$

The variance of the total dose is the sum over the variances of the individual fields:

$$V_i = \sum_{k=1}^{K} V_k^i \tag{5.18}$$

A field k represents the intensity modulated field for beam k and the number of fields K equals the number of beam directions. For compensator based dose delivery, τ_k is the time required to deliver field k. For Step-and-Shoot IMRT, τ_k is the time needed to deliver field k with a compensator divided by the number of fluence levels in the discretized fluence map.

5.2.2 Optimization

For the optimization of the treatment plan, we apply the quadratic objective function 3.11 that is also applied for the prostate case:

$$\begin{aligned} E &= \sum_{i \in CTV} \alpha_{CTV} \left[\left(\langle D_i \rangle - D_{CTV} \right)^2 + V_i \right] \\ &\quad + \sum_n \left[\sum_{i \in OAR_n} \alpha_n \left(\langle D_i \rangle - D_n^{max} \right)_+^2 \right] \end{aligned} \tag{5.19}$$

A complication, which arises in the context of respiratory motion, is as follows: The variance for field k depends on the irradiation time τ_k for this field. The irradiation time, in turn, depends on the maximum beamlet weight in the fluence map for beam k. Hence, the variance term is not simply a quadratic function of the beamlet weights any more. In the evaluation of the gradient of the objective function, we do not account for this dependency. For the calculation of the derivative of the variance with respect to the beamlet weights, τ_k is considered a constant. After the update of the beamlet weights in one gradient optimization step, the irradiation time is then recalculated according to the new beamlet weights. Therefore, the presented results may not exactly represent the minimum of the objective function. The impact on the optimized treatment plan has not been investigated yet.

5.3 Results of probabilistic treatment planning for lung tumors

We consider a patient with a relatively small lung tumor of about 2 cm in diameter. We optimize a treatment plan with five coplanar beams at 0°, 60°, 120°, 210° and 325°. The resolution of voxels is $(2.6\,mm)^3$ and the resolution of beamlets is $(5\,mm)^2$. In order to specify the irradiation time, we assume a dose rate of 600 monitor units per minute. The irradiation time τ_k for the delivery of an intensity modulated field with a compensator is assumed to be given by the monitor units of the maximum beamlet weight divided by the dose rate of the linac. For the estimation of the variance for Step-and-Shoot IMRT we assume that the fluence map is discretized into five equidistant fluence levels so that the imaginary treatment time for Step-and-Shoot IMRT is one fifth of the compensator based treatment time. The CT scan used for the dose calculation is assumed to show the tumor in its exhale position. The amplitude of motion is assumed to be 2.3 cm in CC direction. We compare four different cases:

1. optimization of the expectation value of the dose ($\tau_k \to \infty$)
2. compensator based IMRT delivery
3. Step-and-Shoot IMRT

4. optimization assuming an infinitesimally short irradiation time ($\tau_k \to 0$)

All treatment plans are optimized for a single fraction, i.e. we demand that a widely homogeneous dose is delivered to the tumor in each fraction. Blurring of the static dose distribution is due to respiratory motion within one fraction only.

Figure 5.5 shows on a sagittal CT slice the static dose distribution, the expectation value of the dose and the standard deviation for these four scenarios. Let us first compare the static dose distributions. For the treatment plan optimized under the assumption that the five intensity modulated fields are delivered using compensators, the static dose distribution (figure 5.5a) shows a dose peak in the region where the caudal edge of the tumor is located at exhale. Qualitatively, this was also observed in section 4.5.1 for the idealized model. The height of the peak is approximately 130% of the prescribed dose. This allows for a dose reduction in the area where the tumor is located at inhale, where the values of the static dose field are in the order of 80-90% of the prescribed dose. For the treatment plan optimized for Step-and-Shoot IMRT (using the variance estimation described in section 5.1.5), the static dose distribution (figure 5.5d) shows a similar modulation pattern, however, the dose peak is less pronounced (approximately 120% of the prescribed dose). The dose profiles in CC direction depicted in figure 5.6a show the difference of the two static dose distributions. This result is in agreement with our intuition, since the estimated dose uncertainty is much higher for Step-and-Shoot IMRT than for compensator based IMRT. When only the expectation value of the dose is optimized, the static dose distribution (figure 5.5g) shows a very steep dose peak (approximately 170% of the prescribed dose) and a more dramatic dose reduction in the region where the tumor is at inhale (in the order of 50% of the prescribed dose). In contrast, when we assume an infinitesimal irradiation time for each beam, the static dose distribution represents a safety margin like solution (figure 5.5j). Qualitatively, the results found in section 4.5.1 for an idealized model are reproduced for the considered lung tumor.

The second column in figure 5.5 shows the corresponding expectation values of the dose (figures 5.5b,e,h,k). Dose profiles in CC direction are depicted in figure 5.6b. The expectation values show the potentially better sparing of the lung tissue for increased modulations of the static dose distribution. The third column in figure 5.5 shows the standard deviation of the dose for an infinitesimal irradiation time for each beam (figures 5.5c,f,i,l). The standard deviation for an infinitesimal irradiation time is not the dose uncertainty estimated for the actual treatment. It only depends on the static dose distribution but not on the dose delivery method and is therefore helpful for a plan comparison. The standard deviation distributions illustrate the increased dose uncertainty as a consequence of stronger static dose modulations. Figure 5.5i shows the relatively large dose uncertainty within the tumor when only the expectation value is optimized. In contrast, the dose uncertainty is pushed into the lung tissue for the safety margin like treatment plan (figure 5.5l). This becomes obvious also in the profiles in CC direction (figure 5.7a). Figures 5.8a,b show the absolute values of the standard deviation estimated for compensator based IMRT (figure 5.8a) and

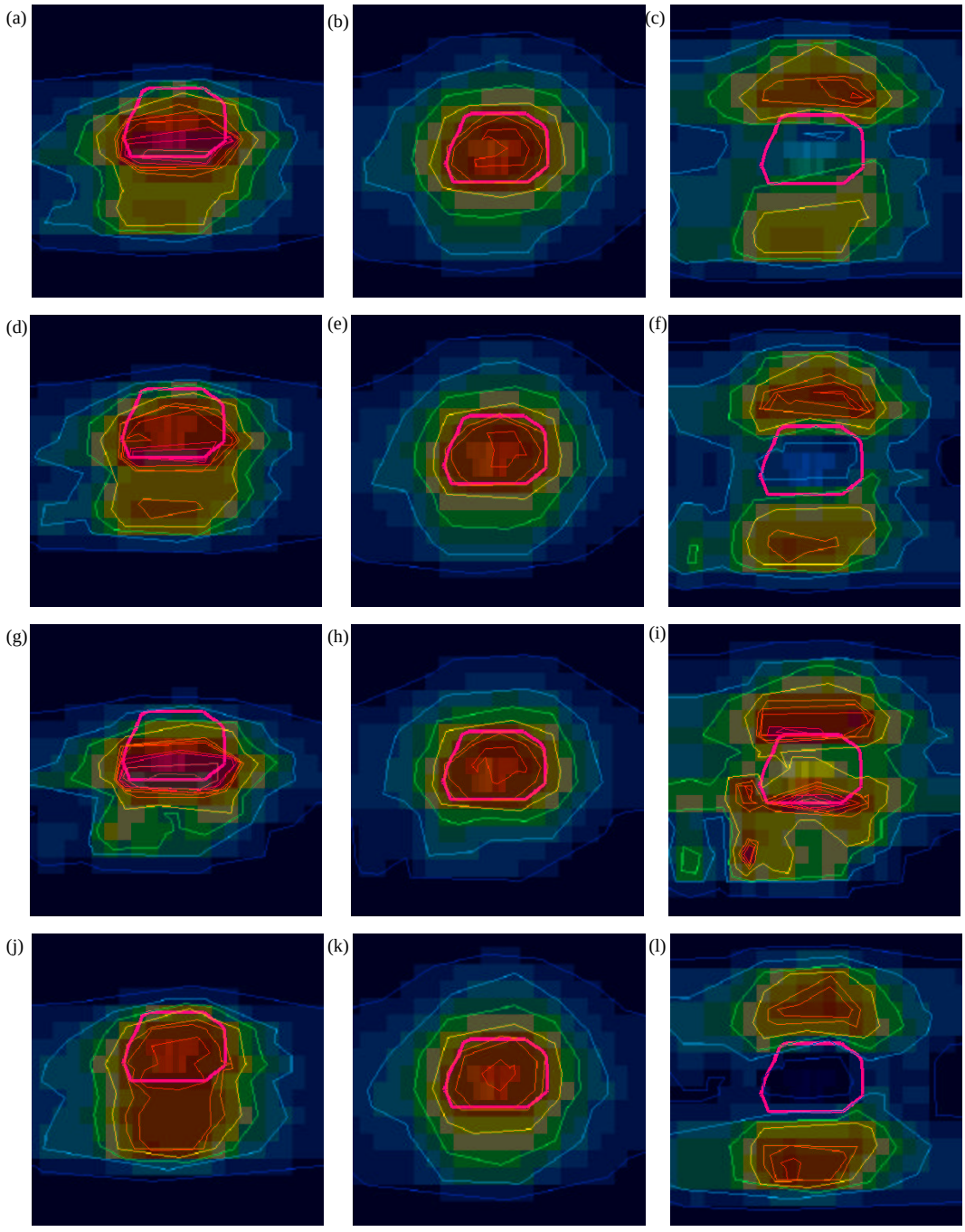

Figure 5.5: 3D distributions for treatment plans optimized for different irradiation times: (a-c) optimized for compensator based IMRT delivery (d-f) optimized for Step-and-Shoot IMRT (g-i) optimization of the expectation value of the dose (infinite treatment time) (j-l) optimized for an infinitesimal short irradiation time. The three columns show: (a,d,g,j) the static dose distribution, (b,e,h,k) the expectation value of the dose and (c,f,i,l) the standard deviation for an infinitesimal irradiation time. The color code legends in figures 5.8c,d apply.

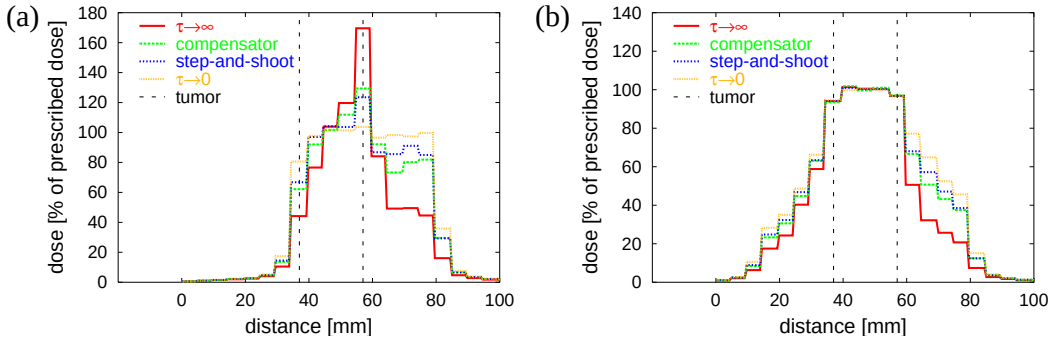

Figure 5.6: Profiles in CC direction through the center of the tumor for the dose distributions in figure 5.5: (a) for the static dose distributions (b) for the expectation values of the dose

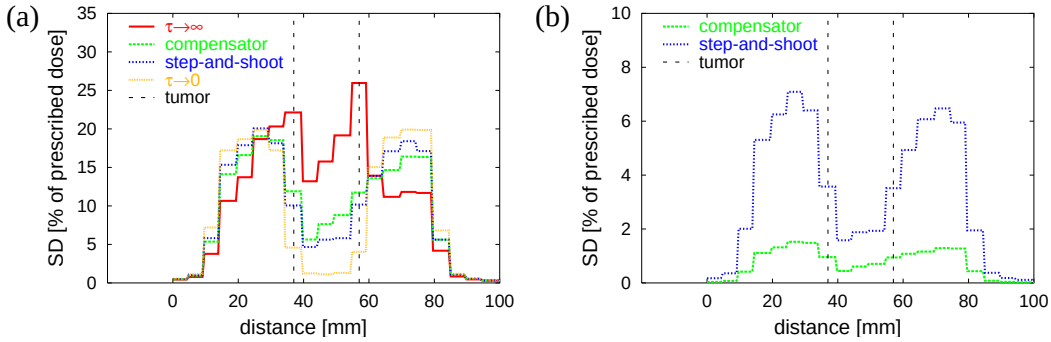

Figure 5.7: Profiles in CC direction through the center of the tumor: (a) for the standard deviation distributions for an infinitesimal irradiation time shown in figures 5.5c,f,i,l (b) for the standard deviations in figures 5.8a,b

Step-andShoot IMRT (figure 5.8b). For compensator based IMRT, the dose uncertainty for one fraction is in the order of 0.5% of the prescribed dose within the tumor and approximately 1.0% of the prescribed dose at the cranial and caudal edge of the tumor. For Step-and-Shoot IMRT the estimated uncertainty is considerably higher due to the reduced virtual irradiation time (figure 5.7b). However, rather crude approximations were made in section 5.1.5, so figure 5.8b is a rough estimate for the standard deviation of the dose. The irradiation time for compensator based IMRT is in the order of 10 seconds per beam. The virtual irradiation time for Step-and-Shoot IMRT is in the order of 2 seconds.

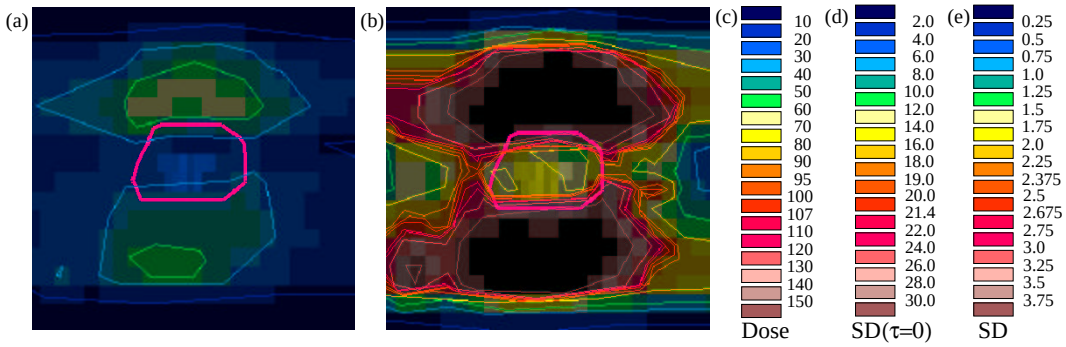

Figure 5.8: (a) Standard deviation of the dose for compensator based IMRT (for the corresponding static dose distribution in figure 5.5a) (b) standard deviation of the dose for Step-and-Shoot IMRT (for the corresponding static dose distribution in figure 5.5d) (c) color code legend for the dose distributions in figure 5.5 (d) color code legend for the standard deviation for an infinitesimal irradiation time in figure 5.5 (e) color code legend for the standard deviation in figures 5.8a,b

5.4 Discussion and future work

The amplitude of motion for lung tumors can be larger than the interfractional movements of the prostate. In addition, the inhomogeneities in the static dose distribution are partly leveled out within a single fraction and not only after a large number of fractions. Therefore, the modulation of the static dose distribution can be more pronounced, which, in turn, allows for a larger improvement compared to the safety margin approach. On the other hand, the description of respiratory motion is more complex and approximations have to be made in order to evaluate the expectation value of the quadratic objective function. One of these approximations is the linear approximation of the characteristic standard deviation function (section 4.3.3). A second one, possibly the most questionable one, is the estimation of the variance for Step-and-Shoot IMRT based on the variance for compensator based IMRT (section 5.1.5).

In order to improve the implementation of probabilistic treatment planning for lung tumors, a number of questions should be addressed in the future. Some are listed below:

1. A 4D CT data set of the patient should be the basis of probabilistic treatment planning. Based on the 4D CT, the tumor trajectory has to be estimated using appropriate image processing methods. In addition, the dose calculation should be improved by incorporating the CT images for different breathing phases not only into the estimation of the tumor trajectory, but also into the dose calculation.

2. The implementation should allow for arbitrary tumor trajectories and should be able to deal with variations in amplitude and exhale position.

3. A single 4D CT data set does not provide all parameters of the motion model. In particular the magnitude of variations of the exhale position and the amplitude cannot be derived from a single 4D CT scan. Other methods like fluoroscopic imaging should be established to estimate the respective parameters.

These three issues are mainly practical aspects that have to be solved in order to come closer to a clinical application. In addition, several conceptual aspects could be subject to further investigation:

4. The approximation of the variance of the dose for Step-and-Shoot IMRT should be further justified or improved (section 5.1.5). In particular, further investigation of this question should include variations in amplitude and exhale position which was not performed in section 5.1.5.

5. The dependency of the irradiation time on the maximum beamlet weight in the fluence map should be treated correctly during the IMRT optimization process (section 5.2.2).

6. Probabilistic treatment planning competes with gating as a strategy to deal with respiratory motion in radiotherapy. In principle, one could combine these two approaches, i.e. incorporate the residual motion within the gating window into the optimization using probabilistic treatment planning.

Chapter 6

Extensions and relations to other approaches

In this chapter, possible extensions and modifications of probabilistic treatment planning as analyzed in chapters 2 to 5 are discussed. Section 6.1 discusses the possibility of evaluating a modified objective function. Section 6.2 shows relations to other approaches to incorporate uncertainties in inverse planning.

6.1 Another objective function

A widely used objective function for treatment plan optimization (without considering organ motion) is [41]

$$\begin{aligned} E &= \sum_{i \in CTV} \alpha_{CTV}^{max} \left(D_i - D_{CTV}^{max}\right)_+^2 \\ &\quad + \sum_{i \in CTV} \alpha_{CTV}^{min} \left(D_{CTV}^{min} - D_i\right)_+^2 \\ &\quad + \sum_n \left[\sum_{i \in OAR_n} \alpha_n \left(D_i - D_n^{max}\right)_+^2 \right] \end{aligned} \tag{6.1}$$

In chapters 2 to 5, we considered the special case that $\alpha_{CTV}^{max} = \alpha_{CTV}^{min}$ and $D_{CTV}^{max} = D_{CTV}^{min}$. When we make the transition to probabilistic treatment planning, the expectation value of the objective for the CTV can, in this case, be written as the sum of the variance and the quadratic difference of expected and prescribed dose. As a consequence, overdosing the CTV is penalized as much as underdosing the CTV. This may not always be desired. Avoiding cold spots within the CTV may be more important than avoiding hot spots. In chapters 3 and 5, we minimized the objective

$$\sum_{i \in OAR_n} \alpha_n \left(\langle D_i \rangle - D_n^{max}\right)_+^2 \tag{6.2}$$

for each organ at risk. This is obviously not the expectation value of the OAR-term in objective function 6.1. In sections 2 and 4, this problem was avoided by setting $D_n^{max} = 0$. In this section, we want to discuss the possibility of evaluating directly the expectation value of objective function 6.1 for general parameters.

Objective function 6.1 is still a voxel-based objective function. It is therefore sufficient to consider a single voxel i. Let us consider the penalty for a potential overdosage of the voxel in the presence of motion:

$$\begin{aligned} E_i &= \left\langle (D_i - D^{max})_+^2 \right\rangle \\ &= \int (D_i - D^{max})^2 \Theta(D_i - D^{max}) P(D_i) dD_i \end{aligned} \tag{6.3}$$

where Θ is the Heavyside step function and $P(D_i)$ is the probability that a certain dose D_i is absorbed in voxel i. Generally, we can not easily calculate $P(D_i)$. However, in certain cases, we can assume that $P(D_i)$ is a Gaussian distribution with expected dose $\langle D_i \rangle$ and variance V_i. If we consider the irradiation of a single fraction, $P(D_i)$ will generally not be Gaussian distributed. However, for a realistic number of 30 fractions it can be a good approximation. If we, for example, consider interfractional movements and consider random errors only, $P(D_i)$ will be extremly close to a Gaussian according to the central limit theorem. However, as soon as systematic errors are taken into account this is not fulfilled any more (see also Bortfeld *et al* [36] for a discussion of this issue in the context of respiratory motion).

We make the approximation that $P(D_i)$ is Gaussian. The probability distribution can thus be parameterized by the expectation value and the variance. Both parameters can be calculated from the fluence profiles with the tools provided in this thesis. The objective for voxel i becomes (the index i is omitted)

$$\begin{aligned} E &= \int_{-\infty}^{\infty} (D - D^{max})^2 \Theta(D - D^{max}) \frac{1}{\sqrt{2\pi V}} \exp\left(-\frac{(D - \langle D \rangle)^2}{2V} \right) dD \\ &= \int_{D^{max}}^{\infty} (D - D^{max})^2 \frac{1}{\sqrt{2\pi V}} \exp\left(-\frac{(D - \langle D \rangle)^2}{2V} \right) dD \end{aligned}$$

Introducing the new variables $\tilde{D} = D - D^{max}$ and $\langle \tilde{D} \rangle = \langle D \rangle - D^{max}$ yields

$$\begin{aligned} E &= \frac{1}{\sqrt{2\pi V}} \int_0^{\infty} \tilde{D}^2 \exp\left(-\frac{(\tilde{D} - \langle \tilde{D} \rangle)^2}{2V} \right) d\tilde{D} \\ &= \frac{1}{\sqrt{2\pi V}} \exp\left(-\frac{\langle \tilde{D} \rangle^2}{4V} \right) \sqrt{V^3} \Gamma(3) \mathcal{Z}_3 \left(-\frac{\langle \tilde{D} \rangle}{\sqrt{V}} \right) \end{aligned} \tag{6.4}$$

where $\mathcal{Z}_n$ is a parabolic cylinder function [42, 43] which obeys the equation

$$\int_0^{\infty} x^{-n-1} \exp\left(-\frac{(x-s)^2}{2\sigma^2} \right) dx = \exp\left(-\frac{s^2}{4\sigma^2} \right) \sigma^{-n} \Gamma(-n) \mathcal{Z}_n \left(-\frac{s}{\sigma} \right) \tag{6.5}$$

The gradient of the objective with respect to the bixel weight Φ_α is given by

$$\frac{\partial E}{\partial \Phi_\alpha} = \int_0^\infty \frac{\tilde{D}^2}{\sqrt{2\pi}} \frac{\partial}{\partial \Phi_\alpha} \left[\frac{1}{\sqrt{V}} \exp\left(-\frac{(\tilde{D} - \langle \tilde{D} \rangle)^2}{2V} \right) \right] d\tilde{D} \tag{6.6}$$

Evaluation of the derivative yields

$$\begin{aligned} \frac{\partial E}{\partial \Phi_\alpha} = & \int_0^\infty \frac{\tilde{D}^2}{\sqrt{2\pi}} \exp\left(-\frac{(\tilde{D} - \langle \tilde{D} \rangle)^2}{2V} \right) \\ & \times \left[\tilde{D}^2 \left(\frac{1}{2\sqrt{V^5}} \frac{\partial V}{\partial \Phi_\alpha} \right) + \tilde{D} \left(-\frac{1}{\sqrt{V^5}} \frac{\partial V}{\partial \Phi_\alpha} + \frac{1}{\sqrt{V^3}} \frac{\partial \langle \tilde{D} \rangle}{\partial \Phi_\alpha} \right) \right. \\ & \left. + \left(-\frac{1}{2\sqrt{V^3}} + \frac{\langle \tilde{D} \rangle}{2\sqrt{V^5}} \frac{\partial V}{\partial \Phi_\alpha} - \frac{\langle \tilde{D} \rangle}{\sqrt{V^3}} \frac{\partial \langle \tilde{D} \rangle}{\partial \Phi_\alpha} \right) \right] d\tilde{D} \end{aligned} \tag{6.7}$$

which can also be expressed in terms of parabolic cylinder functions. Both the objective function itself and its derivatives with respect to the bixel weights can explicitely be written as a function of the bixel weights. In principle, this allows for an evaluation of the expectation value of objective function 6.1 by standard gradient methods (assuming that the objective function is well behaved and does not show local minima).

6.2 Coverage probability, delineation errors and organ motion

Let us assume that N CT scans of a patient exist and that CTV and OARs are contoured in each image. To make it explicit, let us consider interfractional motion of the prostate. Based on the N CT scans, one can estimate the probability that a certain voxel is covered by a certain structure. Assuming that in N_i^T of N CT scans, voxel i is covered by the tumor, we can estimate that the probability to find tumor tissue in voxel i is $C_i = N_i^T/N$ when we assume that each CT scan is a priori equally likely. We could also assume that there is a single CT scan of a patient and different physicians independently delineated the tumor. As a result, one may obtain multiple contours for the tumor which are not identical and can be used to estimate the probabilities C_i to find tumor tissue at voxel i. In a paper by Baum *et al* [44] it was suggested that this probability can be incorporated into a voxel-based objective function as a voxel-dependent penalty factor. In this section, we will define this approach for the quadratic objective function and we show that under certain assumptions the approach is mathematically equivalent to two other approaches that start from entirely different perspectives.

6.2.1 The coverage probability approach

We consider a one-dimensional geometry like in chapter 4 and focus on a boundary between the tumor and an OAR. The boundary is uncertain, either because of motion effects or

because of delineation uncertainties. We assume that the probability to find tumor tissue at position r is given by $C(r)$, the coverage probability. We heuristically suggest the objective function

$$\begin{aligned} E &= \int \alpha_T C(r) \left[D(r) - D_T\right]^2 dr \\ &\quad + \int \alpha_{OAR}(1 - C(r)) D^2(r) dr \end{aligned} \tag{6.8}$$

where the integration range covers the transition region of tumor and OAR. When $C(r)$ is the Heavyside step function objective function 6.8 reduces to the standard quadratic objective function applied in section 4 and 2.

6.2.2 Delineation errors

In this section, we assume that there are no organ movements but a static geometry. We focus on the boundary of the tumor and the adjacent OAR. Let us assume that the boundary is delineated at the coordinate $r = \beta$. The quadratic objective function in the region of interest is

$$E(\beta) = \int \alpha(r, \beta) \left[D(r) - D_{pres}(r, \beta)\right]^2 dr \tag{6.9}$$

where

$$\alpha(r, \beta) = \alpha_{OAR} + (\alpha_T - \alpha_{OAR})\Theta(\beta - r) \tag{6.10}$$

$$D_{pres}(r, \beta) = D_T \Theta(\beta - r) \tag{6.11}$$

where $\Theta(r)$ is the Heavyside step function, i.e. $\Theta(r) = 0$ $(r < 0)$ and $\Theta(r) = 1$ $(r > 0)$. Let us now assume that the boundary between tumor and OAR is uncertain, i.e. the parameter β is uncertain and $P(\beta)$ is the probability density that a particular value of β is the "true" boundary. We apply the same postulate as in section 1.4, which means, we optimize the expectation value of the objective function in order to incorporate the delineation uncertainty into the optimization:

$$\langle E \rangle = \int E(\beta) P(\beta) d\beta \tag{6.12}$$

Evaluating the objective function 6.12 yields

$$\langle E \rangle = \int \int \alpha(r, \beta) \left[D(r) - D_{pres}(r, \beta)\right]^2 dr P(\beta) d\beta \tag{6.13}$$

$$= \int \Bigg[D^2(r) \int \alpha(r, \beta) P(\beta) d\beta \tag{6.14}$$

$$-2D(r) \int \alpha(r, \beta) D_{pres}(r, \beta) P(\beta) d\beta \tag{6.15}$$

$$+ \int \alpha(r, \beta) D^2_{pres}(r, \beta) P(\beta) d\beta \Bigg] dr \tag{6.16}$$

The integral over β in the first term 6.14 can be rearranged to give

$$\begin{aligned} \int \alpha(r,\beta)P(\beta)d\beta &= \alpha_{OAR} + (\alpha_T - \alpha_{OAR}) \int \Theta(r,\beta)P(\beta)d\beta & (6.17) \\ &= \alpha_{OAR}(1 - C(r)) + \alpha_T C(r) & (6.18) \end{aligned}$$

where

$$C(r) = \int \Theta(r,\beta)P(\beta)d\beta \tag{6.19}$$

can be interpreted as the coverage probability since for every position r, $C(r)$ gives the probability that β is larger than r, i.e. that there is tumor tissue at position r. Evaluation of the integrals over β in 6.15 and 6.16 yields

$$\int \alpha(r,\beta)D_{pres}(r,\beta)P(\beta)d\beta = D_T\alpha_T C(r) \tag{6.20}$$

$$\int \alpha(r,\beta)D^2_{pres}(r,\beta)P(\beta)d\beta = D^2_T\alpha_T C(r) \tag{6.21}$$

Substituting this into equation 6.13 gives us

$$\begin{aligned} \langle E \rangle &= \int \alpha_{OAR} D^2(r)(1 - C(r))dr & (6.22) \\ &\quad + \int \alpha_T \left[D^2(r) - 2D(r)D_T + D_T^2\right] C(r)dr & (6.23) \end{aligned}$$

which is equivalent to the coverage probability approach in equation 6.8. Optimizing the expectation value of the objective function in the presence of delineation uncertainties is thus equivalent to the coverage probability approach which was introduced in section 6.2.1 without further justification.

6.2.3 Motion-induced uncertainties

Let us reconsider interfractional organ motion and the incorporation of random errors into the optimization. We need two coordinate systems: let r' denote a position in the static coordinate system and let r denote a position in the tissue which moves as a rigid object. As discussed in section 2.4, the expectation value of the quadratic objective function can be written as

$$\langle E \rangle = \int \alpha(r,\beta) \left[\left(\langle D \rangle(r) - D_{pres}(r,\beta) \right)^2 + \frac{1}{N} \left(\langle D^2 \rangle(r) - \langle D \rangle^2(r) \right) \right] dr \tag{6.24}$$

where

$$\begin{aligned} \alpha(r,\beta) &= \alpha_{OAR} + (\alpha_T - \alpha_{OAR})\Theta(\beta - r) & (6.25) \\ D_{pres}(r,\beta) &= D_T\Theta(\beta - r) & (6.26) \end{aligned}$$

The boundary β between tumor and OAR in the moving coordinate system is assumed to be known, i.e. we consider purely motion effects and no delineation errors. The expectation values $\langle D\rangle$ and $\langle D^2\rangle$ are given by

$$\langle D\rangle(r) = \int D(r')P(r-r')dr' \tag{6.27}$$

$$\langle D^2\rangle(r) = \int D^2(r')P(r-r')dr' \tag{6.28}$$

where $D(r')$ refers to the dose delivered to the static point r' and $P(r-r')$ is the probability to find the tissue element r at position r'. For the special case that only a single fraction is considered ($N=1$) equation 6.24 simplifies to

$$\langle E\rangle = \int \alpha(r,\beta)\left[\langle D^2\rangle(r) - 2D_{pres}(r,\beta)\langle D\rangle(r) + D^2_{pres}(r,\beta)\right]dr \tag{6.29}$$

When we substitute 6.27 and 6.28 into 6.29 we get

$$\begin{aligned}
\langle E\rangle &= \int \alpha(r,\beta)\left[\int \left[D^2(r') - 2D_{pres}(r,\beta)D(r') + D^2_{pres}(r,\beta)\right]P(r-r')dr'\right]dr \\
&= \int\Bigg[\int D^2(r')\alpha(r,\beta)P(r-r')dr \\
&\qquad - \int 2D(r')\alpha(r,\beta)D_{pres}(r,\beta)P(r-r')dr \\
&\qquad + \int \alpha(r,\beta)D^2_{pres}(r,\beta)P(r-r')dr\Bigg]dr' \\
&= \int \alpha_{OAR}D^2(r')(1-C(r',\beta))dr' \\
&\quad + \int \alpha_T\left[D^2(r') - 2D(r')D_T + D_T^2\right]C(r',\beta)dr'
\end{aligned}$$

where

$$C(r',\beta) = \int \Theta(\beta - r)P(r-r')dr$$

is the probability that a point r, which is smaller than β, is at position r', i.e. it is the coverage probability.

We thus find that optimizing the expectation value of the objective function in the presence of a random displacement of the tumor due to interfractional motion is equivalent to the coverage probability approach. However, this equivalence only holds when the dose distribution is optimized for a single fraction. For the more general case where the cumulative dose for multiple fractions is optimized, this equivalence does not apply. Thus, probabilistic treatment planning defined in chapters 2 and 3 is the more general approach to incorporate interfractional organ movements into IMRT optimization. The coverage

probability approach can only reproduce the safety margin like solution, characterized by a homogeneous dose distribution delivered to the tumor in each fraction. However, the coverage probability approach is computationally less complex. Therefore, the equivalence of the coverage probability approach and probabilistic treatment planning for the special case $N = 1$ is helpful if one is only interested in reproducing the safety margin like solution.

Chapter 7

Conclusions

7.1 Summary of concepts and results

General concept

The thesis presents an off-line strategy to incorporate organ movements into inverse IMRT treatment planning. We refer to this approach as "probabilistic treatment planning". Following this approach, the optimization of the fluence maps is based on a mathematical model of organ motion which describes the possible geometric variations of the patient's anatomy. Organ motion is to a large extent a stochastic process. This especially applies to interfractional movements, but also to respiratory motion. The motion model involves a set of random variables that parameterize the anatomical state of the patient and their associated probability distributions. Consequently, the dose delivered to the patient becomes a random variable too and is characterized by an expectation value of the dose and its variance. In order to incorporate the motion model into the optimization, we optimize the expectation value of a quadratic objective function. This objective can be written as a sum of two terms: first the variance of the dose, and second, the quadratic difference of the expectation value of the dose and the prescribed dose (section 1.4).

Interfractional motion

In chapters 2 and 3, interfractional motion is considered. Chapter 2 derives a motion model for interfractional motion (section 2.1) and analyzes the concept of probabilistic treatment planning for an idealized patient geometry. Chapter 3 provides an application to clinical data of prostate patients. The underlying assumption of the motion model is that interfractional displacements of tissue elements can be described by a Gaussian distribution with parameters mean position and distribution width. The distribution width determines the magnitude of motion. The displacement of the tissue element from its mean position may be different in different fractions and is referred to as the random error. The mean position of the tissue element has to be estimated from tomographic images of the patient. Typically, the number of images is small and, therefore, the estimate of the mean position

is uncertain. This is referred to as a systematic error. The magnitude of motion can also be estimated from patient specific images. In addition, clinical studies on organ motion may provide prior knowledge derived from a larger population of patients. The concept of Bayesian inference is applied to derive probability distributions for the mean position and the magnitude of motion based on contributions of the patient specific data and population based knowledge. Bayesian inference, in particular, allows for an interpolation between knowledge from the patient's images and knowledge from clinical studies, which is relevant since the number of CT scans of the individual patient is usually small. The motion model allows for a unified description of random errors and systematic errors.

Probabilistic treatment planning for interfractional motion is first analyzed for an idealized two-dimensional patient geometry (chapter 2). This allows us to demonstrate the mathematical formalism and to discuss the generic features of probabilistic treatment planning. The concept is then implemented into a research version of the inverse planning tool KonRad (chapter 3). The basic features of probabilistic treatment planning observed for the idealized model were mostly reproduced for the application to a clinical prostate case.

The variance of the cumulative dose depends on the number of fractions. Therefore, we obtain different optimal treatment plans for a different number of fractions. For the treatment plan optimized for 30 fractions, the dose distribution delivered to a static patient geometry is characterized by inhomogeneous patterns (sections 2.4, 3.2.3). These inhomogeneities are shaped in such a way that regions where tumor tissue is located only rarely is irradiated with a lower dose than the dose prescribed to the tumor. In order to ensure a sufficient target coverage, this is compensated for by delivering a higher dose to regions that are mostly occupied by tumor tissue. After 30 fractions, a widely homogeneous dose distribution is delivered to the tumor. Optimization of the fluence map for a single fraction reproduces a safety margin like solution, characterized by a homogeneous high dose region in the dose distribution delivered to a static patient geometry (sections 2.4, 3.2.4). For a single fraction, initial dose inhomogeneities could never be compensated for by later fractions. This is "measured" by the variance term which suppresses a modulation of the dose distribution. Inhomogeneities in the dose delivered to a static patient geometry allow for an improved expectation value of the dose distribution compared to the safety margin like solution, i.e. dose gradients at the transition between tumor and healthy tissue are steeper. On the other hand, the standard deviation of the dose increases and makes the dose delivered to the CTV less predictable. An optimization of the expectation value of the dose alone further increases the standard deviation of the dose and makes the assumed benefit of the optimized expectation value questionable (sections 2.4.1, 3.2.5).

The inclusion of systematic errors and an uncertain magnitude of motion into the optimization mainly leads to an extension of the high dose region towards the normal tissue. It does not lead to a major change of the modulation pattern (sections 2.5, 3.6). The inclusion of systematic errors into the optimization demonstrates a general problem in treatment evaluation (section 3.4). In the presence of systematic errors, the expectation value of the

dose is not a good surrogate for the dose distribution as a whole that may be delivered to the patient. It can never be realized at each voxel simultaneously. In the framework of a diploma thesis, a simulation and visualization tool was depeloped, which allows the display of probabilities for an appropriate dose delivery. For each voxel, the probability that the delivered dose is within a predefined dose interval is displayed. Generally, a large variety of distributions can be displayed in order to characterize the dose delivered to the patient. None of them seem to be perfect or sufficent all alone.

For small motion amplitudes in the order of 2 mm or less, the treatment plan optimization becomes widely insensitive to the number of fractions and a mainly safety margin like treatment plan is generated. The distance of hot spots and cold spots in the dose distribution delivered to a static patient geometry has to be in the order of the magnitude of motion. For small motion amplitudes this is not possible due to lateral scattering of the photons and a limited resolution of the MLC.

Respiratory motion

Chapters 4 and 5 deal with the application of probabilistic treatment planning to lung tumors. We model the trajectory of the moving tumor during respiratory motion using a cosine function to the power of four (section 4.2). In order to model the variability of the breathing pattern, we assume that the model parameters amplitude and exhale position are random variables. The irradiation time of one field is generally not a multiple of the breathing cycle. Therefore, the delivered dose depends also on the breathing phase at the time when the irradiation starts. In chapter 4 we derive equations to calculate the expectation value of the dose (sections 4.3.1, 4.4.1) and the associated variance (sections 4.3.2, 4.4.2) for the irradiation of a single field and a one-dimensional geometry. An exact calculation of the variance (within the framework of the motion model) is relatively unhandy. Therefore, we introduce an approximation of the variance where the variance for arbitary irradiation times of the field is approximated based on the variance for an infinitesimal irradiation time (sections 4.3.3, 4.4.3).

The application of this concept to probabilistic treatment planning for lung tumors (chapter 5) is not straightforward. The variance of the dose depends on temporal aspects of the dose delivery process. The entire dose field is not applied at once. For Step-and-Shoot IMRT, an intensity modulated field is realized by a large number of MLC segments which are applied one after another. In order to assess the dose uncertainty for clinical IMRT treatments, we first consider dose delivery with compensators (sections 5.1.1, 5.1.2). Based on the variance for compensator based dose delivery, an approximation of the variance for Step-and-Shoot IMRT is suggested (sections 5.1.3-5.1.5).

The concept is partly implemented into the inverse planning tool KonRad (section 5.2) and applied to a lung tumor (section 5.3). Four different treatment plans are compared: compensator based IMRT, Step-and-Shoot IMRT, treatment planning assuming that the

expectation value of the dose is always realized, and treatment planning assuming an infinitesimal irradiation time. The treatment plans for compensator based IMRT and Step-and-Shoot IMRT show characteristic modulation patterns in the dose distribution that would be delivered to a stationary patient geometry. Roughly speaking, the dose delivered to regions where the tumor is located at exhale is increased. This allows for a reduction of the dose delivered to regions where the tumor is at inhale. The magnitude of modulation is higher for the compensator based IMRT treatment plan compared to Step-and-Shoot IMRT because the estimated dose variance is larger for Step-and-Shoot IMRT. If an infinitesimal irradiation time is assumed for treatment plan optimization, a safety margin like solution can be reproduced. The dose distribution delivered to a stationary patient geometry is homogeneous within the entire region where the tumor can be located. The expectation values of the dose distributions indicate that the modulations of the dose distribution delivered to a stationary patient geometry allow for a better sparing of the healthy tissue compared to the safety margin like treatment plan.

Extensions

The last chapter of this thesis outlines a possible modification of the objective function and shows relations to another approach to deal with uncertainties in radiotherapy. In section 6.2, we discuss the relations between the so called coverage probability approach, the inclusion of delineation uncertainties, and probabilistic treatment planning to incorporate organ motion. In section 6.1, a modification of the quadratic objective function is outlined. This modification would allow for different penalties for overdosage and underdosage of the tumor.

7.2 Discussion and conclusions

The motivation for probabilistic treatment planning can be seen from different perspectives. One aspect is that it seems to be natural to incorporate organ motion into the optimization of an IMRT treatment plan. In the framework of the traditional safety margin approach, organ motion effects are incorporated into the delineation process instead. Based on the available knowledge on organ motion, the appropriate size of the margin has to be determined. Generally, the minimal margin required to expand the CTV to the PTV is non-isotropic and it is not easy to determine the “optimal” margin that allows for the best possible sparing of the adjacent healthy tissue. In the IMRT optimization step, the dose distribution in the artificial PTV is optimized without assessing the dose distribution in the moving tumor itself, which would be of primary interest. Probabilistic treatment planning eliminates the extra step of choosing an appropriate safety margin. The available knowledge on organ motion is incorporated into the optimization of the dose distribution and the optimization routine determines the required expansion of the irradiated volume automatically. In addition, the concept assesses the dose distribution delivered to the anatomical structure and not only the dose delivered to a certain point in space, regardless

of what type of tissue is mostly located at this point.

Apart from that, one can ask for the dosimetric improvements that probabilistic treatment planning can provide in comparison to the safety margin approach. For small amplitudes of motion, probabilistic treatment planning can only reproduce treatment plans that deliver a widely homogeneous dose to the region where the tumor is located. The advantage is that the optimization automatically determines the appropriate expansion of the high dose region around the tumor. For larger amplitudes of motion, probabilistic treatment planning generates treatment plans which are qualitatively different and cannot be produced by a safety margin approach. For such treatment plans, the dose distribution delivered to a stationary patient geometry would be inhomogeneous within the region where the tumor is located. Regions where tumor tissue is expected to be located only rarely are irradiated with a lower dose than the dose prescribed to the tumor. This is compensated for be delivering higher doses to regions where mostly tumor tissue is located. Due to organ movements during the course of treatment, initial dose inhomogeneities level out and a widely homogeneous dose is delivered to the tumor. This modulation allows for a better sparing of the adjacent healthy tissue compared to a safety margin like solution.

On the other hand, treatment plans that would deliver an inhomogeneous dose to a stationary patient geometry bear risks. If organ movements during the course of treatment do not occur in a similar way as assumed in the treatment planning process, the dose distribution applied to the tumor may remain inhomogeneous. The treatment planner has to find a trade-off between the potential benefit and an increased risk. The benefit would be the better sparing of healthy tissues, the risk would be an inhomogeneous cumulative dose distribution within the CTV. By including the variance of the dose into the objective function, the optimal trade-off is in principle defined mathematically. By changing the relative weight of the variance term in the objective function, the treatment planner can control the trade-off between benefit and risk.

It has been suggested previously by other authors that organ motion can be incorporated into IMRT treatment planning via optimizing the objective function evaluated at the expectation value of the dose distribution. For the quadratic objective function this corresponds to a minimization of the quadratic difference of expected and prescribed dose while the variance term is neglected. In this thesis, it was demonstrated that this approach fails for considerably large amplitudes of motion.

7.3 Outlook and future work

This section outlines several aspects of probabilistic treatment planning that could be subject to further investigation in the future. Some aspects are of practical importance in order to implement a clinical application. But there are also a number of conceptual issues. Some aspects apply to both interfractional and respiratory motion, others mainly refer to

interfractional motion. For respiratory motion, a seperate outlook section is provided (section 5.4).

Practical issues

For a clinical application of probabilistic treatment planning, the parameters of the motion model have to be estimated from the available image data of the patient. In order to perform this estimation, elastic image registration tools are required (also referred to as deformable registration methods). Elastic image registration provides the positions of a tissue element in different images, which forms the basis to estimate parameters of the motion model.

In this thesis, the optimization of a treatment plan was performed via a beamlet based optimization which yields an intensity modulated fluence map for each beam. In order to deliver the intensity modulated field in practice using Step-and-Shoot IMRT, the fluence map has to be discretized and decomposed into deliverable apertures using a sequencer. One may hypothesize that treatment plans which deliver a modulated dose distribution to a stationary patient geometry are more sensitive to the discretization of the fluence map and that more MLC segments are needed in order to approximate the beamlet based optimized fluence map sufficiently well. This issue has not been investigated yet.

Conceptual issues

For probabilistic treatment planning incorporating the interfractional movements of the prostate, it was assumed in chapter 3 that a set of CT images is available for treatment planning before the first fraction. In a clinical environment this may not be realistic. The number of CT images increases during the course of treatment. Section 2.7 outlines a concept to optimize two fluence maps simultaneously in order to adapt the treatment plan during the course of treatment. However, an application to clinical data is not straight forward as discussed in the last paragraph in section 2.7. Further work concerning this issue may be beneficial for both practical and conceptual questions.

Probabilistic treatment plan optimization was performed for the quadratic objective function. The quadratic objective function has the advantage that it can be evaluated by considering the movement of each tissue element separately. Practically, the movement of neighboring tissue elements is of course highly correlated. A principal component analysis (PCA) provides a method to parameterize the geometric changes of the patient as a whole [34, 35]. A PCA provides the prevalent deformation modes of the tissue and the entire geometric change of the patient anatomy can be parameterized by a small set of random variables. Although this is not necessary to evaluate the quadratic objective function, it may be beneficial for other reasons. First, it provides a more consistent description of geometric changes. Second, it would be possible to overcome the limitation to objective

functions that are separable with respect to the movement of different tissue elements. And third, it could be used to generate random samples of the cumulative dose distribution and the DVH. The simulation tool described in section 3.3.1 calculates the expectation value and the variance of the dose by simulating displacements for each voxel seperately. This does not allow for generating a realistic sample of the cumulative 3D dose distribution.

When the dose delivered to a static patient geometry is inhomogeneous within the CTV, the dose delivered to an element of tumor tissue is not the same in each fraction. As a consequence, the biological effect is different compared to a uniform fractionation. The biological effect of the non-uniform fractionation could e.g. be assessed in the framework of the linear-quadratic cell survival model by approximating the expectation value of the equivalent uniform fraction dose as the sum of the expectation value of the physical dose and a variance-dependent perturbation [36].

In the future, probabilistic treatment planning could also be investigated for other objective functions. One drawback of the quadratic objective function is that overdosage und underdosage of the tumor are considered equally bad, which may not always be desired. Section 6.1 outlines a modification of the quadratic objective function that can overcome this limitation.

Appendix A

Evaluation of the rotation therapy model

In this section we discuss practical aspects of the evaluation of the expectation value of the dose, its variance and the minimization of the objective function for the idealized model in section 2.

A.1 Calculation of expectation values

In this section we derive the expectation values in equations 2.48-2.52 that are used to calculate the expectation value of the dose and its variance in the presence of systematic errors and an uncertain distribution width. Equations 2.34-2.37 for dose calculations based on random errors alone and equations 2.40-2.44 for systematic errors are simplifications of the general case and can be derived similarly. Further details can be found in the appendix of [1].
The random errors in different fractions are statistically independent. In other words, the probability distribution for a set of displacements $\{\Delta \boldsymbol{g}_\mu\}_1^N$ given the model parameters $(\Delta \boldsymbol{s}, \sigma)$ factorizes:

$$P(\Delta \boldsymbol{g}_1, \ldots, \Delta \boldsymbol{g}_N | \Delta \boldsymbol{s}, \sigma) = \prod_{\mu=1}^{N} P(\Delta \boldsymbol{g}_\mu | \Delta \boldsymbol{s}, \sigma)$$

where $P(\Delta \boldsymbol{g}_\mu | \Delta \boldsymbol{s}, \sigma)$ is given by equation 2.53 for all $\mu = 1, \ldots, N$. For the expectation value of the cumulative dose we obtain

$$\begin{aligned}
\langle D_c \rangle(r) &= \int \cdots \int \left[\sum_{\mu=1}^{N} D(\boldsymbol{r} | \Delta \boldsymbol{g}_\mu) \right] P(\Delta \boldsymbol{g}_1, \ldots, \Delta \boldsymbol{g}_N | \Delta \boldsymbol{s}, \sigma) \\
&\qquad \times P(\Delta \boldsymbol{s} | \sigma, \{\Delta \boldsymbol{p}_\mu\}) P(\sigma | \{\Delta \boldsymbol{p}_\mu\}) \, d\Delta \boldsymbol{g}_1 \cdots d\Delta \boldsymbol{g}_N \, d\Delta \boldsymbol{s} \, d\sigma \\
&= \sum_{\mu=1}^{N} \int \int \int D(\boldsymbol{r} | \Delta \boldsymbol{g}_\mu) P(\Delta \boldsymbol{g}_\mu | \Delta \boldsymbol{s}, \sigma) \\
&\qquad \times P(\Delta \boldsymbol{s} | \sigma, \{\Delta \boldsymbol{p}_\mu\}) P(\sigma | \{\Delta \boldsymbol{p}_\mu\}) \, d\Delta \boldsymbol{g}_\mu \, d\Delta \boldsymbol{s} \, d\sigma
\end{aligned}$$

which yields equations 2.48 and 2.50. For the expectation value of the cumulative dose squared we obtain

$$\begin{aligned}
\langle D_c^2 \rangle(r) &= \int \cdots \int \left[\sum_{\mu=1}^{N} D(\boldsymbol{r} | \Delta \boldsymbol{g}_\mu) \right]^2 P(\Delta \boldsymbol{g}_1, \ldots, \Delta \boldsymbol{g}_N | \Delta \boldsymbol{s}, \sigma) \\
&\qquad \times P(\Delta \boldsymbol{s} | \sigma, \{\Delta \boldsymbol{p}_\mu\}) P(\sigma | \{\Delta \boldsymbol{p}_\mu\}) \, d\Delta \boldsymbol{g}_1 \cdots d\Delta \boldsymbol{g}_N \, d\Delta \boldsymbol{s} \, d\sigma \\
&= \sum_{\mu=1}^{N} \int \int \int D^2(\boldsymbol{r} | \Delta \boldsymbol{g}_\mu) P(\Delta \boldsymbol{g}_\mu | \Delta \boldsymbol{s}, \sigma) \\
&\qquad \times P(\Delta \boldsymbol{s} | \sigma, \{\Delta \boldsymbol{p}_\mu\}) P(\sigma | \{\Delta \boldsymbol{p}_\mu\}) \, d\Delta \boldsymbol{g}_\mu \, d\Delta \boldsymbol{s} \, d\sigma \\
&\quad + \sum_{\substack{\mu,\eta=1 \\ \mu \neq \eta}}^{N} \int \int \int \int D(\boldsymbol{r} | \Delta \boldsymbol{g}_\mu) D(\boldsymbol{r} | \Delta \boldsymbol{g}_\eta) P(\Delta \boldsymbol{g}_\mu | \Delta \boldsymbol{s}, \sigma) P(\Delta \boldsymbol{g}_\eta | \Delta \boldsymbol{s}, \sigma) \\
&\qquad \times P(\Delta \boldsymbol{s} | \sigma, \{\Delta \boldsymbol{p}_\mu\}) P(\sigma | \{\Delta \boldsymbol{p}_\mu\}) \, d\Delta \boldsymbol{g}_\mu \, d\Delta \boldsymbol{g}_\eta \, d\Delta \boldsymbol{s} \, d\sigma
\end{aligned}$$

which yields equations 2.49, 2.51 and 2.52. All expectation values are radially symmetric functions and do not depend on the azimuthal angle φ but only on the radial coordinate r.

A.2 Numerical aspects

In this section we discuss the numerical evaluation of the rotation therapy model in section 2. For simplicity, we consider the optimization problem in section 2.4 which includes random errors only. The objective function in sections 2.5 and 2.6 can be evaluated in a similar way.

For numerical evaluation of the model we discretize the fluence profile, i.e. the fluence is constant on intervals $[i\Delta x, (i+1)\Delta x]$ $(i \in \mathbb{N}_0)$. Each segment of the fluence profile is referred to as a *bixel*. To calculate the dose contribution of a bixel i to a point (r, φ) in the patient given a displacement $\Delta \boldsymbol{g} = (\Delta g, \Delta \varphi)$ the following integral has to be solved numerically:

$$d_i(r, \varphi | \Delta g \Delta \varphi) = \frac{1}{2\pi} \int_0^{2\pi} \Theta(\psi, i, r, \varphi, \Delta g, \Delta \varphi) \exp(-\mu z(r, \varphi, \psi)) \, d\psi \tag{A.1}$$

where

$$\Theta\left(\psi, i, r, \varphi, \Delta g, \Delta\varphi\right) = \begin{cases} 1 & \left(\left|x\left(r, \varphi, \Delta g, \Delta\varphi, \psi\right)\right| \in [i\Delta x, (i+1)\Delta x]\right) \\ 0 & otherwise \end{cases} \tag{A.2}$$

and x and z are given by equation 2.26 and 2.27, respectively. The dose distribution can now be rewritten as a sum:

$$D\left(r, \varphi|\Delta g\Delta\varphi\right) = \sum_i d_i\left(r, \varphi|\Delta g\Delta\varphi\right)\Phi_i$$

where Φ_i is the fluence in bixel i. To calculate the expectation value of the dose

$$\langle D\rangle\left(r\right) = \int_0^{2\pi}\int_0^{\infty} D\left(r, \varphi|\Delta g\Delta\varphi\right) P\left(\Delta g, \Delta\varphi|\Delta\boldsymbol{s}, \sigma\right)\Delta g\, d\Delta g\, d\Delta\varphi \tag{A.3}$$

an effective dose contribution function $\bar{d}_i(r)$ is defined as

$$\bar{d}_i\left(r\right) = \int_0^{2\pi}\int_0^{\infty} d_i\left(r, \varphi|\Delta g\Delta\varphi\right) P\left(\Delta g, \Delta\varphi|\Delta\boldsymbol{s}, \sigma\right)\Delta g\, d\Delta g\, d\Delta\varphi$$

which is independent of φ, so that

$$\langle D\rangle\left(r\right) = \sum_i \bar{d}_i\left(r\right)\Phi_i$$

holds. To calculate the expectation value

$$\left\langle D^2\right\rangle = \int_0^{2\pi}\int_0^{\infty} D^2\left(r, \varphi|\Delta g\Delta\varphi\right) P\left(\Delta g, \Delta\varphi|\Delta\boldsymbol{s}, \sigma\right)\Delta g\, d\Delta g\, d\Delta\varphi \tag{A.4}$$

for a single fraction, we define the variance contribution function $\bar{q}_{ij}\left(r\right)$ by

$$\bar{q}_{ij}\left(r\right) = \int_0^{2\pi}\int_0^{\infty} d_i\left(r, \varphi|\Delta g\Delta\varphi\right) d_j\left(r, \varphi|\Delta g\Delta\varphi\right) P\left(\Delta g, \Delta\varphi|\Delta\boldsymbol{s}, \sigma\right)\Delta g\, d\Delta g\, d\Delta\varphi \tag{A.5}$$

so that

$$\left\langle D^2\right\rangle\left(r\right) = \sum_{i,j} \bar{q}_{ij}\left(r\right)\Phi_i\Phi_j \tag{A.6}$$

applies.
The optimisation problem can be solved by a standard gradient method since the objective function can explicitly be written as a quadratic function of the fluence in each bixel. The objective function 2.39 can now be expressed as

$$\begin{aligned} E &= \int \alpha(r)\left[\sum_i \bar{d}_i(r)\Phi_i - D_{pres}(r)\right]^2 r dr \\ &\quad + \int \alpha(r)\frac{1}{N}\left[\sum_{i,j}\bar{q}_{ij}(r)\Phi_i\Phi_j - \left(\sum_i \bar{d}_i(r)\Phi_i\right)^2\right] r dr \end{aligned}$$

and the gradient is hence

$$\begin{aligned}\frac{\partial E}{\partial \Phi_i} &= \int \alpha(r) 2\bar{d}_i(r) \left(\sum_j \bar{d}_j(r)\Phi_j - D_{pres}(r) \right) r dr \\ &\quad + \int \alpha(r) \frac{1}{N} \left[2 \sum_j \bar{q}_{ij}(r)\Phi_j - 2\bar{d}_i(r) \left(\sum_j \bar{d}_j(r)\Phi_j \right) \right] r dr\end{aligned}$$

A.3 Calculation of P_{95} probabilities

We want to calculate the probability $P_{95}(r)$ that the cumulative dose at a point with a radial coordinate r exceeds 95% of the prescribed tumor dose. We consider the most general case which accounts for systematic errors and uncertainties in the magnitude of motion (section 2.6). The calculation of P_{95} for considering random errors only is a straightforward simplification. To calculate $P_{95}(r)$ we simulate the treatment of a large number n of patients according to the following steps:

1) Randomly choose σ from the distribution 2.55 or 2.57.

2) Choose a systematic error $\Delta \boldsymbol{s}$ from the distribution 2.54. Without loss of generality set $\sum_{\mu=1}^{M} \Delta p_\mu = 0$.

3) Choose a set of N treatment positions $\{\Delta \boldsymbol{g}_\mu\}$ from the distribution 2.53.

4) Calculate the cumulative dose $D_c^i(\boldsymbol{r})$ according to equation 2.32.

The probability $P_{95}(r)$ is then approximately given by

$$P_{95}(r) = P_{95}(\boldsymbol{r}) \approx \frac{1}{n} \sum_{i=1}^{n} \Theta \left(D_c^i(\boldsymbol{r}) - 0.95 N D_{pres} \right) \tag{A.7}$$

where i is a patient index and Θ is the Heavyside step function, i.e. $\Theta(D) = 1$ $(D > 0)$ and $\Theta(D) = 0$ $(D < 0)$.

Bibliography

[1] J. Unkelbach and U. Oelfke. Inclusion of organ movements in IMRT treatment planning via inverse planning based on probability distributions. *Phys. Med. Biol.*, 49:4005–29, 2004.

[2] J. Unkelbach and U. Oelfke. Incorporating organ movements in inverse planning: assessing dose uncertainties by Bayesian inference. *Phys. Med. Biol.*, 50:121–139, 2005.

[3] J. Unkelbach and U. Oelfke. Incorporating organ movements in IMRT treatment planning for prostate cancer: Minimizing uncertainties in the inverse planning process. *Med. Phys.*, 32(8):2471–83, 2005.

[4] J. Unkelbach and U. Oelfke. Inclusion of stochastic organ movements in IMRT treatment planning. *Radiother. Oncol.*, 68(Sup. 1):S101, 2003.

[5] J. Unkelbach and U. Oelfke. Organ movements in IMRT treatment planning: inverse planning based on probability distributions. In B. Y. Yi, S. D. Ahn, E. K. Choi, and S. W. Ha, editors, *Proc. 14th Int. Conf. on the Use of Computers in Radiation Therapy*, pages 104–107, Seoul, South Korea, 2004. Jeong Publishing.

[6] J. Unkelbach and U. Oelfke. Inverse planning incorporating organ movements via probability distributions of voxel locations. *Radiother. Oncol.*, 73(Sup. 1):S347, 2004.

[7] J. Unkelbach, D. Maleike, and U. Oelfke. On Probabilistic treatment planning: A novel concept for including organ motion into IMRT optimization. *Med. Phys.*, 32(6):1976, 2005.

[8] J. Unkelbach and U. Oelfke. A concept for the estimation of dose uncertainties caused by respiratory motion in radiotherapy. *Radiother. Oncol.*, 76(Sup. 2):S93, 2005.

[9] D. Maleike. *Calculation and visualization of dose uncertainties in radiation therapy due to organ motion*. Diploma thesis, University of Heidelberg, 2005.

[10] M. van Herk, P. Remeijer, C. Rasch, and J. V. Lebesque. The probability of correct target dosage: dose-population histograms for defining treatment margins in radiotherapy. *Int. J. Radiat. Oncol. Biol. Phys.*, 47(4):1121–1135, 2000.

[11] D. A. Jaffray, D. G. Drake, M. Moreau, A. A. Martinez, and J. W. Wong. A radiographic and tomographic imaging system integrated into a medical linear accelerator for localization of bone and soft-tissue targets. *Int. J. Radiat. Oncol. Biol. Phys.*, 45(3):773–789, 1999.

[12] C. W. Cheng, J. Wong, L. Grimm, M Chow, M. Uematsu, and A. Fung. Commissiong and clinical implementation of a sliding gantry ct scanner installed in an existing treatment room and early clinical experience for precise tumor localization. *Am. J. Clin. Oncol.*, 26(3):28–36, 2003.

[13] T. Tücking, S. Nill, B. Hesse, R. Bendl, and U. Oelfke. Application of a kv cone beam equipment on a siemens linac for image guided radiotherapy. *Radiother. Oncol.*, 73(Sup. 1):51, 2004.

[14] D. Yan, D. Lockman, D. Brabbins, L. Tyburski, and A. Martinez. An off-line strategy for constructing a patient-specific planning target volume in adaptive treatment process for prostate cancer. *Med. Phys.*, 48:289–302, 2000.

[15] Y. Seppenwoolde, H. Shirato, K. Kitamura, S. Shimizu, M. van Herk, J. V. Lebesque, and K. Miyasaka. Precise and real-time measurement of 3D tumor motion in lung due to breathing and heartbeat, measured during radiotherapy. *Int. J. Radiat. Oncol. Biol. Phys.*, 53(4):822–34, 2002.

[16] P. C. Cheung, K. E. Sixel, R. Tirona, and Y. C. Ung. Reproducibility of lung tumor position and reduction of lung mass within the planning target volume using active breathing control. *Int. J. Radiat. Oncol. Biol. Phys.*, 57(5):1437–42, 2003.

[17] V. M. Remouchamps, N. Letts, F. A. Vicini, M. B. Sharpe, L. L. Kestin, P. Y. Chen, A. A. Martinez, and J. W. Wong. Initial clinical experience with moderate deep-instiration breath hold using an active breathing control device in the treatment of patients with left-sided breast cancer using external beam radiation therapy. *Int. J. Radiat. Oncol. Biol. Phys.*, 56(3):704–715, 2003.

[18] K. M. Langen and D. T. L. Jones. Organ motion and its management. *Int. J. Radiat. Oncol. Biol. Phys.*, 50:265–278, 2001.

[19] B. K. Lind, P. Källman, B. Sundelin, and A. Brahme. Optimal radiation beam profiles considering uncertainties in beam patient alignment. *Acta Oncologica*, 32(3):331–342, 1993.

[20] J. Löf, B. K. Lind, and A. Brahme. Optimal radiation beam profiles considering the stochastic process of patient positioning in fractionated radiation therapy. *Inverse Problems*, 11:1189–1209, 1995.

[21] J. Löf, B. K. Lind, and A. Brahme. An adaptive control algorithm for optimization of intensity modulated radiotherapy considering uncertainties in beam profiles, patient set-up and internal organ motion. *Phys. Med. Biol.*, 43:1605–28, 1998.

[22] J. G. Li and L. Xing. Inverse planning incorporating organ motion. *Med. Phys.*, 27:1573–78, 2000.

[23] M. Birkner, D. Yan, M. Alber, J. Liang, and F. Nüsslin. Adapting inverse planning to patient and organ geometrical variation: algorithm and implementation. *Med. Phys.*, 30(10):2822–31, 2003.

[24] W. L. Hays and R. L. Winkler. *Statistics - probability, inference and decision.* Holt, Rinehart and Winston Inc, 1970.

[25] H. L. Harney. *Bayesian inference - parameter estimation and decisions.* Springer, 2003.

[26] P. Baldi and S. Brunak. *Bioinformatics - The Machine Learning Approach.* MIT Press, Cambridge, Massachusetts, 1998.

[27] A. Brahme, J. E. Roos, and I. Lax. Solution of an integral equation in rotation therapy. *Phys. Med. Biol.*, 27:1221–29, 1982.

[28] U. Oelfke and T. Bortfeld. Inverse planning for x-ray rotation therapy: a general solution of the inverse problem. *Phys. Med. Biol.*, 44:1089–104, 1999.

[29] T. Bortfeld, M. van Herk, and S. B. Jiang. When should systematic patient positioning errors in radiotherapy be corrected. *Phys. Med. Biol.*, 47:N297–N302, 2002.

[30] S. Nill, U. Oelfke, and T. Bortfeld. A new planning tool for imrt treatments: Implementation and first application for proton beams. In W. Schlegel and T. Bortfeld, editors, *Proc. 13th Int. Conf. on the Use of Computers in Radiation Therapy*, pages pp 326–328, Heidelberg, 2000. Springer.

[31] S. Nill. *Development and Application of a Multi-Modality Inverse Treatment Planning System.* PhD thesis, University of Heidelberg, 2001.

[32] F. Lohr, J. Debus, C. Frank, K. Herfarth, O. Pastyr, B.Rhein, M. L. Bahner, W. Schlegel, and M. Wannenmacher. Non-ivasive patient fixation for extracranial stereotactic radiotherapy. *Int. J. Radiat. Oncol. Biol. Phys.*, 45(2):521–27, 1999.

[33] K. Herfarth, A. Pirzkall, F. Lohr, D. Schulz-Ertner, J. Spoo, C. Frank, M. L. Bahner, O. Pastyr, and J. Debus. First experiences with a non-invasive patient set-up system for radiotherapy of the prostate. *Strahlenther. Onkol.*, 176(5):217–22, 2000.

[34] M. Söhn, M. Birkner, M. Alber, and F. Nüsslin. Modelling patient geometric variation based on dominant eigenmodes of organ deformation. *Radiother. Oncol.*, 73(Sup. 1):49, 2004.

[35] M. Birkner and F. Nüsslin. Automatic modelling of rigid and non-rigid setup inaccuracies for precise head and neck treatments. *Radiother. Oncol.*, 73(Sup. 1):215, 2004.

[36] T. Bortfeld, K. Jokivarsi, M. Goitein, J. Kung, and S. B. Jiang. Effects of intra-fraction motion in imrt dose delivery: statistical analysis and simulation. *Phys. Med. Biol.*, 47:2203–20, 2002.

[37] A. E. Lujan, E. W. Larsen, J. M Balter, and R. K. Ten Haken. A method for incorporating organ motion due to breathing into 3d dose calculations. *Med. Phys.*, 26(5):715–20, 1999.

[38] D. M. Shepard, M. A. Earl, X. A. Li, S. Naqvi, and C. Yu. Direct aperture optimization: a turnkey solution for step-and-shoot IMRT. *Med. Phys.*, 29(6):1007–18, 2002.

[39] Y. Li, J. Yao, and D. Yao. Genetic algorithm based deliverable segments optimization for static intensity-modulated radiotherapy. *Phys. Med. Biol.*, 48:3353–3374, 2003.

[40] T. Bortfeld, D. L. Kahler, T. J. Waldron, and A. L. Boyer. X-ray field compensation with multileaf collimators. *Int. J. Radiat. Oncol. Biol. Phys.*, 28(3):723–730, 1994.

[41] U. Oelfke and T. Bortfeld. Inverse planning for photon and proton beams. *Medical Dosimetry*, 26(2):113–124, 2001.

[42] M. Abramowitz and I. A. Stegun. *Handbook of mathematical functions*. Dover Publications, New York, 1972.

[43] I. S. Gradshteyn and I. M. Ryzhik. *Table of integrals, series, and products*. San Diego, Academic Press, 1994. (A. Jeffrey, editor).

[44] C. Baum, M. Alber, M. Birkner, and F. Nüsslin. Robust treatment planning for intensity modulated radiotherapy of prostate cancer based on coverage probabilities. *Radiother. Oncol.*, 2005. in press.